Modelling the glucocorticoid receptor dimerisation cycle

Christopher James Barry

Thesis presented in partial fulfillment of the requirements for the degree

Master of Science in Biochemistry

in the Faculty of Science at Stellenbosch University

Supervisor: Prof. J. M. Rohwer

Co-supervisor: Prof. A. Louw

March, 2017

Declaration

By submitting this thesis electronically, I declare that the entirety of the work contained therein is my own, original work, that I am the sole author thereof (save to the extent explicitly otherwise stated), that reproduction and publication thereof by Stellenbosch University will not infringe any third party rights and that I have not previously in its entirety or in part submitted it for obtaining any qualification.

Christopher Barry

Date: March, 2017

Summary

The Nobel prize winning discovery of the human glucocorticoid (GC), cortisol, was instrumental in steroidal anti-inflammatory medication development. GCs are employed to combat diseases caused by malfunctions in the immune response such as rheumatoid arthritis, allergies, asthma, sepsis, acute transplant rejection and graft-versus-host disease. However, as with many members of the steroid class, GCs regulate a plethora of biological processes and consequently therapeutic use is associated with a number a side effects.

The majority of GC effects are mediated through activation of their cognate steroid receptor, the glucocorticoid receptor (GR). In the inactive form, the GR resides in the cytoplasm as a monomer. Upon ligand binding the receptor-ligand complex translocates into the nucleus. Once inside the nucleus, the GR can either remain a monomer and act as a *trans*-acting transcriptional repressor, which is associated with the positive effects of GC treatments. Alternatively, the GR can dimerise and act as a *cis*-acting transcriptional activator, associated with the side effects of GC treatments. Therefore, ligand binding and dimerisation are major factors that determine GC signal transduction and subsequent induction or repression of transcription.

Ligand activation of GR can follow two pathways, which occur simultaneously: either via the "classical pathway", which consists of ligand binding to monomeric GR, which subsequently dimerises, or via the "alternative pathway", where GR dimerises independently of ligand and ligand subsequently binds to the dimer.

Being hydrophobic, GCs are able to pass through the cell membrane without transporters, hence, at any given time, their cellular concentration is roughly equal in most tissues. Conversely, GRs are present throughout the body at different concentrations depending on tissue type, inter individual variation, physiological conditions and disease state. Taken together, GR level is likely a primary cause of variations in GC activity.

Until recently, the influence of GR concentration on GC activity had not been quantified nor had the molecular mechanism been elucidated. In 2013, Robertson *et*

al. showed that the Hill coefficient and potency of GR-Dexamethasone (Dex) binding increased with an increase in GR concentration. The shifts in Hill coefficient and potency were abolished when dimerisation was abrogated using a dimerisation deficient mutant. The same study showed that high levels of wild type GR displayed ligand-independent dimerisation, which is a prerequisite for cooperative ligand binding.

A major outcome of this project was the formulation of a mathematical model of the GR dimerisation cycle and Dex binding. Significantly, this model captured GR concentration-dependent shifts in potency and Hill coefficient when simulating GR-Dex saturation binding experiments, albeit not to the same extent as experimental data from literature. This correlates with the increase in potency and Hill coefficient with an increase in GR concentration shown by Robertson *et al.*.

Furthermore, this model is capable of simultaneously predicting GR-GC binding in cells with different GR concentrations, which more closely resembles a transiently transfected cell population. Using a method developed in this study, the specific binding of a population of cells can be scaled to the relative distribution of GR within that cell population.

The kinetic basis for the increase in potency was determined in this study as a GR concentration-dependent decrease in k_{off} as k_{on} remained constant. This decrease in k_{off} was eliminated when dimerisation was abrogated and therefore the concentration-dependent shift in potency is most likely attributed to the dimerisation reactions present in both the classical and alternate pathways of GR activation.

This project comprised a novel approach of simulating GR-GC binding, considered a requisite step of GR activation. The findings demonstrate that the GC signal transduction system is more sensitive to GR concentration than has been previously anticipated. This has implications for GC signal transduction research, steroid research in general, as well as for therapeutic regimes and the development of GC resistance.

Opsomming

Die ontdekking van die menslike glukokortikoïed (GC) kortisol, wat met die Nobelprys bekroon is, het 'n belangrike bydrae gelewer tot die ontwikkeling van steroïedale anti-inflammatoriese medikasie. GCs word gebruik om siektes wat deur gebreke in die immuunstelsel veroorsaak word, soos rumatoïede artritis, allergieë, asma, sepsis, akute oorplanting verwerping en ent-versus-gasheer siekte, te behandel. Soos met baie lede van die steroïed-klas van molekule, reguleer GCs egter 'n wye reeks van biologiese prosesse, en om hierdie rede gaan terapeutiese gebruik dikwels gepaard met 'n aantal newe-effekte.

Die meerderheid van die GC-effekte word bemiddel deur aktivering van die glukokortikoïed-reseptor (GR). Die onaktiewe vorm van GR kom in die sitoplasma voor as 'n monomeer en beweeg na die selkern wanneer dit aan 'n gepaste steroïed bind. Sodra die GR binne die selkern is kan dit as monomeer as 'n transkripsionele onderdrukker optree, wat geassosieer word met die positiewe effekte van GC behandeling. Alternatiewelik kan die GR optree as 'n dimeer, in hierdie geval as 'n transkripsiefaktor deur te bind aan GC responselemente om gene te aktiveer. Hierdie meganisme van werking word geassosieer met die newe-effekte van GC behandeling. Dus bepaal ligandbinding en reseptor-dimerisering die seintransduksie van GCs en die daaropvolgende induksie of repressie van transkripsie.

Die aktivering van GR deur ligandbinding kan twee weë volg wat gelyktydig plaasvind: in die "klassieke pad" bind die ligand eers aan monomeriese GR wat later dimeriseer, terwyl GR in die "alternatiewe pad" 'n dimeer vorm in die afwesigheid van ligand, waaraan die ligand daarna bind.

Omdat GCs hidrofobies is, is dit in staat om sonder transportproteïene deur die selmembraan te beweeg, dus is hul sellulêre konsentrasie min of meer gelyk in die meeste weefsels. Aan die ander kant is GRs teenwoordig in verskillende konsentrasies in die liggaam, afhangende van die tipe weefsel, variasie tussen individue, fisiologiese toestande en siektes. Met hierdie punte in gedagte kan daar afgelei word dat die GR waarskynlik die belangrikste bydraende faktor is wat differensiële GC aktiwiteit bepaal.

Tot onlangs was die invloed van GR konsentrasie op GC aktiwiteit, asook die molekulêre meganisme hiervan, nie bepaal nie. In 2013 het Robertson *et al.* getoon dat die Hill koëffisiënt van GR-dexametasoon binding asook die potensie toegeneem het wanneer die totale GR konsentrasie verhoog word. Dieselfde studie het gewys dat hoë vlakke van wilde-tipe GR ligand-onafhanklike dimerisering kan toon, 'n voorvereiste vir koöperatiewe ligandbinding. Ten slotte kon die verskuiwings in Hill koëffisiënt, potensie en ligand-onafhanklike dimerisering opgehef word deur die gebruik van 'n GRdim mutant wat nie tot dimerisering in staat is nie.

'n Kern uitkoms van hierdie projek was die formulering van 'n wiskundige model van GR dimerisering en Dex binding. Hierdie model kon die eksperimenteel waargenome skuiwe in potensie en Hill koëffisiënt met verandering in GR konsentrasie naboots, wanneer Dex-GR versadigings-bindingseksperimente gesimuleer word, al was die grootte van hierdie verskuiwings nie dieselfde as in eksperimentele data uit die literatuur nie. Hierdie studie bevestig dus die toename in potensie en Hill koëffisiënt met 'n toename in GR konsentrasie, wat oorspronklik deur Robertson *et al.* is aangetoon.

Verder is hierdie model in staat om GR-GC binding te voorspel in selle met verskillende GR konsentrasies. Daar word berig oor die ontwikkeling van 'n metode om die spesifieke binding in 'n populasie van selle te skaleer tot die relatiewe verspreiding van GR binne daardie populasie.

Die onderliggende kinetiese grondslag vir die toename in potensie is in hierdie studie bepaal, nl. 'n GR konsentrasie-afhanklike afname in k_{off} terwyl k_{on} min of meer konstant bly. Hierdie afname in k_{off} word geëlimineer wanneer dimerisering uitgeskakel word, en derhalwe kan die konsentrasie-afhanklike verskuiwing in potensie waarskynlik toegeskryf word aan die dimeriseringsreaksies in beide die klassieke en alternatiewe roetes van GR aktivering.

Hierdie projek behels 'n nuwe benadering tot die simulering van GR-GC binding, wat beskou word as 'n noodsaaklike stap in GR aktivering. Die bevindinge toon dat die GC seintransduksie-stelsel meer gevoelig is vir veranderinge in GR konsentrasie as wat voorheen verwag was. Dit het implikasies vir navorsing oor GC seintransduksie, steroïede in die algemeen, asook vir steroïed-terapieë en die ontwikkeling van weerstand teen GCs.

In loving memory of Robert Barry

Acknowledgements

I would hereby like to express my sincerest gratitude to the following persons and institutions:

Prof. Johann Rohwer, for your continual patience, expertise and encouragement. Thank you for always making time for me, this thesis would not have been the same without you.

Prof. Ann Louw, for your consistent guidance and troubleshooting. As well as for accommodating me and making me feel part of your lab.

Dr. Nicolette Verhoog, for introducing me to wet lab work and always being willing to teach.

Carmen Langevelt and Arrie Arends, for your excellent technical assistance and for being great lab managers.

My mother, Joan Barry, without whom none of this would have been possible. I will forever be grateful for your support and love as well as the opportunities you have afforded me.

Fellow students, with special mention to Elzette Pretorius for all your help, encouragement, love and belief in me.

University of Stellenbosch and the NRF, for financial support.

Contents

List of Figures

List of Tables

Abbreviations

General

ACTH	Adrenocorticotrophic hormone
BSA	Bovine Serum Albumin
CBG	Corticosteroid binding globulin
CFP	Cyan fluorescent protein
COS-1	Monkey Kidney Fibroblast-like Cells
CRH	Corticotrophin Releasing hormone
DBD	DNA binding domain
Dex	Dexamethasone
DMEM	Dulbecco's Modified Eagle Medium
DMSO	Dimethyl sulfoxide
FACS	Flourescent Activated Cell Sorting
FBS	Fetal Bovine Serum
FITC	Fluorescein isothiocyanate
FRET	Fluorescent resonance energy transfer
GC	Glucocorticoid
GR	Glucocorticoid receptor
GRE	Glucocorticoid response element
$t_{(1/2)}$	Half-life
HPA	Hypothalamic–pituitary–adrenal axis
Hsp	Heat shock protein
IL	Interleukin
LBD	Ligand Binding Domain
MAPK	Mitogen-activated protein kinase
nGRE	negative glucocorticoid response element
NR	Nuclear Receptor
NTD	N-terminal domain
PBS	Phosphate Buffered Saline

PySCeS	Python simulator for cellular systems
RE	Response elements
TNF	Tumor necrosis factor
TPR	Tertratricopeptide repeat
YFP	Yellow fluorescent protein
WHO	World Health Organisation

Enzymes

3β-HSD	3-beta-hydroxysteroid dehydrogenase
CYP11A1	Cytochrome P450 cholesterol side chain cleavage
CYP11B1	Cytochrome P450 11β-hydroxylase
CYP17A1	Cytochrome P450 17α-hydroxylase/17,-20-lyase
CYP21A2	Cytochrome P450 steroid 21-hydroxylase

Chapter 1

Project motivation and outline

Steroids and their cognate receptors mediate a plethora of biological processes in the human body. Glucocorticoids (GCs) regulate the immune, cardiovascular and metabolic systems, to name a few, and have been exploited as inflammation suppressors for over 60 years. GCs mediate the majority of their effects through the glucocorticoid receptor (GR) and while this field of signal transduction has been studied for many years, it still regularly yields novel findings. Furthermore, there is no indication that this will cease and with the proliferation of computational techniques, more aspects of the GC signal transduction system are becoming available for study. While there are many mechanisms of action employed by the GC/GR system, this thesis focuses specifically on its classical role of a signal transduction mechanism.

The GR-GC signal transduction system is a therapeutic target, which has the potential to vastly improve the quality of life of many patients. However, there are still a number of gaps in our understanding that limit our ability to use this system to its fullest capacity. Taking into account that GC activity varies between tissues, GC concentration is relatively equal throughout the body at a specific time. Since GCs exert much of their effects through the GR and that GR concentration varies between tissues, it seems likely that GR concentration is a major factor that determines GC activity. For example, a study has shown that increasing GR concentration from 67.0 to 283.9 fmol GR/mg protein increases the potency of Dexamethasone (Dex) via the GR 2600-fold and that this concentration-dependent increase in potency is eliminated when dimerisation of the GR protein was abrogated[1]. For this reason, research into GR dimerisation could elucidate the mechanism underlying the difference in GC activity between tissues and disease states. Specifically, this project focused on producing a mathematical model capable of predicting liganded and unliganded GR monomer and dimer species concentrations over a range of GR concentrations

during Dex stimulation.

Attainment of this goal required a number of incremental aims to be achieved. First, the mathematical framework of the model was formulated based on the reaction scheme shown in **Figure 2.8**. Second, the model was populated with kinetic parameters such that it was able to replicate experimental data. Furthermore, these kinetic parameters were determined using a combination of existing experimental data and newly generated experimental data when necessary. Finally, the model was used to simulate ligand binding to GR under different conditions to examine the behavior of this system.

Briefly, the remainder of the thesis is organized as follows:

Chapter 2 serves as a summary of the literature relevant to this project. Succeeding chapters draw heavily on the information on glucocorticoids, the glucocorticoid receptor and modelling signal transduction mechanisms presented in this chapter.

In Chapter 3, the results of the *in vitro* and *in silico* experiments performed in the course of this study are presented. These entail the details of the formulation of a mathematical model of the GR dimerisation cycle, the processes used to determine the parameters of this model, a whole cell binding time course, a transfection time course and the formulation of a compartmental model of the GR dimerisation cycle.

In Chapter 4, the broader context of the results of this study are discussed including the limitations encountered in this project as well as potential future work.

Finally, in Chapter 5, the techniques used in this project are described in sufficient detail for replication. This entails descriptions of *in vitro* and *in silico* experimental protocols as well as the details of reagent procurement.

Chapter 2

Introduction to glucocorticoids, the glucocorticoid receptor and nuclear receptor modelling

2.1 Glucocorticoids

Steroids are a group of organic molecules found in many species across the prokaryotic and eukaryotic kingdoms. Their primary functions in eukaryotes are signal transduction and cellular membrane fluidity regulation. Steroids contain a distinctive 17-carbon atom, 4-ring structure, called a gonane, shown in **Figure 2.1 (A)**. **Figure 2.1 (B)** shows the prototypical animal steroid, cholesterol, from which all other steroids are derived. In animals, there are 5 classes of steroids: estrogens, androgens, progesterones, mineralocorticoids and GCs.

The name "glucocorticoid" is derived from the role of these steroids in glucose metabolism (gluco), their production location in the adrenal cortex (corti) and their steroidal (oid) structure. Since the Nobel Prize winning discovery of cortisol, shown in **Figure 2.1 (C)**, by Edward Kendall and Harold Mason[2,3], GCs have been used to treat rheumatoid arthritis as well as other rheumatological and inflammatory conditions. Exogenous GCs, such as cortisone or Dex, cause an upregulation in anti-inflammatory proteins and a downregulation in pro-inflammatory proteins. Unlike androgens and estrogens, GCs are not particularly associated with one of the sexes and are found throughout the human body.

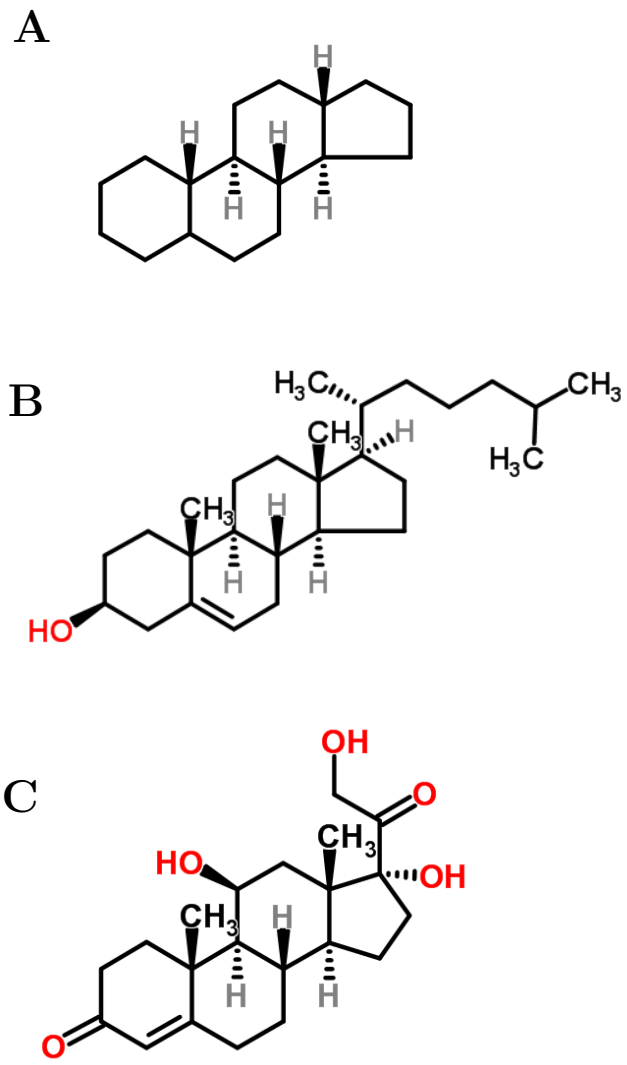

Figure 2.1: Steroid structure. **(A)** gonane, the nucleus of steroid molecules. **(B)** cholesterol, the prototypical animal steroid. **(C)** cortisol, the classical glucocorticoid.

2.1.1 Biosynthesis

GCs are produced in the *zona fasciculata* of the adrenal cortex in the adrenal gland, as shown in **Figure 2.2**, and transported to tissues throughout the body via the circulatory system. Cortisol is synthesized after cholesterol undergoes side chain cleavage by the Cytochrome P450 cholesterol side chain cleavage enzyme (CYP11A1), 17α-hydroxylation by the Cytochrome P450 17α-hydroxylase/17,-20-lyase enzyme (CYP17A1), oxidation by the 3-beta-hydroxysteroid dehydrogenase enzyme (3β-HSD), 21-hydroxylation by the Cytochrome P450 steroid 21-hydroxylase enzyme (CYP21A2) and 11β-hydroxylation by the Cytochrome P450 11β-hydroxylase enzyme (CYP11B1) shown in **Figure 2.3**. Being hydrophobic, GCs are able to pass through the cell membrane without transporters, therefore their cellular concentration is approximately equal at any given time in most tissues with adaquate access to the blood system.

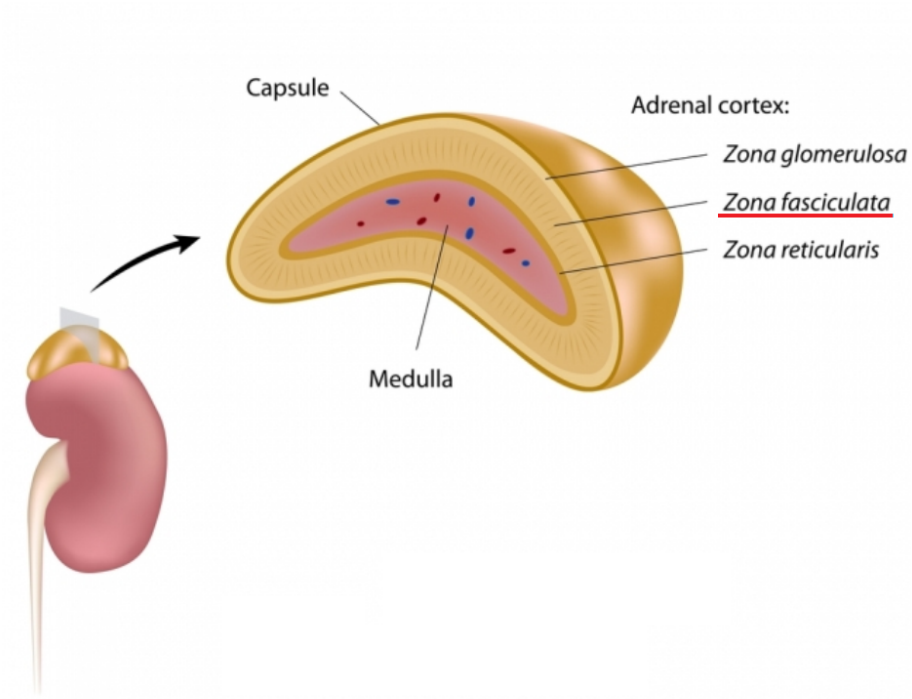

Figure 2.2: The adrenal gland and a cross-section of its subdivisions. The adrenal gland is located above the kidney. It contains the medulla, capsule and the andrenal cortex. The adrenal cortex is partitioned into three zones, notably the *zona fasciculata* where glucocorticoids are produced. Reproduced from Michigan Surgery[a].

[a] http://michigansurgery.com/general-surgery/adrenal-gland/

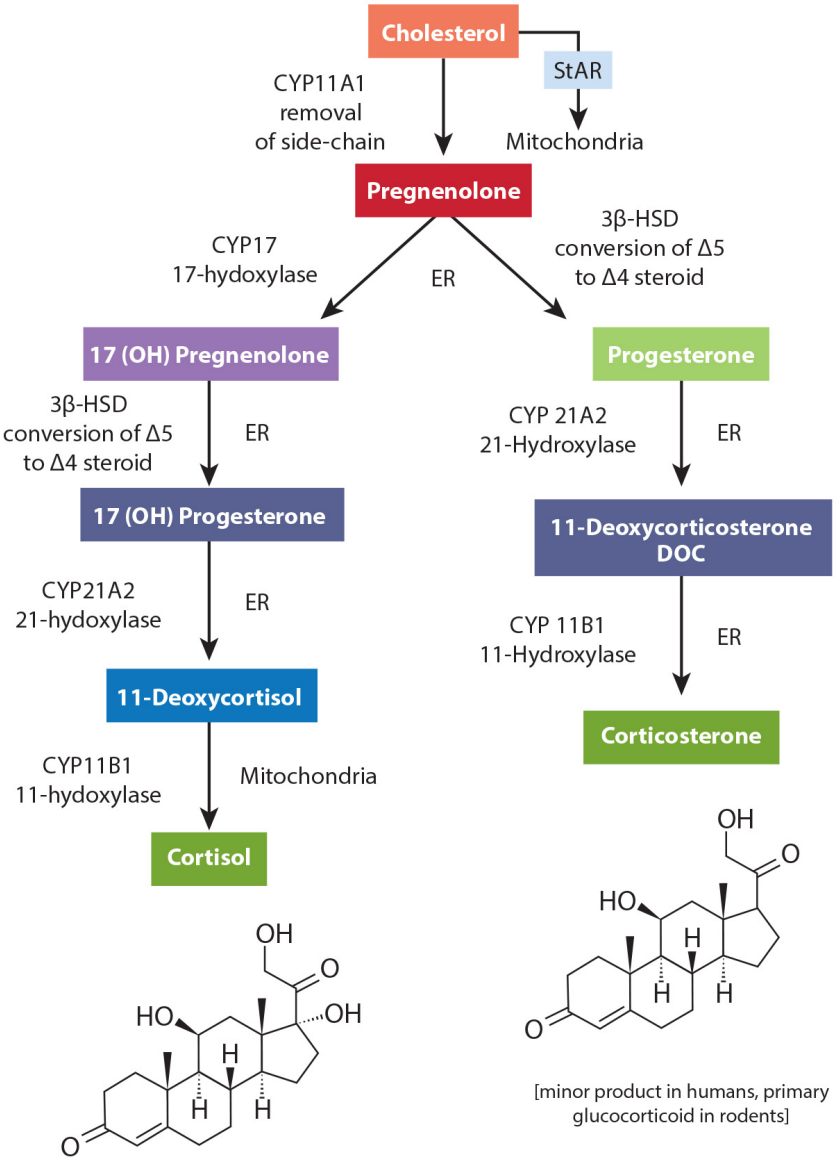

Figure 2.3: The biosynthetic pathways of two glucocorticoids: cortisol and corticosterone. Cortisol is synthesized after cholesterol undergoes side chain cleavage by Cytochrome P450 cholesterol side chain cleavage (CYP11A1), 17α-hydroxylation by Cytochrome P450 17α-hydroxylase/17,-20-lyase (CYP17A1), oxidation by 3-beta-hydroxysteroid dehydrogenase (3β-HSD), 21-hydroxylation by Cytochrome P450 steroid 21-hydroxylase (CYP21A2) and 11β-hydroxylation by Cytochrome P450 11β-hydroxylase (CYP11B1). ER, endoplasmic reticulum; StAR, Steroidogenic acute regulatory protein. Reproduced from Point Institute[a].

[a] http://www.pointinstitute.org/category/blog/

2.1.2 Regulation of glucocorticoid levels

HPA axis

GCs are the primary mediators of the stress response via the hypothalamic–pituitary–adrenal axis (HPA)[4]. The HPA includes the hypothalamus, pituitary and adrenal glands and is regulated by negative feedback mechanisms by cortisol as shown in **Figure 2.4**. The hypothalamus acts as an interpreter by converting neural stimuli into a hormonal signal. Hormonal signals have the advantage over neural signals in that they are delivered to the entire body over a longer period of time[5]. The HPA plays a critical role in regulating the immune response to effectively deal with threats as well as to limit autoimmune harm from inflammatory responses[6–8].

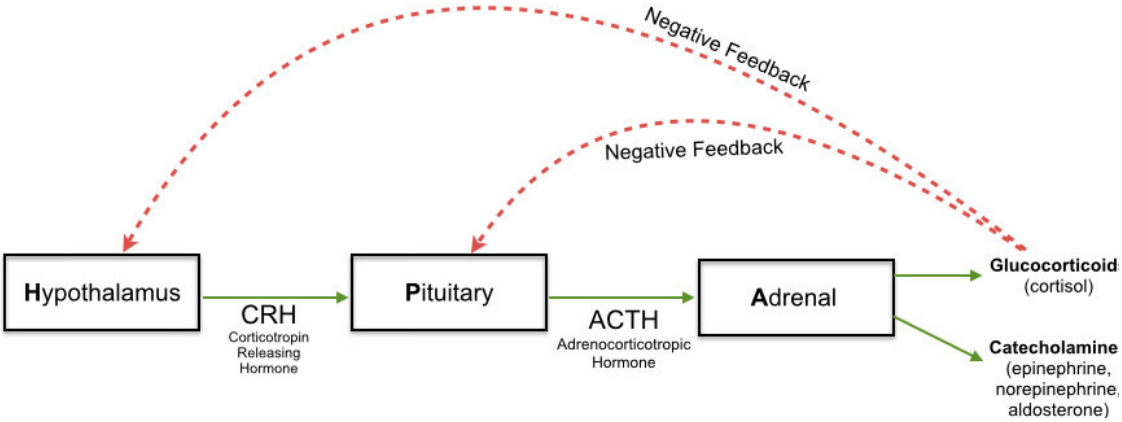

Figure 2.4: The hypothalamic–pituitary–adrenal axis consists of the hypothalamus, the pituitary and adrenal glands. The hypothalamus produces corticotrophin releasing hormone (CRH). CRH stimulates the pituitary to produce adrenocorticotrophic hormone (ACTH). ACTH stimulates the adrenal gland to produce glucocorticoids, which, in turn, inhibit the hypothalamus and pituitary to produce less CRH and ACTH respectively, thereby forming a negative feedback loop. Reproduced from Adrenal Fatigue Solution[a].

[a] https://adrenalfatiguesolution.com/hpa-axis/

Cortisol production is initiated when neurons in the hypothalamus are stimulated to produce corticotrophin releasing hormone (CRH)[9]. This CRH travels to the anterior pituitary via the hypophyseal portal system and stimulates the release of adrenocorticotrophic hormone[10] (ACTH). CRH mediated release of ACTH is responsible for the diurnal rythm of cortisol levels as well as responses to psychiatric disturbances, adrenergic agonists, interleukins and other stresses. ACTH travels via the bloodstream to the adrenal gland where it stimulates the production of GCs in the *zona fasciculata* via activation of melanocortin receptor 2[11,12]. Both ACTH and

CRH production are under negative feedback by circulating cortisol[13].

Plasma circulation

Circulating cortisol is distributed in various forms with 80-90% bound to corticosteroid binding globulin[14,15] (CBG), 5-10% bound to albumin[15] and 3-10% free[15], biologically active cortisol[16]. The level of free cortisol is regulated by negative feedback of glucocorticoids within the HPA. Accordingly, when the level of CBG or albumin is increased or decreased, resulting in either lower or higher plasma cortisol levels, ACTH levels are increased or decreased, which up- or downregulates cortisol production and restores plasma levels.

2.1.3 Mechanism of action and modes of DNA binding

The classical explanation of GC-GR activity is shown in **Figure 2.5**. Initially, the unliganded GR resides in the cytoplasm as a monomer. When ligand enters the cytoplasm, it binds to the GR and this complex trans-locates into the nucleus. Once inside the nucleus, the GR remains a monomer and acts as a transcriptional repressor by tethering to the transcription factors associated with the promotors of other genes; this transrepression is associated with the positive effects of GC treatments. Alternatively, the GR dimerises and acts as a transcription factor by binding to GC response elements (GRE) and activating genes; this transactivation is associated with the negative side effects of GC treatments[17,18]. The GR-GRE complex recruits co-factors such as histoneacetyltransferases, which open the chromatin structure. This causes upregulation of transcription, usually within a few hours after GC exposure[19].

However, the range of GR activation mechanisms has been greatly expanded to include liganded GR homodimers binding to negative GREs (nGRE) either upstream or downstream of the transcription start site, resulting in downregulation of transcription[20–22]. The consensus sequence of nGREs differs from that of GREs and, upon GR binding, results in the recruitment of co-repressors, such as nuclear receptor co-repressor 1 and 2, instead of co-activators[23]. Additionally, liganded monomeric GR has been shown to tether to other DNA interacting transcription factors and thereby upregulate the genes they control[24,25] as well as to occupy monomeric-binding sites and drive transcription[26,27].

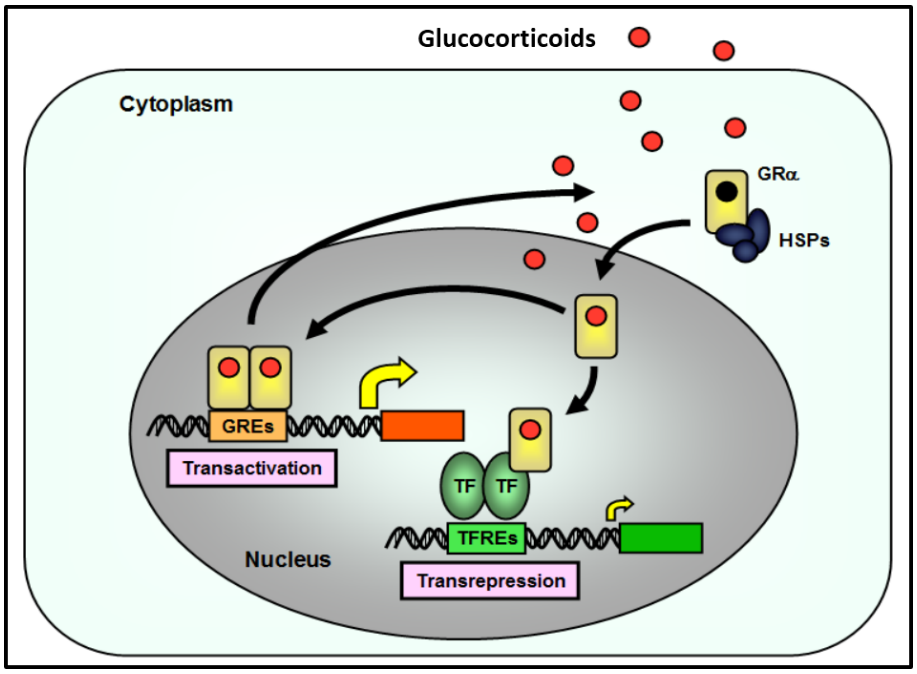

Figure 2.5: Classical activation of the glucocorticoid receptor (GR). The classical explanation of glucocorticoid (GC) GR activity is that the GR resides in the cytoplasm as a monomer. When ligand is added, it binds to the GR and this complex trans-locates into the nucleus. The GR now can either dimerise and act as a transcription factor binding to glucocorticoid response element (GRE) and activating genes or it remains a monomer and acts as a transcriptional repressor by binding to the transcription factors associated with the promoters of other genes. HSP, Heat shock protein; GRα, Glucocorticoid Receptor subtype-alpha; TF, transcription factor; TFRE, transcription factor response element.
Reproduced from Brain Immune[a].

[a] http://brainimmune.com/the-glucocorticoid-receptor/

2.1.4 Biological effects

The effects of GCs are classified primarily as either immunological or metabolic but a significant number of effects also involve development and homeostasis. The majority of effects of GCs studied to date are mediated through interaction with the GR, usually leading to regulation of transcription.

Metabolic effects

The role of cortisol and hydroxycortisol in glucose metabolism was discovered shortly after their inflammation suppressing qualities[28–31]. In many respects GCs play an antagonistic role to insulin in glucose metabolism and maintain or increase blood glucose levels. High GC levels result in insulin resistance-like symptoms such as up-regulation of hepatic gluconeogenesis and reduced peripheral glucose uptake[32].

In early fasting, GCs stimulate gluconeogenesis by upregulation of phosphoenolpyruvate carboxykinase, an enzyme in gluconeogenesis, particularly in the liver, resulting in non-hexose production of glucose[33]. In late fasting, GCs stimulate glycogenesis in preparation for starvation. Under conditions that lead to high insulin levels, such as while recovering from stress, glycogen accumulation is promoted by GCs[34]. Additionally, GCs reduce blood flow and therefore reduce glucose mobility and delivery in the body[35]. The effects of GCs have the effect of amplifying the response to other metabolic regulation stimuli[36].

GCs also stimulate extrahepatic amino acid mobilization, inhibit muscular and adipose tissue glucose uptake as well as stimulating lipolysis in adipose tissue[34,37,38]. *In vitro* studies show that GCs induce adipocytes to release free fatty acids[39]. In cells activated by growth hormone, GCs increase the lipolysis stimulation caused by catecholamines. However, in the presence of insulin, GCs reduce the basal lipolytic rate and responsiveness to catecholamines[40]. Therefore, in adipose tissue, the uptake and turnover of fatty acids as well as response to stimuli such as insulin or catecholamines are modulated by GCs, similar to their role in glucose/glycogen metabolism.

Immunological effects

Overall, GCs act as immunosuppressants by regulating a number of specific lymphocyte processes. GCs regulate T-lymphocyte homeostasis and development[41], inhibition of T-lymphocyte migration to inflammatory sites and the enhancement of scavenger mechanisms leading to the cleanup of microorganisms, dead cell bodies and antigens[42,43]. In addition, many inflammatory cytokines, such as interleukin (IL)-

1β, tumor necrosis factor (TNF)α, IL-6, IL-8, IL-12 and IL-18, are downregualted by GCs while anti-inflammatory cytokines, such as IL-10 and transforming growth factor-β[44–47], are upregulated. T-cells constantly produce "survival signals" that allow peptide or major histocompatibility complex recognition by T-cell receptors to avoid the induction of apoptosis[41]. Apoptosis is the major mechanism of T-cell removal and these survival signals are downregulated by GCs.

GCs regulate the immune system primarily through apoptosis, however the governing mechanisms are not completely understood and vary with cell type. GCs activate apotosis in a number of cell types through the Bcl-2 protein family by upregulation of the pro-apoptotic members, Bim, Bid and Bad[48–50], and downregulation of the anti-apoptotic members, Bcl-2, Mcl-1 and Bcl-xL[50–52]. GCs stimulate phosphatidylinositol 3-kinase and the protein kinase AKT[53], which cause rapid changes in the cytoplasmic environment leading to endothelial nitric oxide synthase activation and nitric oxide-dependent vasorelaxation[54]. Additionally, GC induced GR translocation has been observed in GC responsive cells and not GC resistant cells, indicating that GCs influence apoptosis through the mitochondrial pathway[55,56].

Cognitive effects

Patients using GC medication or suffering from Cushing's syndrome, discussed in Section 2.1.5, frequently suffer from impaired attention, concentration and memory[57–60]. The cognitive effects of GCs are effected by their action on the hippocampus, amygdala and frontal lobes. Long term memory potentiation is optimal at mildly elevated GC levels and inhibited at low or high GC levels[61]. Memory recollection is impaired during times of mildly raised GC levels. During an emotionally stressful event, GCs enhance flashbulb memory formation related to that event and inhibit memory formation of details not related to the event[62].

2.1.5 Role in modern medicine

There are 44 million prescriptions for GCs in the US annually[63] and long term prescription in the UK has increased by 34% in the last 20 years[64]. GCs are the primary treatment for an array of medical conditions, primarily as an anti-inflammatory drug. The wide spread use of GCs has led to the development of many synthetic variations, such as Dex described below. However, endogenous GCs regulate a number of other biological processes besides inflammation and therefore GC therapies are linked to many side effects as well as the development of GC resistance.

Anti-inflammatory drugs

GCs are employed pharmacologically to combat diseases brought about by the immune system such as rheumatoid arthritis, allergies, asthma, sepsis, acute transplant rejection and graft-versus-host disease. Sepsis, an autoimmune condition brought about by infection[65], is estimated to be responsible for 60% of deaths in the developing world*. GCs are prescribed as pills or as topical applications such as creams, nasal sprays and inhalers owing to the reduced side effect profile of these formulations. The anti-inflammatory effects of GCs are elicited through a number of mechanisms and at different levels. GC activated GR induces upregulation of the annexin 1 protein, which inhibits the activity of phospholipase $A_2\alpha$, an enzyme involved in inflammation via the production of the pro-inflammatory prostaglandins. TNFα, a cytokine involved in acute inflammatory response, has an unstable mRNA, which is stabilized when cells are stimulated by proinflammatory signals[66]. GCs negate this stabilization by stimulating proteins, such as tristetraprolin, which promote degradation of proinflammatory mRNAs[67]. Mitogen-activated protein kinase (MAPK) signalling pathways, which activate a number of inflammatory genes, are downregulated by GCs through induction of a MAPK downregulator, mitogen-activated protein kinase phosphatase-1[68,69]. Activated GR reduces the transcriptional activity of the pro-inflammatory transcription factor nuclear factor kappa-light-chain-enhancer of activated B cells (NF-κB) through interaction with co-repressor molecules that reduce RNA polymerase 2 chromatin remodelling as well as histone acteylation via histone deacetylase-2[68,70].

Dexamethasone

Dex is a synthetic glucocorticoid developed in 1957 by MERCK[71] and is used in both medicine, for its anti-inflammatory and immunosuppressant effects, and research, as a GR agonist. It has a long half-life and is 25 times more potent an agonist for the GR than cortisol[72], while having a minimal mineralocorticoid effect. In accordance with it's critical role in public health, Dex is on the WHO list of essential medicines[73†].

Side effects

Considering the wide use of GC medication, the effects of GCs at therapeutic levels constitutes a class of effects on their own. For example, drug induced high GC levels

*http://www.world-sepsis-day.org/CONTENTPIC/2015_WSD_FactSheet_long_English.pdf

†http://www.who.int/medicines/publications/essentialmedicines/EML2015_8-May-15.pdf

have been shown to cause osteoporosis[74], delayed wound healing[75], myopathy[76–78], increased risk of infection[79], hyperglycemia and "steroid diabetes"[80]. Repeated exposure to GCs over long periods of time has been shown to permanently damage memory recollection leading to "steroid dementia"[60,81,82].

Selective glucocorticoid receptor modulators (SEGRMs) are a class of drugs, which exhibit the desirable properties of glucocorticoids but have reduced side effect profiles[83]. SEGRMs achieve dissociation of positive and negative side effects of GCs by selectively activating GR mechanisms of action, usually increasing transrepression and decreasing transactivation. For example, compound A[84], a non-steroidal SEGRM, has agonist activity for the GR but does not induce GR dimerisation, therefore the activated GR remains a monomer and induces transrepression. Cushing's syndrome is a collection of symptoms brought about by sustained high levels of GC exposure[85], primarily in the form of medication but in some cases by GC secreting tumors. The symptoms include: high blood pressure, abdominal obesity, round red face, a fat lump between the shoulders, weak muscles, weak bones, acne and fragile skin. Usually, this condition is treatable either by tapering off GC medication or removal of GC secreting tumors; however, if the pituitary is damaged medication is required to replace its lost function.

Resistance

GC resistance is caused by a variety of mechanisms such as familial resistance[86], GR modification and downregulation[87,88], defective histone acetylation[70,89], increased GRβ expression[90–92], GC efflux[93,94], pro-inflammatory transcription factors[95,96] and upregulation of macrophage migration inhibitory factor[97]. Owing to the high demand for anti-inflammatory treatments, a number of therapeutic options for reversing GC resistance are being investigated and developed such as the GC efflux blockers, verapamil and quinidine, among others[98]. Small molecule inhibitors and monoclonal antibodies are being developed to inhibit the action of macrophage migration inhibitory factor[99] and there is interest in the ability of SEGRMs to restore GR levels as either concomitant with or subsequent to GC therapies. The diverse mechanisms of GC resistance are often simultaneously active, which frustrates attempts to ameliorate them and, together with the side effects of GCs, present a major obstacle to the development of long term GC based treatments.

2.2 The glucocorticoid receptor

The GR mediates the effects of cortisol and other endogenous[50,100,101] and synthetic[102–104] GCs. Ligand activated GR acts as a transcription factor[104], binding to positive or negative GREs, up or down regulating genes, or as a repressor, binding to other transcription complexes, as shown in **Figure 2.5**. Like other steroid hormone receptors, the primary function of the GR is to regulate protein-coding genes that effect development, metabolism and immune responses, as discussed in Section 2.1.4. GRs are present throughout the body[105] albeit at varied concentrations depending on tissue type[106], inter individual variation[107], physiological conditions[108] and disease state[109]. Considering the anti-inflammatory affects of GCs, further study into the GR is warranted.

2.2.1 Protein structure

The GR is a member of the nuclear receptor superfamily of steroid receptors. The members of this family have common structural layout with a moderately conserved activation domain, which includes the N-terminal domain (NTD), a highly conserved DNA binding domain and the moderately conserved ligand-binding domain (LBD), which encompasses the C-terminal of the GR protein, shown in **Figure 2.6**. The NTD contains the activation function 1, which plays a critical role in the activation of transcription[110–112] and interacts with multiple transcription factors including the TATA and CREB binding proteins. Serine phosphorylation of S203, S211 and S226 also influences GR function[113–115]. The DBD contains regions necessary for dimerisation, DNA binding and transcription factor association. The LBD possesses a globular ligand binding pocket of 12 helices and includes regions necessary for dimerisation, co-factor association, transcription factor association[116] as well as regions involved in transactivation. Following ligand-binding, a ligand specific conformational change is induced in helix 12 of the GR, which affects binding of transcriptional intermediary factor 2, a co-activator protein, resulting in differential activity between GR ligands[117].

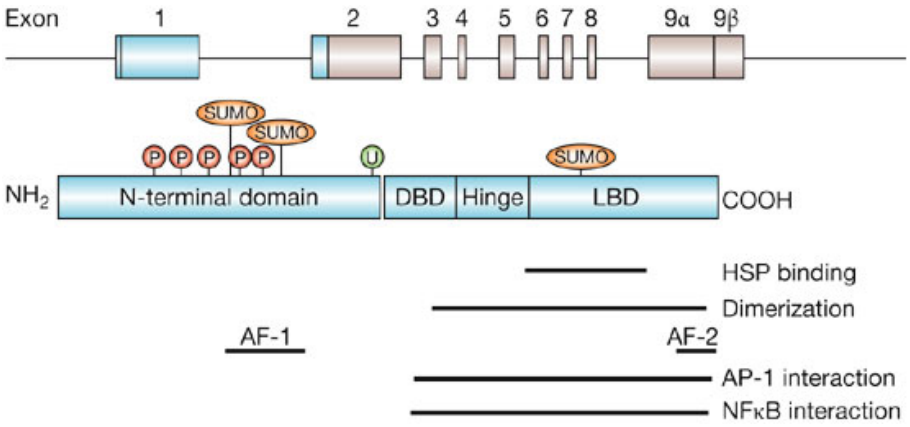

Figure 2.6: Schematic representation of the glucocorticoid receptor gene intron and exon layout as well protein structure and functional domains. The common structural layout of nuclear receptor consists of a moderately conserved N-terminal domain, which includes the activation domain, a highly conserved DNA binding domain (DBD) and the moderately conserved ligand-binding domain (LBD), which encompasses the C-terminal of the receptor protein. AF-1, Activation function 1; AF-2, Activation function 2; AP-1, Activator protein 1; HSP, Heat shock protein; NF-κB, nuclear factor kappa-light-chain-enhancer of activated B cells. Reproduced from Andrew McMaster and David W. Ray[118].

2.2.2 Glucocorticoid receptor distribution

The promoter region of the human GR is activated by a broad range of transcription factors that ensure its constitutive expression under multifarious physiological conditions. As mentioned previously, GR concentration varies between tissues, which governs the different effects GCs have on different parts of the body. Within the cell, the GR protein is localized to specific locations with consequent effects on GR-GC signal transduction.

Inter-tissue distribution

The level of GR varies between individuals[107], tissues[106], under different physiological conditions[108]and under different disease states[109]. For example, GR in bone marrow ranges from 1106 to 27000 GR molecules/cell[108]. MCF-7, a breast cancer cell line, contains 29995 GR/cell[119], SiHa, a uterine cervical cancer cell line, contains 81000 GR/cell and Hep3B, a hematoma cell line, contains 43000 GR/cell[120]. Considering this, and that there are tissue specific variations of GC activity while GC concentration is similar between tissues, the GR level is likely the causative parameter leading to differential GC activity between tissues[120].

Intra-cellular distribution

In the unliganded state, the GR resides as a protein complex with heat shock protein (Hsp) 90, Hsp70, p23 and one of the tertratricopeptide repeat (TPR)-domain proteins[121]. Nuclear localization is governed by NL1 from amino acid 479-506[122–124] and NL2 from 526-777[122,124]. Upon ligand binding, the association with Hsp90[121,125] changes and TPR FK506-binding protein 52[126] and importin-α[127] bind. This complex is translocated into the nucleus along the cytoskeleton by dynein. Nuclear localisation occurs in equilibrium without ligand-binding, however it shifts dramatically towards nuclear import upon ligand-binding[124,128]. Following ligand withdrawal, the GR rapidly dissociates from the DNA[129] and relocates to transcriptionally inactive sites within the nucleus[130]. Nuclear retention is mediated by the nuclear retention signal of amino acids 442-456[131]. Export is slow and does not consume ATP, therefore it is likely via passive diffusion. Immunofluorescent nuclear import and export studies with GRwt and compound A show similar results to the dimerisation deficient GR mutant, GRdim, and Dex[132,133], indicating that dimerisation may play a role in nuclear import and export.

2.2.3 Ligand binding

The macromolecular GR protein contains a binding pocket that is sterically and electronically complimentary to both natural ligand (owing to evolutionary pressure) and synthetic ligand (owing to the associated increase in activity). This complementarity network stabilizes the ligand-receptor complex such that it is thermodynamically favoured over the dissociated complex[134,135].

In the conventional lock and key model for receptor ligand interaction[136], the receptor-ligand complex remains static after ligand binding and therefore association and dissociation occurs as a single reversible reaction. Thus, drug activity can be quantified by conventional equilibrium parameters such as IC_{50} and K_d. However, high-affinity drug-target reactions, those which bind in the nM or lower K_d range, usually include a conformational change in the receptor-ligand complex, which increases complex stability[134,135,137–140]. This conformational change is usually described by either the conformational selection model or the induced fit model.

Conformational selection model

The conformational selection model states that there is an equilibrium between a number of protein conformations with varied ligand binding affinity[141]. Upon addition of ligand, the ligand binds to the receptor at a rate proportional to the

quantity and affinity of each state. Regardless of the equilibrium position between various states, this will result in the majority of receptors binding to ligand, as ligand binding removes the higher affinity forms from the unliganded receptor conversion substrate pool.

Induced fit model

In the induced fit model, a conformational change, which increases ligand affinity to the receptor, occurs after ligand has bound to the receptor[142,143]. The complementarity network in the ligand binding pocket is not optimally conformed for ligand binding. After ligand binding, the receptor undergoes an isomerisation reaction where the conformation of the complementarity network in the ligand binding pocket adjusts in such a way that the affinity for the ligand increases.

The conformational selection and induced fit models are not mutually exclusive and indeed most mechanisms are a compromise or combination of the two, which results in the optimal affinity for a particular system[144,145]. The stable, ligand-bound state reached in both models should be characterized by a potential energy trough, which prevents interconversion between forms. The majority of conformational changes which occur result in modulation of recognition elements formed in the original receptor ligand interaction. Thermodynamically, both models are equivalent as the reaction path does not affect Gibbs free energy change. The shift in affinity associated with these conformational changes can be quite substantial with reports of changes up to 6 orders of magnitude[146].

Residence time

The idea that receptor ligand half-life ($t_{1/2}$) is a key factor determining *in vivo* effectiveness of ligands has been put forward by multiple researchers[137,138,140,147]. The drug-receptor complex $t_{1/2}$ is the time for half of the receptor ligand complex to dissociate and is calculated as $\frac{\ln(2)}{k_{\text{off}}}$. The residence time is directly proportional to the stability of the states of the receptor-ligand complex with higher ligand affinity and thus the energy barriers between these states[148]. In the *in vivo* environment, drug and target concentrations fluctuate over time, whereas many metrics by which drug activity is measured, such as K_{d} (Section 2.3.1) and IC_{50}, are determined under equilibrium conditions. Often residence time will be inadvertently optimized during the optimization of K_{d}[137–139]; therefore, understanding the relationship between structure and function is crucial to drug discovery.

2.2.4 Variants and mutants

The GR protein has a number of naturally occurring splice variants such as GRα, GRβ and GRγ as well as artificial mutants generated for the purposes of research such as GRdim and GRmon. The two primary splice variants, GRα and GRβ occur as a result of alternative splicing of exon 9[149,150], as shown in **Figure 2.6**. Generally, papers referring to the GR are referring to GRα as it is the most widely expressed and transcriptionally active isoform of the GR protein[151,152]. The GRβ splice variant has substituted 50 C-terminal amino acids with 15 nonhomologous amino acids, which, in concurrence with previous studies on steroid receptors, prevent binding of agonists and subsequent activation[153–155]. The intact DNA binding domain is still able to bind to GREs, therefore the GRβ acts as a dominant negative inhibitor with respect to GRα[156]. Recent studies have shown that GRβ participates in the regulation of a set of genes distinct from those regulated by GRα[157].

GRdim

The majority of research into GR homodimerisation has focused on the DBD where it has been shown that dimerisation is dependent on the 5 amino acids in the second zinc finger of the DBD[158]. A dimerisation deficient mutant, GRdim, was established in 1998 with a point mutation, by an alanine to threonine conversion at amino acid 458, in the region responsible for dimerisation, supposedly abrogating the process[158]. GRdim mutants have been constructed for human[159], GR^{A458T}, mouse[160], GR^{A465T}, and rat[161], GR^{A477T}. GRdim has become the most widely characterized GR dimerisation mutant and has been used extensively in studies to elucidate the relevance of dimerisation in GC activity. The validity of the GRdim mutant, as a model for dimerisation deficiency, has been recently questioned as it has been shown to dimerise partially[159,162].

GRmon

In response to the growing concerns about GRdim, described above, a fully dimerisation deficient mouse GR mutant, GRmon, has been developed[162]. This mutant, which contains two mutations, one in the LBD, I634A, and one in the DBD, A465T, showed no dimerisation at 0.1 μM Dex and severely abrogated dimerisation at 1 μM Dex[162]. This suggests that there are multiple regions within the GR protein that promote dimerisation to varying degrees.

2.2.5 Concentration-dependent effects

As mentioned previously, GC concentration is nearly equal throughout the human body at any given time whether under natural or exogenously stimulated conditions, while GR concentration is known to vary. A study by Robertson *et al.* showed that GR concentrations of 67.0, 152.6 and 283.9 fmol GR/mg protein, representing a two- and four-fold GR increase over physiological concentrations, showed a basal induction increase of three- and ten-fold, and an efficacy increase of four- and 12-fold[1]. Furthermore, over the same GR range, a potency increase of 650- and 2600-fold was shown while the fold induction was 9, 10 and 11 for the low, medium and high GR concentrations respectively. Wild type GR showed increased transactivation potency at higher receptor concentrations, which was not mirrored by increased concentrations of GRdim shown in **Figure 2.7**, therefore, dimerisation is crucial for dose-dependent increase of GR potency.

Until recently, the GR concentrations causing these effects had not been measured nor had the molecular mechanism been described. A recent study by Robertson *et al.*[1] showed that ligand-independent dimerisation is responsible for positive cooperative ligand binding as well as an increase in affinity and that ligand-independent dimerisation increases the GC potency and causes a shift in bio-character. Their observations showed an increase in potency far greater than could be accounted for by cooperative binding alone, suggesting basal priming of the GR through ligand-independent dimer loading onto DNA.

Chromatin Immunoprecipitation studies show that unliganded GR dimers bind GRE while monomers do not[1]. This supports earlier electromobility shift assays which showed that ligand independent dimers can bind to DNA with much greater affinity than unliganded monomers, with K_ds of 1.21 and 62 nM, respectively[163]. This is substantiated by fluorescent resonance energy transfer (FRET) results showing unliganded dimers in the nucleus[1]. This indicates a hierarchy of binding affinity to DNA: liganded dimerised GR > unliganded dimerised GR $\geq$ liganded monomeric GR > unliganded monomeric GR.

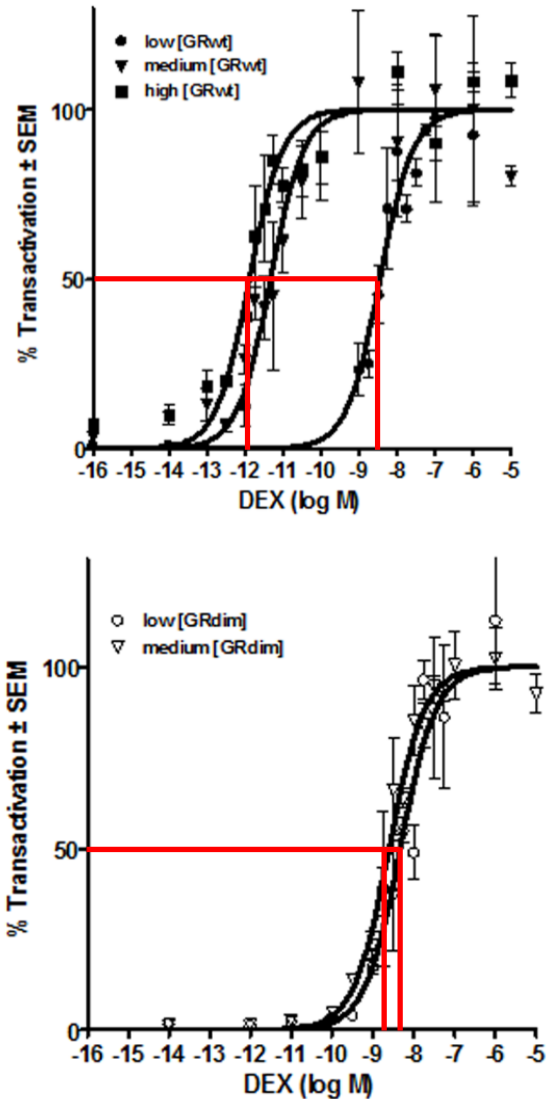

Figure 2.7: Potency of dexamethasone-induced transactivation increases with increased wild-type glucocorticoid receptor concentration but not with the dimerisation deficient mutant. Robertson *et al.* found that GC transactivation potency increased 2600-fold with an increase in GR concentration and that this effect was eliminated when dimerisation was abrogated[1].

2.3 Modelling glucocorticoid receptor signal transduction

Conceptually, steroids are signals, sent from one part of the body to another, which are received by their cognate steroid receptors. A plethora of factors, such as hydrophobicity of the ligand[164], shuttling of receptor across boundaries within the cell[128] and cellular co-factor milleu[165], influence the transduction of this signal often in seemingly paradoxical ways. Great strides have been made in delineating these factors[166], specifically with a systems approach, and as such there is an opportunity for the development of functionally useful predictive models in this field. Molecular biological systems are complex and contain numerous intricately cross-linked systems, which vary in their degree of influence on each other. Therefore computational models have a large scope for expansion that improves their function. The formulation of a model requires a working understanding of which systems to include or exclude and how to compensate for any influences excluded systems may have.

2.3.1 Pharmacodynamic characteristics

Various measurements have been developed to describe drug reaction pharmacodynamics, such as K_d and Hill coefficient. These form the basis of mathematical modelling studies in this field.

Dissociation constant

The dissociation constant, K_d, is a type of equilibrium constant, which describes the propensity for a complex to dissociate into two molecules. The physical interpretation of K_d is that when the concentration of one of the substrates is equal to K_d, half of the molecules of the other substrate will be complexed with the first substrate. Given the reaction:

$$[R] + [L] \underset{k_\mathrm{off}}{\overset{k_\mathrm{on}}{\rightleftharpoons}} [RL]$$

The affinity between the receptor, R, and ligand, L can be described by K_d:

$$K_\mathrm{d} = \frac{[R][L]}{[RL]}$$

The smaller the K_{d}, the higher the affinity of R for L. Less commonly, the propensity that a liganded or unliganded receptor has for dimerisation is also described by K_{d}:

$$[R] + [R] \underset{k_{\mathrm{off}}}{\overset{k_{\mathrm{on}}}{\rightleftharpoons}} [RR]$$

$$K_{\mathrm{d}} = \frac{[R]^2}{[RR]}$$

At equilibrium the rates of the forward and reverse reactions are equal, which leads to a kinetic definition of K_{d}:

$$[R][L]k_{\mathrm{on}} = [RL]k_{\mathrm{off}}$$

$$\frac{[R][L]}{[RL]} = \frac{k_{\mathrm{off}}}{k_{\mathrm{on}}}$$

$$K_{\mathrm{d}} = \frac{k_{\mathrm{off}}}{k_{\mathrm{on}}}$$

The K_{d} rate equation presumes that there are no competing reactions present; however, it can be expanded to include these.

Hill equation and cooperative binding

The relationship between ligand concentration and occupancy of a receptor the reaction of a ligand binding to a macromolecule is given by the Hill equation[167] below:

$$\sigma = \frac{[L]^n}{{K_{\mathrm{d}}}^n + [L]^n}$$

where σ represents the fractional occupancy of the receptor, $[L]$ represents the free ligand concentration, K_{d} represents the apparent dissociation constant (often using the symbol $K_{0.5}$) and n represents the Hill coefficient, the degree of cooperativity. Cooperativity is a measure of the degree to which binding of a ligand influences the binding of subsequent ligands. A Hill coefficient > 1 indicates that a ligand binding enhances the binding of subsequent ligands while a Hill coefficient < 1 indicates the inverse, that a ligand binding inhibits the binding of subsequent ligands. Naturally, multiple binding sites are a prerequisite for cooperative binding to occur. In terms of application, this equation can be fit to a saturation binding curve to determine K_{d} and Hill coefficient.

$$[L] = \frac{B_{\mathrm{max}}}{10^{n \times (\log K_{\mathrm{d}} - \log [L])} + 1}$$

where B_{max} represents the maximum amount of specific binding or the total receptor concentration.

2.3.2 Topological aspects of nuclear receptor signal transduction

Accurate model generation requires a thorough understanding of the subject mechanism as well as of connected systems, which may need to be compensated for, if not incorporated, in the model. Several mechanisms have been identified that modulate the response of a nuclear receptor system to changes in the concentration of ligand[166].

Non-DNA bound nuclear receptors

In the classical model of nuclear receptor activation the nuclear receptors are not present in the cytoplasm[168,169], but are bound to response elements on the DNA, waiting to be activated by ligand. However, the nuclear receptors greatly outnumber the response elements, so that the majority of nuclear receptors are not DNA bound. For example, the number of GRs is approximately 100-fold higher than the number of active response elements calculated from the number of GRE[170,171] and GR[172,173] per cell (although the GR has been shown to bind to other DNA elements[174]). A higher concentration of nuclear receptor leads to a higher concentration of liganded nuclear receptor when ligand is added and, consequently, results in more liganded nuclear receptor bound to the response element, thereby vastly improving responses over DNA bound nuclear receptor alone. Additionally, DNA-bound nuclear receptor is targeted for ubiquitination and degradation[175], which constitutes a futile cycle when the nuclear receptor is unliganded.

Nuclear receptor in the cytoplasm

The nuclear receptors derive their name from initial studies that observed them located mostly in the nucleus, despite them mediating extracellular signals[168]. Simulations with nuclear receptor exclusively in the nucleus show a slow response to addition of ligand; however, the magnitude of the steady-state response is increased[166] relative to simulations with nuclear receptor in cytoplasm. The rate at which unchaperoned ligand diffuses across the cytoplasm is not sufficient to match the rate of ligand sequestration by nuclear receptor in the nucleus[166]. This is in part owing to the hydrophobic nature of steroids, which causes them to remain bound to the plasma membrane rather than enter the cytoplasm with partition coefficients[164] of over 1000. Furthermore, the width of the plasma membrane is significantly smaller than the radius of the cytoplasm. For example, the diffusion rate for cortisol is estimated at approximately 6×10^{-12} $m^2.s^{-1}$ and the diffusion rate for nuclear receptor is

one sixth of this amount, as determined from protein diffusion constants[166]. It may therefore appear paradoxical that cytoplasmic nuclear receptor would shuttle ligand across the cytoplasm. However the concentration of nuclear receptor vastly exceeds that of free ligand and therefore cytoplasmic nuclear receptor shuttles ligand to the nucleus at rates of up to 25 times higher than if the nuclear receptor were present in the nucleus alone.

Nuclear shuttling

In nuclear receptor signal transduction models that do not include nuclear shuttling, ligand would have to be released at and diffuse across the nuclear membrane before binding to nuclear nuclear receptor to cause a transcriptional response. This slows down the transcriptional response[166]; however, this problem is circumvented by translocation of ligand-bound cytosolic nuclear receptor into the nucleus. Following addition of ligand, cytosolic and nuclear nuclear receptor reach an equilibrium with a lower nuclear nuclear receptor concentration than if nuclear receptor were present in the nucleus alone, resulting in a lower transcriptional response[166]. Adjusting the ratio between nuclear and cytosolic nuclear receptor will shift the system either towards a faster response or a more sensitive one and provides a mechanism by which responsiveness in nuclear receptor systems can be modulated to the cell's requirements.

Another aspect that modulates nuclear receptor system responsiveness is the absolute rate of shuttling, as increasing the rate at which liganded nuclear receptors are moved into the nucleus will always improve the speed of the transcriptional response[166]. However, the increased shuttling rate results in reduced specificity. Completely non-discriminatory shuttling at any rate would result in equal concentrations of liganded nuclear receptor on either side of the nuclear membrane. This lowers system responsiveness relative to specific shuttling as cytoplasmic liganded nuclear receptor is increased, inhibiting ligand binding to nuclear receptor, and nuclear liganded nuclear receptor concentration is decreased, weakening the transcriptional outcome. Therefore a compromise needs to be reached between the absolute rate of shuttling and the import/export ratio[166].

The specificity of the nuclear receptor import system is achieved by binding of importins selective to liganded nuclear receptor, which flag these nuclear receptors for nuclear import[166]. These importins have to dissociate from the nuclear receptor once inside the nucleus and travel back to the cytoplasm to regenerate the cytoplasmic importin pool. This results in an increase in the concentration of nuclear importin, which, at high enough concentrations, will inhibit transcriptional response

by sequestration of liganded GR[166]. Therefore, an importin gradient that drives nuclear import of importin-bound liganded nuclear receptor and active importin export, likely coupled to GTP hydrolysis, is optimal.

2.3.3 The glucocorticoid receptor dimerisation cycle

GR and ligand conversion reactions include an array of different species, as shown in **Figure 2.8**, the concentrations of many of which are not feasible to be determined experimentally. These reactions include the formation of heterodimers with other steroid hormone receptors, oligomer states above dimers as well as incompletely liganded dimers and higher oligomers. A partially liganded state can be achieved either when a single ligand binds to the dimerised unliganded GR complex, as two ligands cannot bind to an unliganded GR simultaneously, or when a liganded GR binds to an unliganded GR. These states could be incorporated into the a model using the Adair equation, however these additional states exist for short times and have little influence on activity. Therefore, the exclusion of these reactions and species should not significantly detract from the accuracy of a model of GR-ligand binding.

A GR-^{3}H-Dex radiolabelled ligand-binding study found a shift in Hill coefficient from 1 to 1.72 over a GR concentration range of 67.0 $\pm$ 8.8 to 283.9 $\pm$ 23.8 fmol/mg protein, which indicates an increase in cooperativity[1]. Ligand-independent dimerisation and partially liganded states are a prerequisite for cooperative binding as each GR monomer contains a single ligand binding pocket[116]. The same study showed that cooperative ligand binding and increased ligand binding affinity were abolished when dimerisation was abrogated with the GRdim mutant. Binding of a single ligand to a unliganded GR dimer increases the affinity of the dimer for a second ligand by altering the energetics of binding[176].

Thermodynamics

One of the principles of Gibbs energy is that the total standard Gibbs[177] free energy, and therefore K_{eq}, for the conversion from the substrates to the products is the same regardless of which pathway is taken. The result is that the K_{d} of a reaction could be determined arithmetically by setting the product of all the K_{d}s of a pathway equal to those of another pathway or the K_{eq} of the entire pathway. In the case of the GR i.e.,

$$K_{\mathrm{d1}}^2.K_{\mathrm{d2}} = K_{\mathrm{d3}}.K_{\mathrm{d4}} = K_{\mathrm{eq}}$$

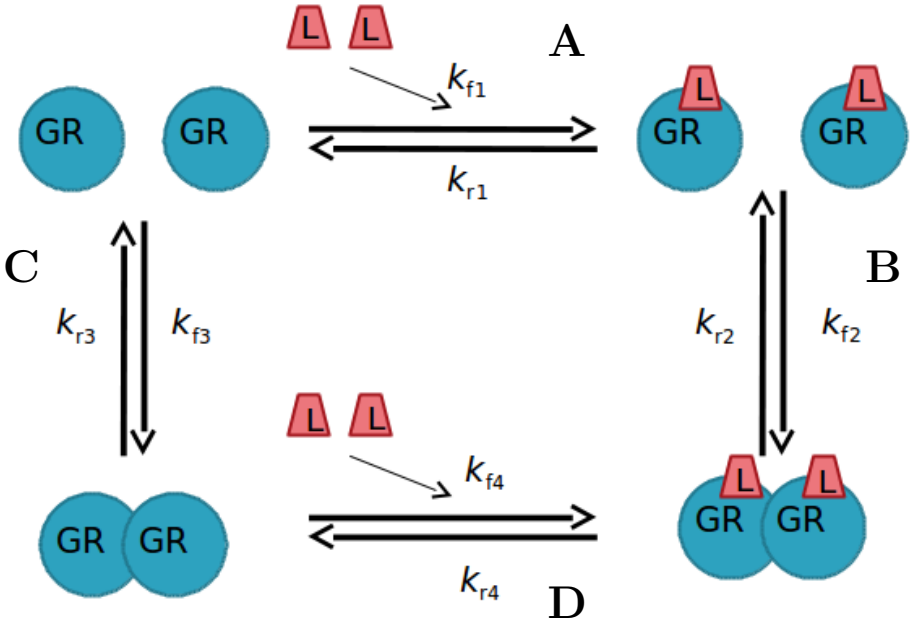

Figure 2.8: The glucocorticoid receptor (GR) dimerisation cycle. **(A)** Reaction 1, ligand binding to monomeric GR produces monomeric liganded GR. **(B)** Reaction 2, monomeric liganded GR associates to form dimeric liganded GR. **(C)** Reaction 3, unliganded GR associates to form dimeric unliganded GR. **(D)** Reaction 4, ligand binding to dimeric GR producing dimeric liganded GR.

the dimerisation of ligand bound GR is difficult to determine experimentally, however the ligand binding to monomeric and dimeric GR as well as the ligand independent association can be determined. **Figure 2.8** shows the two pathways for the conversion of unliganded monomeric GR to liganded dimeric GR.

In the next chapter, the formulation of the model for the GR dimerisation cycle will be described, as well as an analysis of the GR ligand binding system.

Chapter 3

Modelling the glucocorticoid receptor dimerisation cycle

The central focus of this project was to develop a mathematical model of the reactions of the GR dimerisation cycle that included: ligand binding to GR monomer, dimerisation of liganded GR, ligand-independent dimerisation of GR and binding of ligand to unliganded GR dimers **(Figure 2.8)**. The variables of this model were populated using experimental values obtained from literature[1]. Additionally, GR-^{3}H-Dex whole cell time course binding experiments were conducted at 20 nM and 40 nM ^{3}H-Dex in order to the determine kinetic parameters necessary to perform time dynamic simulations with the model. A compartmental model was formulated that included three compartments, representing cells with different concentrations of GR. Finally, these models were to used to simulate saturation binding data at different GR concentrations and distributions, providing insights into the influence of dimerisation on GR signal transduction.

3.1 Formulation of the mathematical model

Reaction kinetic models require both rate and stoichiometric equations to perform computational simulations. The reaction scheme in **Figure 2.8** was used as the basis for formulating a model capable of simulating the GR dimerisation cycle. The following equations were used in the model, they are numbered for easier differentiation between reaction rates as well as reaction rate constants:

Reaction 1, ligand binding to unliganded GR monomer (**Figure 2.8 (A)**):

$$R + L \underset{k_{r1}}{\overset{k_{f1}}{\rightleftharpoons}} RL$$

$$v_1 = k_{f1}[R][L] - k_{r1}[RL]$$

Reaction 2, dimerisation of liganded GR monomer (**Figure 2.8 (B)**):

$$2RL \underset{k_{r2}}{\overset{k_{f2}}{\rightleftharpoons}} (RL)_2$$

$$v_2 = k_{f2}[RL]^2 - k_{r2}[(RL)_2]$$

Reaction 3, dimerisation of unliganded GR monomer (**Figure 2.8 (C)**):

$$2R \underset{k_{r3}}{\overset{k_{f3}}{\rightleftharpoons}} R_2$$

$$v_3 = k_{f3}[R]^2 - k_{r3}[R_2]$$

Reaction 4, binding of two ligands to unliganded GR dimer (**Figure 2.8 (D)**):

$$R_2 + 2L \underset{k_{r4}}{\overset{k_{f4}}{\rightleftharpoons}} (RL)_2$$

$$v_4 = k_{f4}[R_2][L]^2 - k_{r4}[(RL)_2]$$

where R represents receptor, L represents ligand, v represents reaction rate and k_f and k_r represent forward and reverse reaction rate constants, respectively. These reactions were compiled in ".psc" files for use in Python based simulations using the PySCeS environment[178], see **Appendices A to C** for more details. All species and ligand concentrations as well as rate constants were in nM.

Internal consistency

Following formulation, the model was tested for internal inconsistencies. **Figure 3.1** shows that all reaction rates reached zero and the concentrations of all GR species reached equilibrium when the model was initiated with 20 nM ligand. This simulation was performed with k_{off} values of 52.3, 6.4, 83.0 and 211.5 min^{-1} for reactions 1 to 4 respectively, a k_{on} value of 1 $nM^{-1}.min^{-1}$ for reactions 1 to 3 and 1 $nM^{-2}.min^{-1}$ for reaction 4 and a GR concentration of 54 nM. The k_{off} values used in this simulation were determined in Section 3.2. The system simulated in this project was thermodynamically closed, with no external addition or removal of GR species. In a closed system, the results of this simulation demonstrates that the stoichiometry of the model does not violate the law of conservation of matter and that the reaction scheme is logically consistent.

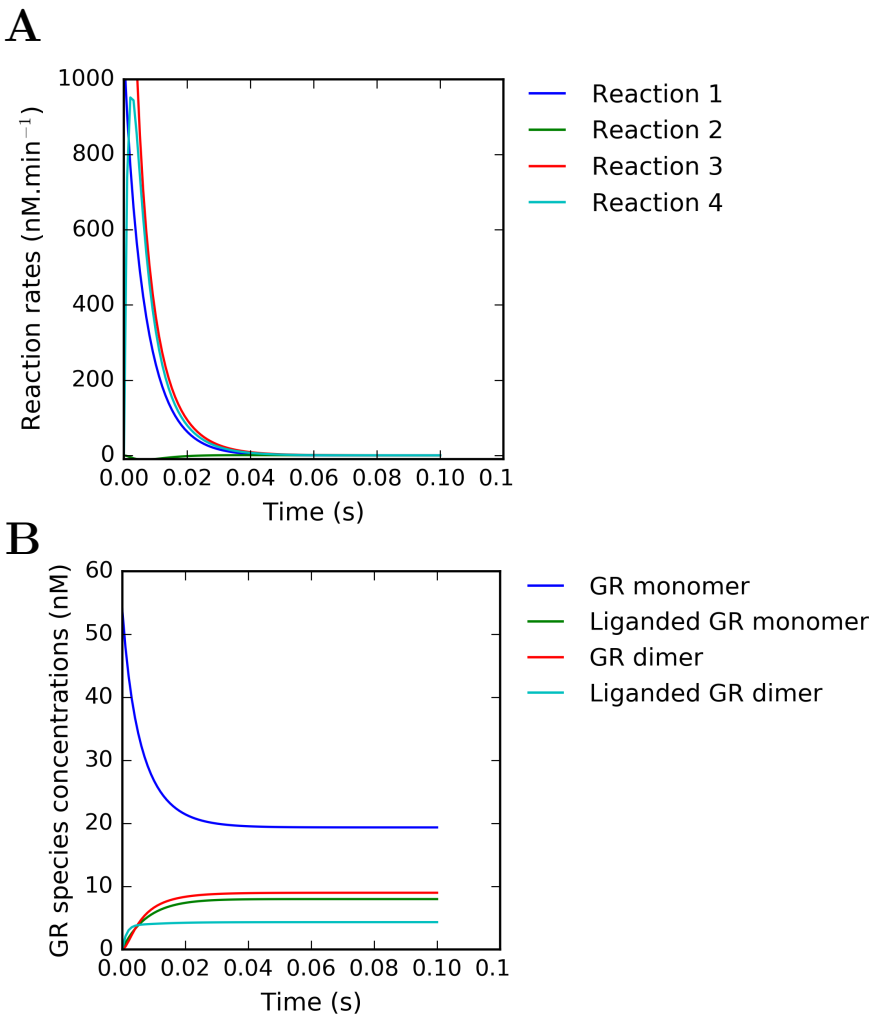

Figure 3.1: The GR dimerisation cycle mathematical model is internally consistent. The model was initiated with k_{off} values of 52.3, 6.4, 83.0 and 211.5 min^{-1} for reactions 1 to 4 respectively, a k_{on} value of 1 $\text{nM}^{-1}.\text{min}^{-1}$ for reactions 1 to 3 and 1 $\text{nM}^{-2}.\text{min}^{-1}$ for reaction 4, a GR concentration of 54 nM and a ligand concentration of 20 nM and simulated until the concentrations of all GR species and free ligand reached equilibrium and all reaction rates reached zero. **(A)** The rates for all reactions reached zero. **(B)** All GR species concentrations reached equilibrium. R1, reaction 1, ligand binding to unliganded GR monomer; R2, reaction 2, dimerisation of liganded GR monomer; R3, reaction 3, dimerisation of unliganded GR monomer; R4, reaction 4, binding of two ligands to unliganded GR dimer.

Excluded reactions

The model formulated in this project aimed only to include the reactions of **Figure 2.8** as it was hypothesized that this would allow simulation of the influence of GR concentration on K_d and Hill coefficient, as discussed in Section 2.3.3. Proximate reactions, such as those shown below, were examined for potential ancillary influences on the hypothesis and simulations.

Reaction 4 (two ligands binding to dimerised GR) assumes 100% cooperativity, which is physically impossible as one ligand cannot force another to bind immediately. This could be resolved by splitting this reaction into two sequential binding reactions as shown below:

$$R_2 + L \rightleftharpoons R_2L$$

$$R_2L + L \rightleftharpoons (RL)_2$$

The first reaction pair describes a single ligand binding to an unliganded GR dimer. The second reaction pair describes a ligand binding to a GR dimer with a single ligand already bound. The latter reaction would likely have a lower K_d, indicating a higher ligand affinity, owing to an increase in cooperativity brought about by the binding of the first ligand. Obtaining the binding constants for these reactions was not possible at this time as they could not be isolated from the rest of the GR dimerisation cycle. Considering that there is no evidence that a GR dimer bound to a single ligand is biologically active and that the thermodynamic influence of a linear reaction path is maintained when combining multiple reactions, including these reactions individually was deemed unnecessary.

Currently, there is no evidence to support or reject the potential reaction of a liganded GR monomer binding to a unliganded GR monomer, shown below:

$$RL + R \rightleftharpoons R_2L$$

The product of this reaction would be a single ligand bound to GR dimer, which would feed into the second reaction above. This reaction was excluded on the basis that the products formed would be rapidly converted to the end product, minimizing any impact they have on the system.

A recent study has shown that the GR forms oligomerisation states higher than dimer[179]. It is unclear whether this applies to both liganded and unliganded oligomers. Oligomers could be formed by sequential addition of ligand, shown in

the equation below, or by concatenation of GR oligomers of any order.

$$R_n + R \rightleftharpoons R_{n+1}$$

These reactions were excluded on the basis that there is limited evidence for their existence and influence on GR function.

Various additional time-dependent influences on the ligand-GR system may become relevant depending on the situation being simulated. For example, steroids are removed from the cells by glucuronidation[180], which lowers ligand concentration over time, causing all GR species to revert to their unliganded forms. In this model it was assumed that free ligand concentration remains stable as the simulations were run over relatively short periods of time. Under this condition, ligand would be continually replenished by an endogenous or exogenous source. Additionally, sequestration of liganded GR to DNA removes this species from the product pool of the GR dimerisation cycle thereby increasing the flux through this pathway until the GREs became saturated. Presumably, the binding of GR dimers to DNA is a major reaction determining the transcriptional outcome of the ligand-GR system and would be incorporated into a model that aimed to simulate this.

Ligand depletion

The initial formulation of the model did not have ligand concentration fixed. Without ligand fixed, the simulated saturation binding data slope shifted to the right for medium and high GR concentrations (**Figure 3.2**), despite the expected increase in cooperativity, which should have resulted in a shift to the left. This observation can be attributed to ligand sequestration, where ligand bound to GR is removed from the reactant pool lowering the effective free ligand concentration, thereby giving a result that falsely appears as if potency had lowered. In *in vivo* binding assays, total ligand greatly exceeds total receptor. Consequently, ligand depletion in binding experiments is negligible, usually $< 5\%$, and was justifiably fixed in the model.

Shifts in K_d and Hill coefficient

One of the objectives of this project was to identify the aspects of the GR dimerisation cycle mechanism that causes K_d to decrease and the Hill coefficient to increase as GR concentration is increased, as discovered by Robertson *et al.*[1]. To this end, the model was reduced into two simpler versions, the classical GR activation pathway, containing Reaction 1 (**Figure 2.8**), ligand binding to unliganded GR monomer and Reaction 2, dimerisation of liganded GR monomer, as well as the alternate GR

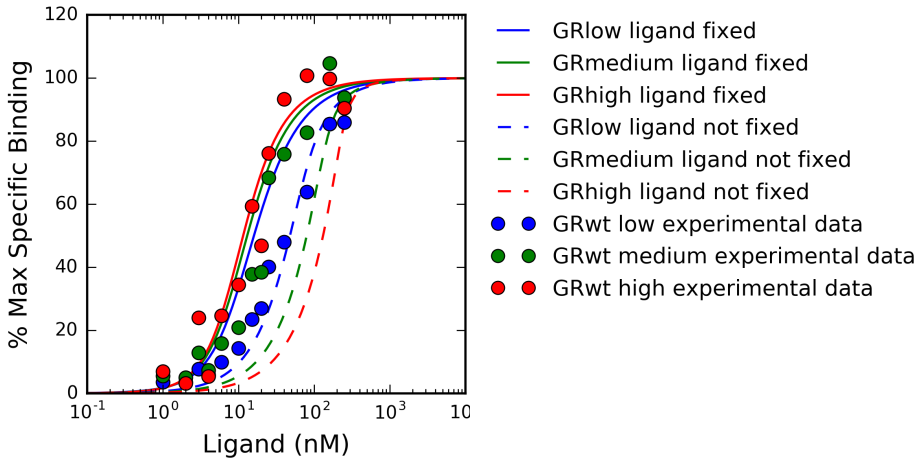

Figure 3.2: Model simulation showing ligand depletion. The model was initiated with k_{off} values of 52.3, 6.4, 83.0 and 211.5 min^{-1} for reactions 1 to 4 respectively and a k_{on} value of 1 $nM^{-1}.min^{-1}$ for reactions 1 to 3 and 1 $nM^{-2}.min^{-1}$ for reaction 4, GR concentrations of 54, 123 and 229 nM and saturation binding data was simulated with and without ligand fixed.

activation pathway containing Reaction 3, dimerisation of unliganded GR monomer and Reaction 4, binding of two ligands to unliganded GR dimer. Saturation binding data was simulated and Hill equations fitted, using the method described in Section 5.2.1, at GR concentrations from 50 to 250 nM and with values of 52.3, 6.4, 83.0, 211.5 nM for k_{r1}, k_{r2}, k_{r3} and k_{r4} respectively (**Figure 3.3**); refer to Section 3.2 for determination of these values. The complete model showed that K_d decreased from 27.1 to 21.7 nM as GR concentration increased and the Hill coefficient increased from 1.36 to 1.60 (**Figure 3.3 (A)**). The classical pathway only model showed that K_d reduced from 20.7 to 10.8 nM as GR concentration increased, Hill coefficient increased from 1.23 to 1.30 (**Figure 3.3 (B)**). The alternate pathway only model, showed the K_d reduced from 35.9 to 24.6 nM as GR concentration increased, while Hill coefficient increased from 1.56 to 1.72 (**Figure 3.3 (C)**). These results show that the complete, classical and alternate pathways contain the mechanism by which K_d and Hill coefficient shift in response to a change in GR concentration. The greater shift in Hill coefficient generated by the alternate only pathway when compared to the classical only pathway may indicate that this pathway contributes more to this phenomenon.

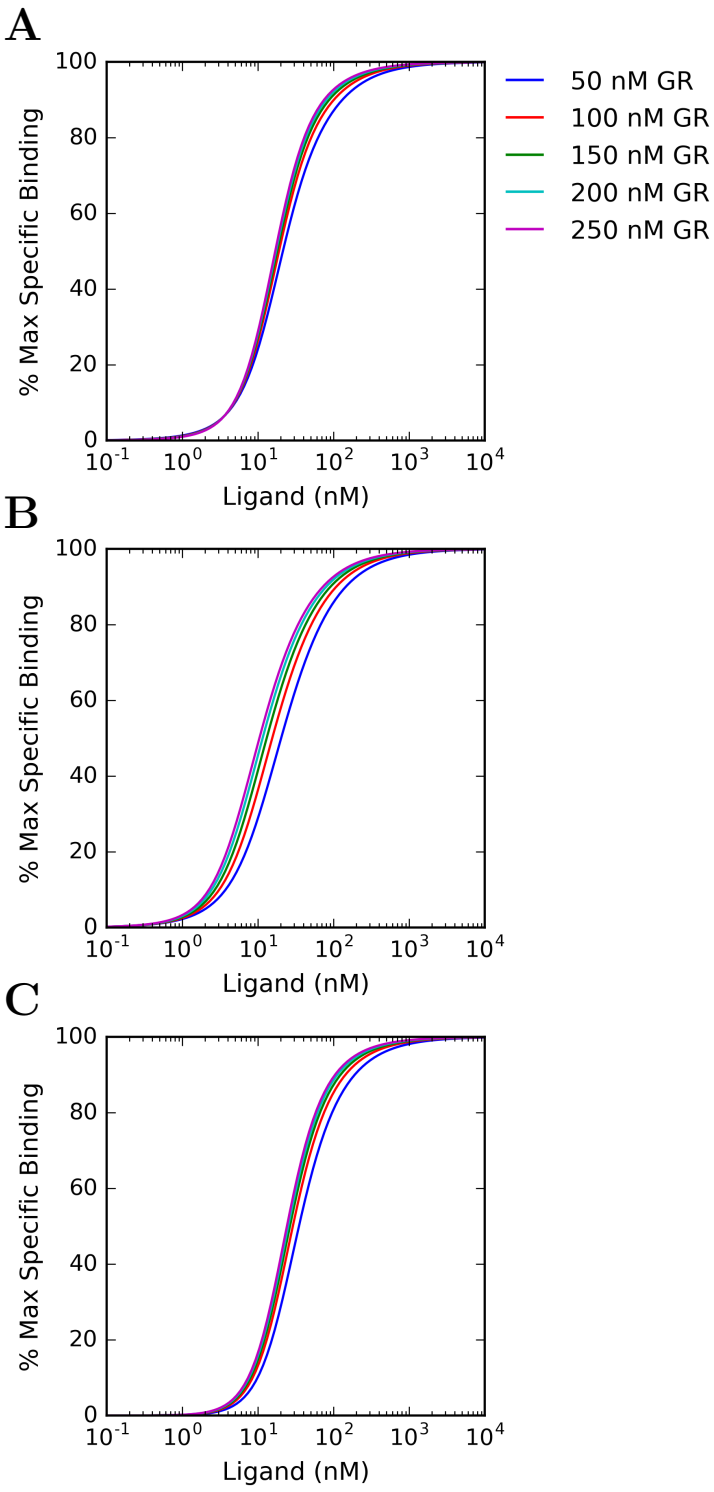

Figure 3.3: The K_d and Hill coefficient of the classical, alternative and combined pathways change in response to a change in GR concentration. Simulated saturation binding data was generated over a range of GR concentrations using the model containing **(A)** both pathways, **(B)** only the classical pathway; ligand binding to GR monomer and dimerisation of liganded GR dimers and **(C)** only the alternate pathway; ligand-independent dimerisation and ligand binding to GR dimer.

3.2 Populating model variables at equilibrium

The reactions of the GR dimerisation cycle are reversible, therefore both forward and reverse reaction rate constants need to be populated before the model can be simulated. Populating the reaction rate constants is easier at equilibrium as dissociation constants can be used instead of reaction rate constants, which are more difficult to obtain. This is owing to the fact that the position of equilibrium is not determined by the absolute values of the forward and reverse reaction rate constants but instead by their ratio, as discussed in Section 2.3.1. Therefore, in terms of populating model variables, the reverse reaction rate constant can be taken as the dissociation constant and the forward reaction rate constant can be taken as 1.

3.2.1 Ligand binding to glucocorticoid receptor monomer (k_{r1})

The dissociation constant for reaction 1, **Figure 2.8 (A)**, ligand binding to GR monomer, was determined in a system where dimerisation was eliminated, thereby isolating this reaction from the rest of the GR dimerisation cycle. GRdim represents this system and a K_d of 52.3 nM was obtained from GRdim ^{3}H-Dex saturation binding experiments found in literature[1], which was used to populate k_{r1} in the model. The literature showed that the K_d did not significantly change in response to an increase in GRdim concentration[1]; however, considering that GRdim is known to dimerise to some extent[159,162], the K_d used in the model was taken from experiments at the lowest GRdim concentration available.

3.2.2 Ligand independent dimerisation (k_{r3})

Similarly to reaction 1, the dissociation constant for reaction 3, **Figure 2.8 (C)**, unliganded GR dimerisation, was determined in a system where this reaction was isolated from the rest of the GR dimerisation cycle, by measuring dimerisation before ligand addition. Data, generated in Monkey Kidney Fibroblast-like Cells (COS-1) cells transiently transfected with both Cyan fluorescent protein (CFP)- and Yellow fluorescent protein (YFP)-tagged GRwt and measured for FRET before and after Dex stimulation, was taken from literature[1] and shown in **Table 3.1**.

The percentage of the GR molecules present as monomers and dimers was calculated (**Table 3.2**) from the concentration of monomers and heterodimers in **Table 3.1**. K_d was calculated from these and an average value of 83 nM was obtained.

Table 3.1: Ligand-independent dimerisation of three concentrations of GR before addition of Dex. COS-1 cells were transiently transfected with both CFP- and YFP-tagged GRwt and measured for FRET before and after Dex stimulation. Saturation binding, used to determine GR concentration, and FRET data were obtained from literature[1]. Equal transfection and expression of CFP- and YFP-tagged GR was assumed. Therefore, CFP-GR and YFP-GR total was calculated as 1/2 total GR. Maximum CFP-GR-YFP-GR heterodimer (CY) was calculated as $1/6^{th}$ of the total GR. CY was calculated as the ratio of FRET before and after Dex stimulation multiplied by the maximum CY concentration. CFP-GR and YFP-GR monomer concentrations were calculated as described by Robertson *et al.*[1].

	Total [GR] (nM)	**Total [CFP- or YFP-GR] (nM)**	**Maximum [CY] (nM)**	**[CY] t=0 (nM)**	**[CFP- or YFP-GR] t=0 (nM)**
Low	54	27	9.0	3.71	15.9
Medium	123	61.5	20.5	11.83	25.9
High	229	114.5	38.2	24.94	39.4

Table 3.2: Calculation of the K_d of ligand-independent dimerisation. % GR monomers was calculated by taking the ratio of CFP-GR or YFP-GR without Dex stimulation (**Table 3.1**) to the total CFP- or YFP-GR. % GR dimers was calculated from % GR monomers. GR concentration was determined by saturation binding. K_d was calculated by converting the % GR monomers and % GR dimers to concentrations and using the mass action form of the K_d formula.

	% GR monomers	**% GR dimers**	**[GR] monomer (nM)**	**[GR] dimer (nM)**	$\boldsymbol{K_d}$ **(nM)**
Low	59	41	31.8	11.1	91
Medium	42	58	51.8	35.5	75
High	34	66	78.8	74.8	83
				Average $\boldsymbol{K_d}$	83

3.2.3 Liganded receptor dimerisation and ligand binding to glucocorticoid receptor dimer (k_{r2} and k_{r4})

Obtaining the K_d for reactions 1 and 3 was made possible by the availability of a convenient means of isolating these reactions from the rest of the GR dimerisation cycle. However, this is not the case for reactions 2 and 4. Consequently, these dissociation constants were determined by fitting model-simulated saturation-binding data to experimental saturation binding data generated using COS-1 cells transiently transfected with either 40, 400 or 4000 ng GRwt-encoding plasmid DNA. There is a thermodynamic relationship between K_{d4} and K_{d2}, shown below, which relates these values by a constant, $\frac{K_{d3}}{K_{d1}}$, determined previously and therefore only a single variable needs be fitted to determine both.

$$K_{d1}^2 \cdot K_{d2} = K_{d3} \cdot K_{d4}$$

$$K_{d2} = \frac{K_{d3}}{K_{d1}^2} \cdot K_{d4}$$

Fitting of k_{r2} and k_{r4} by simultaneous regression

One of the goals of formulating the model was to use it to simulate specific binding over a range of GR concentrations, therefore binding constants were determined by fitting to data sets generated with a low, medium or high GR concentration. This was achieved by simultaneous regression of simulated saturation binding data to low, medium and high GR experimental saturation binding data sets obtained from literature[1] using the method described in Section 5.2.3. A k_{r4} of 211.5 min^{-1} and a k_{r2} of 6.4 min^{-1} was fitted and incorporated into the model.

Weighting of data points

The data sets used for fitting k_{r2} and k_{r4} were derived from multiple saturation binding experiments and the confidence in each individual data point varied. Three methods of fitting were attempted in an effort to reduce the chance of the results being detrimentally affected by error in the data. First, the distance between model-simulated saturation binding data and the average of each experimental data set was minimized without weighting. Second, the distance between model-simulated saturation binding data and the average of each experimental data set was minimized with weighting. Third, the distance between model-simulated saturation binding data and each experimental data point individually was minimized. Fitting to unweighted averages can skew the data therefore this method was discounted.

Regression on all data points individually resulted in fitted values for k_{r4} and k_{r2} that more closely simulated experimental data (**Figure 3.4**) than regression to the weighted averages of each data point, therefore these values were used further.

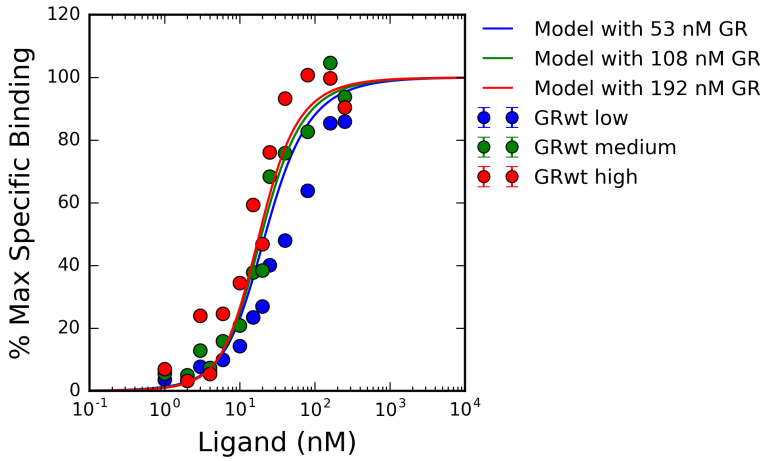

Figure 3.4: Experimental GRwt saturation binding data plotted against model-simulated saturation binding data. COS-1 cells were transiently transfected with either low, medium or high amounts of GRwt and incubated with a range of ^{3}H-Dex for 4 h. The k_{r4} and k_{r2} values of the GR dimerisation cycle model were fitted by simultaneous regression between the low (53 nM), medium (108 nM) and high (192 nM) GR experimental data and simulated saturation binding data generated with the same GR concentrations. Displayed above are the low, medium and high GR experimental data sets (blue, green and red dots respectively) and simulated saturation binding data generated at low, medium and high GR (blue, green and red lines respectively) with the best-fit values of k_{r4} and k_{r2}, 211.5 and 6.4 min^{-1} respectively. Experimental data reproduced from Robertson *et al.*[1].

3.2.4 Model comparison to experimental data

The accuracy of the model was assessed by comparing simulated saturation binding data to Hill equations fitted to experimentally generated saturation binding data. Hill equations were fitted to GRwt saturation binding data, obtained from Steven Robertson and shown in **Figure 3.5**, which produced K_ds of 42.2, 19.8 and 13.2 nM and Hill coefficients of 1.11, 1.56 and 1.64 for low, medium and high GR, respectively. These results differed slightly from their study of origin, which reported K_ds of 49.1, 23.9 and 16.8 nM and Hill coefficients of 1.08, 1.57 and 1.72 for low, medium and high GR, respectively. This discrepancy was due to fitting a single site hyperbola to the data to obtain the K_d and B_{max} before fitting Hill equations to obtain Hill coefficients

with these values as parameters, whereas in this study K_d, Hill coefficient and B_{max} were obtained from a single fit of a Hill equation. The results showed that the GR binding to Dex increases in potency, i.e. has a lower K_d, when GR concentration is increased, which is consistent with previous findings.

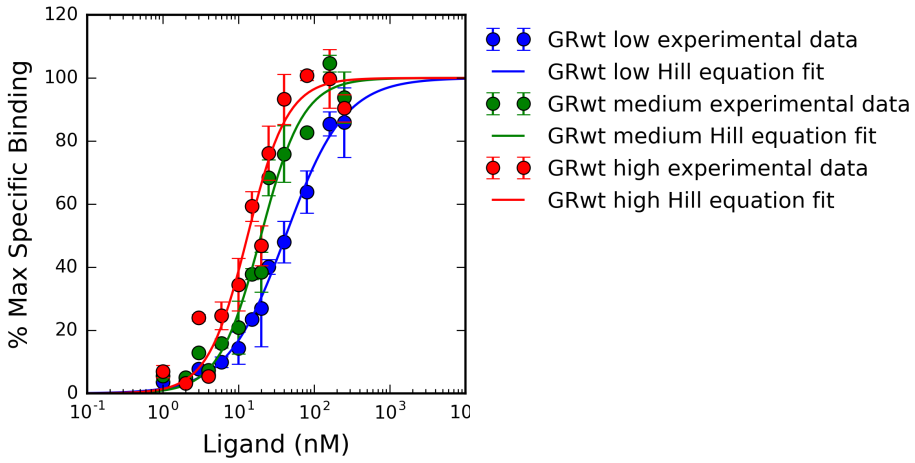

Figure 3.5: Experimental GRwt saturation binding data fitted with a Hill equation. COS-1 cells were transiently transfected with GRwt and incubated with a range of ^{3}H-Dex for 4 h. Experimental data were obtained from Robertson *et al.*[1]. Hill equations were fitted to each data set individually and plotted.

Model simulated saturation binding data was generated at low, medium and high GR, fitted with Hill equations and plotted against experimental data, shown in **Figure 3.4**. The K_ds for model-simulated saturation binding data were 22.3, 19.6 and 18.2 nM, while the Hill coefficients were 1.45, 1.57 and 1.65 for low, medium and high GR, respectively. The r^2 values for the model-simulated saturation binding data fitted to the experimental data were 0.860, 0.969 and 0.890 for low, medium and high GR, respectively. Therefore, model simulations were most accurate at medium GR concentrations and less so at low and high GR concentrations. To sum up, the model was able to replicate a shift in K_d and Hill coefficient with a change in GR concentration, while keeping the kinetic rate constants of each component reaction the same in all cases. However, the observed parameter changes were not as dramatic as those seen in the experimental data.

3.2.5 System analysis using the GR dimerisation model with populated variables

Once the model parameters had been populated, the model was used to further analyse the behavior of the GR dimerisation system. Simulated saturation binding

data was generated, as described above, over a range of GR concentrations and Hill equations were fitted at each concentration, displayed in **Figure 3.6** against experimental saturation binding data. The model-simulated saturation binding data at 5 nM and 10000 nM GR represent the theoretical limits of the model system and the results were comparable to the saturation binding data of COS-1 cells transfected with 40 and 4000 ng DNA, respectively. Model simulations at a GR range between 38 to 230 nM represent physiologically relevant levels of GR and were comparable to saturation binding data of COS-1 cells transfected with 400 ng plasmid DNA. The slope shifted to the left with an increase in GR concentration indicating that the K_d decreased and therefore ligand binding to GR became more potent. The GR concentration-dependent shift in specific binding was greater at higher ligand concentrations than at lower concentrations, resulting in a steeper slope. This indicates that the Hill coefficient increased as GR concentration increased and that the increase in specific binding in response to ligand was greater at higher GR concentrations.

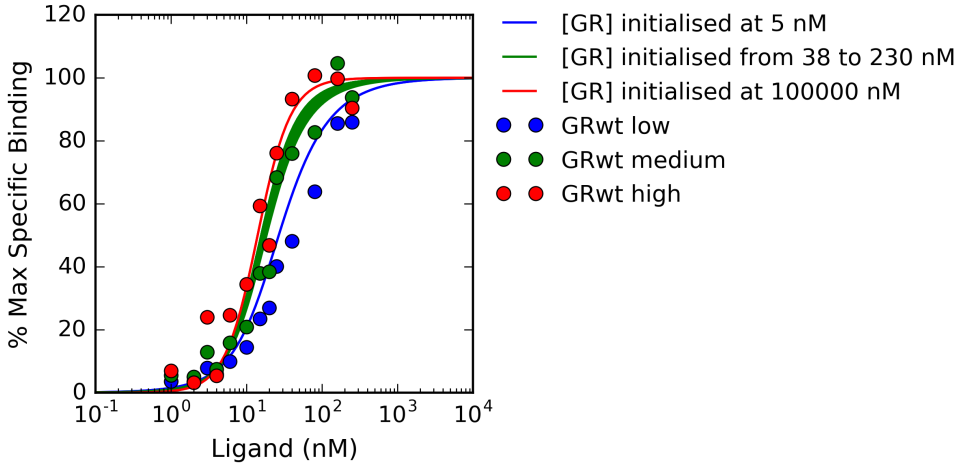

Figure 3.6: Hill equations fitted to model-simulated saturation binding data generated over range of GR concentrations. The GR dimerisation cycle model was used to simulate saturation binding experiments at GR concentrations of 5 nM (blue line), 100000 nM (the red line) and a range from 38 to 230 nM (green lines). COS-1 cells were transiently transfected with either low, medium or high (blue, green and red dots respectively) amounts of GRwt and incubated with a range of ^{3}H-Dex for 4 h. Experimental data reproduced from Robertson *et al.*[1].

Hill equations were fitted to the simulated saturation binding experiments performed in **Figure 3.6** to obtain Hill coefficients, shown in **Figure 3.7 (A)**, and the dissociation constants, shown in **Figure 3.7 (B)**, over a range of GR con-

centrations. The Hill coefficient increased from 1.35 at 34 nM to 1.65 at 249 nM and K_d decreased from 25 to 18 nM over the same range. Both these trends were non-linear, indicating that the GR concentration-dependent shifts in K_d and Hill coefficient are greater at lower GR concentrations than at higher concentrations. This simulated GR dependent shift in K_d and Hill coefficient was consistent in direction with findings in literature, however it did not mimic the magnitude of the shift found experimentally[1].

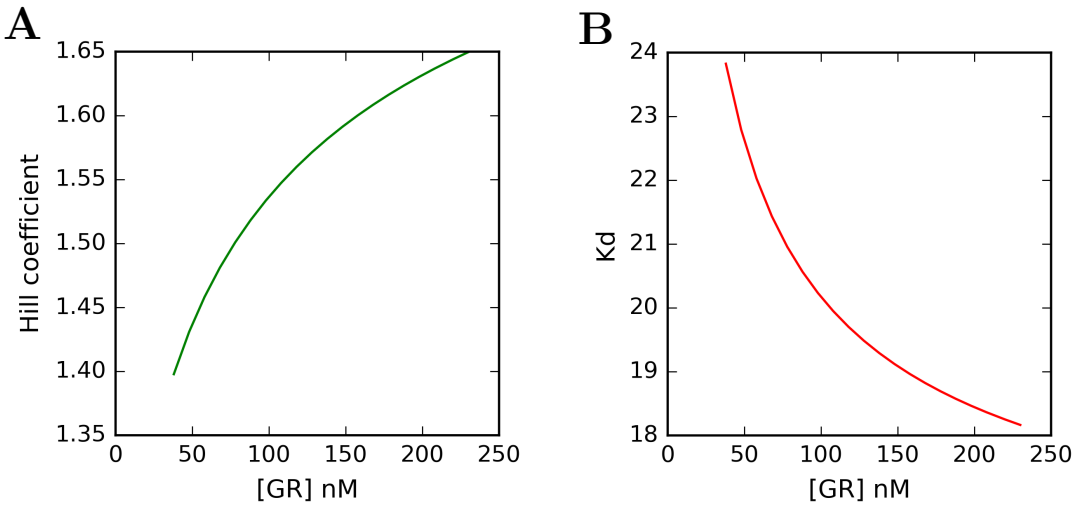

Figure 3.7: Model generated **(A)** Hill coefficients and **(B)** K_d values plotted against GR concentration. Simulated saturation binding data was generated over a range of GR concentrations and a Hill equations were fitted at each concentration.

The model was run to equilibrium without ligand with GR concentrations from 38 to 230 nM and the percentage of the GR population as unliganded GR dimers was calculated. This effectively reduced the model to only the ligand-independent dimerisation reaction and showed that the percentage of the GR population as unliganded "pre-formed" dimers increased as GR concentration increased. The same trends were observed when K_d (**Figure 3.8 (B)**) and Hill coefficients (**Figure 3.8 (A)**) were plotted against GR dimers. Ligand-independent dimerisation is likely the mechanism by which cooperativity increases as GR monomers only contain a single ligand binding site and therefore cooperativity is impossible, while GR dimers contain two ligand binding sites. The formation of ligand-independent dimers correlated linearly with an increase in Hill coefficient (**Figure 3.8 (A)**) and with a decrease in K_d (**Figure 3.8 (B)**). This was consistent with the hypothesis presented by Robertson *et al.*[1] that an increase in GR leads to an increase in ligand-independent dimers, which causes an increase in cooperativity and ligand affinity. However, con-

sidering that **Figure 3.3 (B)** showed that this shift will occur even in the absence of ligand-independent dimers, it is likely that there are additional mechanisms that cause this effect.

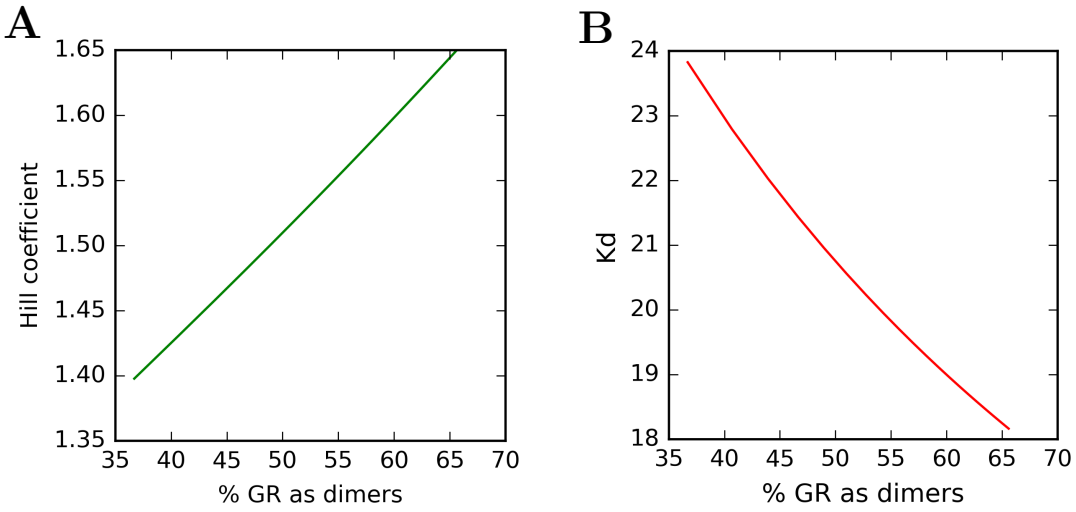

Figure 3.8: Model generated Hill coefficients **(A)** and K_d values **(B)** versus percentage total GR as dimers. The model was simulated to equilibrium without ligand over a range of GR concentrations and the % of the GR population as GR dimers was calculated. Saturation binding data was simulated using the model over a range of GR concentrations and a Hill equation was fitted from which Hill coefficients and K_d were obtained at each concentrations.

3.3 Whole cell binding time course

In order to make the model time dynamic the kinetic parameters of the model would have to be determined. To this end, whole cell binding experiments at 20 nM and 40 nM ^{3}H-Dex with COS-1 cells transiently transfected with with 40, 400 or 4000 ng of either GRwt or GRdim plasmid were conducted and used to determine the k_{on} and k_{off} values of ^{3}H-Dex-GR binding. Representative graphs of each experimental condition consisting of at least two individual experiments performed in triplicate normalized to 40 nM binding at 4 h and pooled are shown in **Figure 3.9**. With the 40 nM ^{3}H-Dex incubation, binding of ^{3}H-Dex to GR reached a plateau at approximately 90 min for GRwt and 120 min for GRdim. However, with the 20 nM ^{3}H-Dex incubation the specific binding appeared not to reach a plateau within the 4 h range of the experiment. This is shown on the graph as a lack of convergence between the 20 and 40 nM model fits despite B_{max} being shared between both lines. The model fits to the 20 nM specific bindings appear to converge to the model fits to the 40 nM

specific bindings earlier for GRwt than for GRdim indicating that dimerisation may increase the rate with which Dex binds to GR at lower ^{3}H-Dex concentrations.

Transfection with 40, 400 and 4000 ng GRwt-encoding plasmid and subsequent whole cell binding yielded K_{d}s of 8.3, 2.23 and 0.91 nM, respectively. Although these were not statistically significantly different, a trend of decreasing K_{d} with increasing GR was shown (**Figure 3.10 (A)**). This trend was not observed for GRdim, which yielded K_{d}s of 8.23 18.55 and 7.97 nM for the same transfection conditions. The k_{off} values obtained from GRwt transfected cells decreased from 0.00739 to 0.00121 and 0.00070 min^{-1} for 40, 400 and 4000 ng plasmid DNA, respectively (**Figure 3.10 (B)**). Again, this trend was not observed for GRdim transfected cells where values of 0.00454, 0.00591 and 0.00635 min^{-1} were obtained for the same quantities of plasmid DNA, respectively. No trend can be observed for k_{on} where values of 8.91×10^{5}, 5.44×10^{5} and 7.64×10^{5} M^{-1}.min^{-1} were found for GRwt, and 5.51×10^{5}, 3.19×10^{5} and 7.97×10^{5} M^{-1}.min^{-1} were found for GRdim, for 40, 400 and 4000 ng, respectively (**Figure 3.10 (C)**). Therefore, the basis for the GRwt concentration-dependent decrease in K_{d} can be found in the decrease in k_{off} rather than an increase in k_{on}. Additionally, the k_{off} values of medium and high GRwt transfections were approximately 5 and 10 times less than those of their respective GRdim conditions. This is in contrast to k_{on} where there was no discernible pattern with respect to dimerisation or GR concentration. This implicates dimerisation as a potential mechanism that increases the ability of GR to hold on to ligand in a concentration-dependent manner.

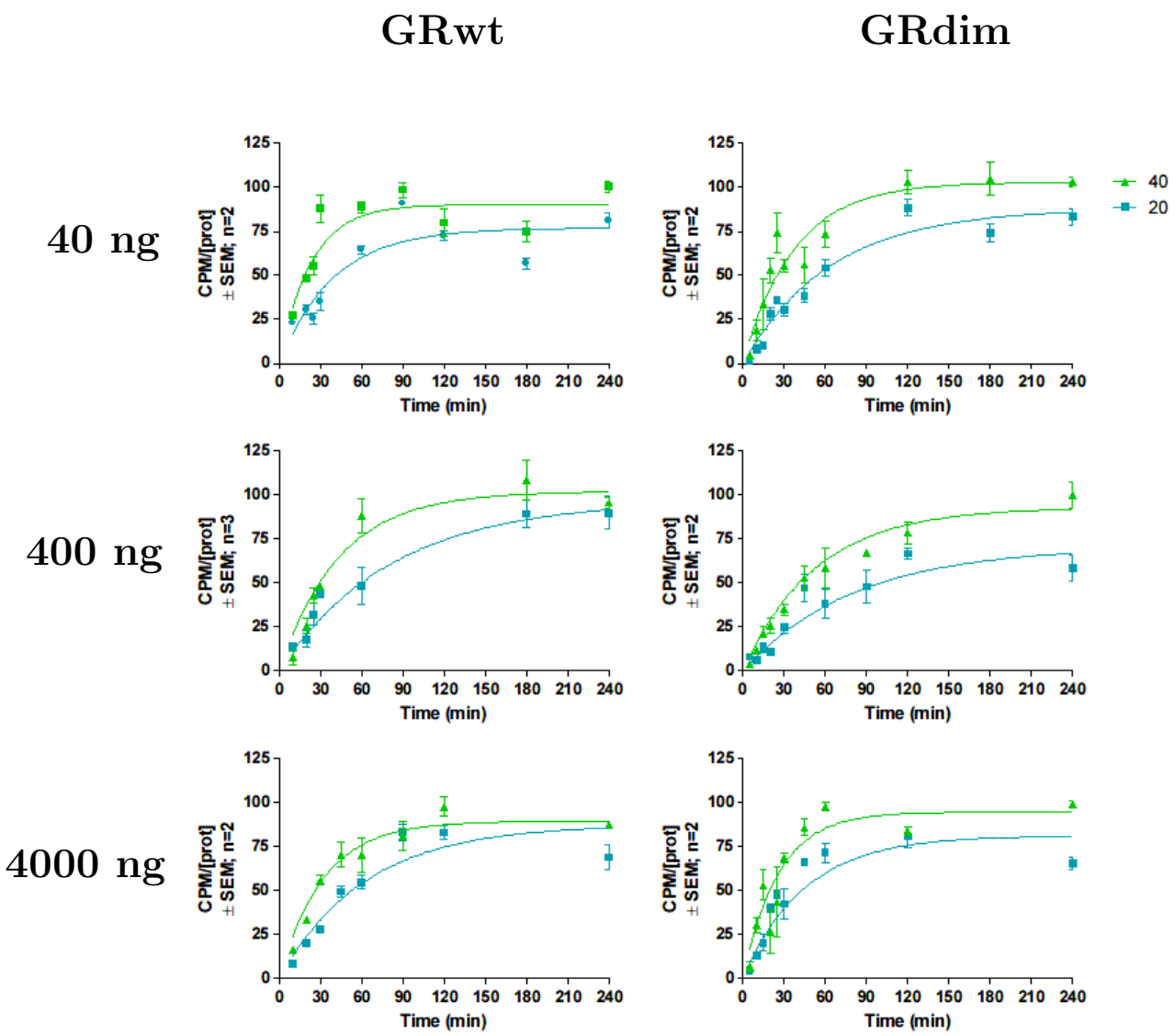

Figure 3.9: Whole cell time course binding experiments with low, medium and high GRwt and GRdim. COS-1 cells were transiently transfected with 40, 400 or 4000 ng of GRwt or GRdim plasmid DNA and incubated with either 20 or 40 nM ^{3}H-Dex for up to 4 h. Binding was determined by scintillation counting, scaled to the 40 nM 4 h time point and the data was pooled for each experimental condition. Lines represent fits of the kinetic parameter model described in Section 5.1.3 to both data sets. Results represent at least two independent experiments performed in triplicate.

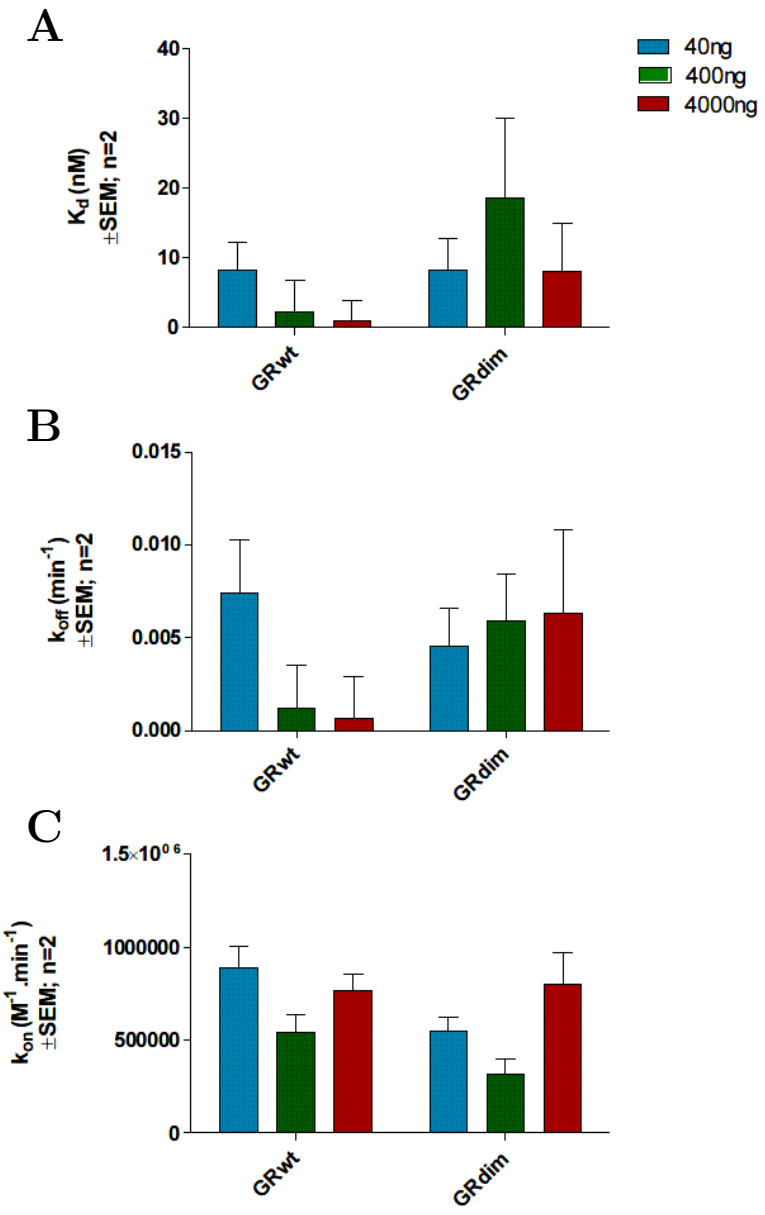

Figure 3.10: K_d, k_{off} and k_{on} values for low, medium and high GRwt and GRdim. k_{off} and k_{on} were fitted to the data shown in **Figure 3.9** using the kinetic parameter model described in Section 5.1.3 to both data sets with B_{max}, K_d, k_{on} and k_{off} shared. Unpaired t-tests were performed within each GR mutant and no statistically significant differences were found. Results represent at least two independent experiments performed in triplicate.

3.4 Transfection efficiency and distribution time course

Previous work on GR dimerisation has been based on the assumption that transfecting with a greater quantity of GR-coding plasmid would result in a higher average GR concentration per transfected cell. In order to evaluate this assumption, as well as to optimize the Fluorescence-Activated Cell Sorting (FACS)-whole cell binding experimental design, the level of GR expression in COS-1 cells transiently transfected with eGFP-GR was tested over 120 h using FACS (**Figure 3.11**).

Expression of GR increased significantly from 24 to 48 h for 40, 400 and 4000 ng transfected DNA (**Figure 3.11 (A)**). No significant differences were found between expression at 48, 72 and 96 h although there appears to be a slight decrease in expression at 96 h for all transfection conditions. There was a significant decrease in GR expression at 120 h for all transfection conditions. Additionally, increasing the quantity of transfected DNA from 40 to 400 ng caused a near two-fold increase in the proportion of the population expressing GR after 48 h. Similarly, an increase in transfected DNA to 4000 ng resulted in a near 3-fold increase over 40 ng DNA at 48 h with similar differences being observed at the other times tested. There is only a single nucleotide difference between GRwt and GRdim genes[160] and both expression plasmids in this study were based on the pEGFP-C2 plasmid and therefore their expression is expected to be comparable.

Cells were further categorized as expressing low, medium or high levels of GR. This distribution is relative to the total number of transfected cells (**Figure 3.11 (B)**). No significant differences were found in the relative proportion of the population expressing low, medium or high GR between the 40, 400 and 4000 ng DNA transfected populations at 48 or 72 h. This contradicts the analysis of previous studies[1], which showed that an increase in the quantity of transfected GR plasmid caused an increase in K_{d} and Hill coefficient and attributed this to the increase in GR concentration per cell.

The distribution relative to the whole population is shown in **Figure 3.11 (C)**. The number of cells expressing a low amount of GR increased with an increase in plasmid DNA although no statistically significant difference was found. In terms of cells expressing a medium amount of GR, the same trend was observed with statistically significant increases in cell numbers from 40 to 400 ng DNA and from 400 to 4000 ng at 48 h as well as from 40 to 400 and 4000 ng at 72 h. The trend strengthened with high GR expressing cells where highly statistically significant increases in cell numbers were found between 40 to 400 ng DNA transfected populations at 48

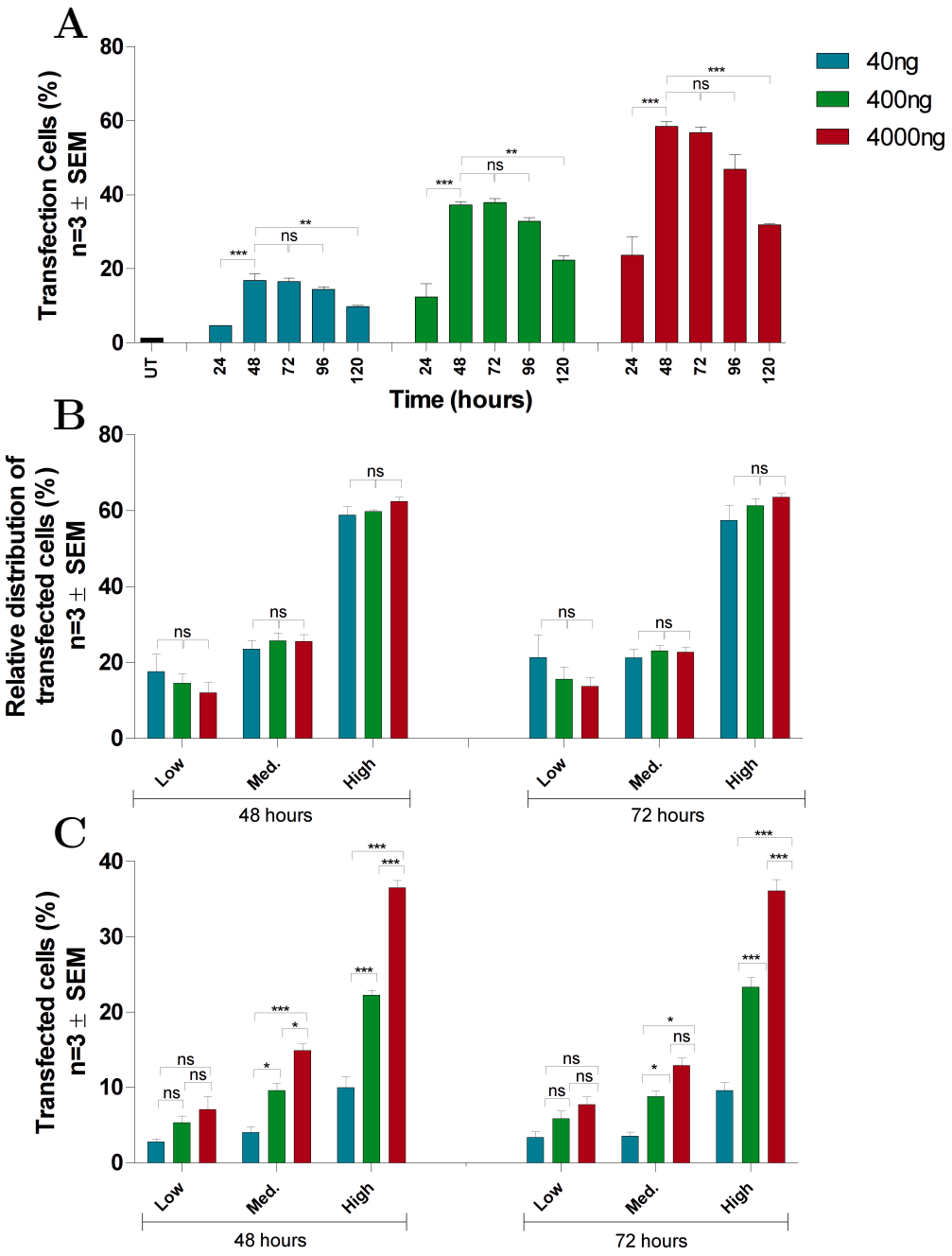

Figure 3.11: GR expression after tranfection with increasing plasmid DNA over 120 h. COS-1 cells were transiently transfected with 40, 400 or 4000 ng eGFP-GR expressing plasmid and **(A)** expression, as a proxy for transfection, of this plasmid was monitored every 24 h up to 120 h by FACS. eGFP-GR expressing cells were further characterized as either low, medium or high expressing represented as (**B**) proportional to the total amount of transfected cells and (**C**) relative to the total cell population. Results were analyzed using one-way ANOVA followed by Dunnett's multiple comparisons test. Statistically significant differences are indicated by *, **, *** for $p<0.05$, $p<0.01$ or $p<0.001$, respectively and "ns" where no statistically significant difference was found.

and 72 h. Therefore, the ratio of low, medium and highly transfected cells remained constant in response to increased plasmid DNA, while the overall percentage of the population transfected increased from 16.8% to 58.5% at 48 h. Additionally, the numbers of low, medium and high cells were maximal at 48 h and when 4000 ng GR plasmid DNA was used for transfection.

3.4.1 Cell sorting to create a homologous population

Transfection of GR plasmid resulted in a heterogeneous distribution of GR expressing cells, with cells expressing low, medium, high or no GR present simultaneously in a population (**Figure 3.11**). This presented a challenge to model simulations as the model could only simulate cells of a single GR concentration at a time. To resolve this, cells were sorted into low, medium and high GR expressing populations using FACS with the intent of generating homogeneous populations for ^{3}H-Dex whole cell binding experiments 24 h later. Harvesting a 10 cm plate of COS-1 cells transfected 48 h prior with 4000 ng plasmid DNA yielded 1.62×10^5, 1.06×10^5 4.24×10^5 cells of low, medium and high GR, respectively. However, 24 h after replating, the cells had not survived and/or adhered sufficiently to perform a whole cell binding experiment. Additionally, 24 h after sorting and replating, cells were tested for transfection distribution and it was discovered that the transfection distribution had redistributed to pre-sort levels.

3.5 Compartmental model

Generation of a homologous population of transfected cells was not possible at the time, therefore an alternate strategy was required to accurately simulate whole cell binding experiments on heterogeneously GR transfected populations. To this end, a compartmental model of the GR dimerisation cycle capable of taking into account the population distribution of transfected cells was formulated. This compartmental model was formulated using the same rate and stoichiometric equations as the original model (Section 3.1) except that it contained three GR dimerisation cycles, using the same kinetic rate constants but different GR concentrations. Therefore, the compartmental model could concurrently simulate binding in three cell populations, each with a different concentration of GR. Thereafter, this binding would be scaled to the relative proportion of the total population of each category of cells, as described in Section 5.2.4.

Compartmental model internal consistency

The compartmental model was tested for internal consistency in the same way as the original model was in Section 3.1. **Figure 3.12** shows that all reaction rates reached zero and the concentrations of all GR species reached equilibrium when the model was initiated with 20 nM ligand. Therefore, the stoichiometry of the compartmental model, similarly to the original model, does not violate the law of conservation of matter and shows that the reaction scheme is logically consistent.

Compartmental model can be reduced to the non-compartmental model

There was a possibility that the compartmental model contained additional factors not found in the non-compartmental model. To investigate this, saturation binding data was simulated using the compartmental model with 100% of cells in either the low, medium or high compartments. This resulted in r^2 values of 0.87, 0.99 and 0.93 for low, medium and high GR, respectively (**Figure 3.13**), identical to the simulated saturation binding data generated by the non-compartmental model at 53, 108 and 192 nM (**Figure 3.4**). This demonstrates that the compartmental model reduces to the non-compartmental model when 100% of the transfected cells are in a single GR transfection category.

Compartmental model-simulated shifts in K_d and Hill coefficient

The ability of the compartmental model to simulate shifts in K_d and Hill coefficient with relation to a shift in GR concentration distribution was investigated (**Figure 3.14**). To simplify the analysis, only the low and high GR compartments were used in these simulations, which was sufficient to demonstrate the proof of concept. The total GR was fixed to the number of GR molecules contained in the population when 20% of the cells are medium transfected cells and the other 80% are untransfected. Adjusting the distribution of GR so that more of the total GR is concentrated in high GR cells resulted in a decrease in K_d from 22.3 to 18.2 nM and additionally, at the minimally and maximally concentrated GR levels K_ds of 29.0 and 14.6 nM, respectively. Furthermore, the same adjustments resulted in a shift in Hill coefficient from 1.45 to 1.65 and 1.27 and 2 at the minimally and maximally concentrated levels respectively. Therefore, the K_d and Hill coefficient of a saturation binding experiment is able to shift in response to a change in the distribution of GR in a population.

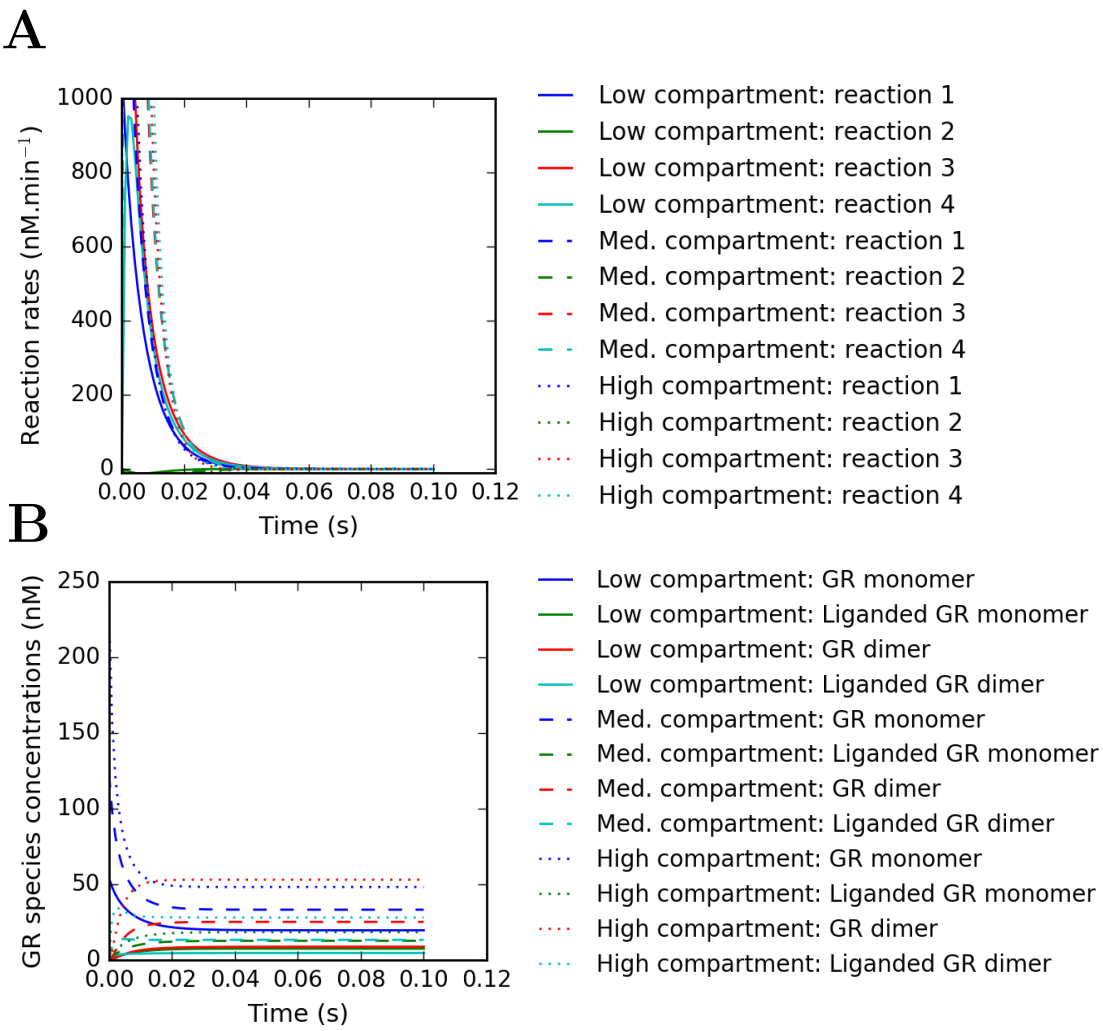

Figure 3.12: The GR dimerisation cycle compartmental mathematical model is internally consistent. The model was initiated with k_{off} values of 52.3, 6.4, 83.0 and 211.5 min^{-1} for reactions 1 to 4 respectively and their respective counterparts in the medium and high compartments, a k_{on} value of 1 nM^{-1}.min^{-1} for reactions 1 to 3 and 1 nM^{-2}.min^{-1} for reaction 4, a GR concentrations of 54, 123 and 229 nM for the three compartments, a ligand concentration of 20 nM and simulated until the concentrations of all GR species reached equilibrium and all reaction rates reached zero. **(A)** All reaction rates reach zero. **(B)** All GR species concentrations reach equilibrium. A description of the abbreviations can be found in **Appendix D**.

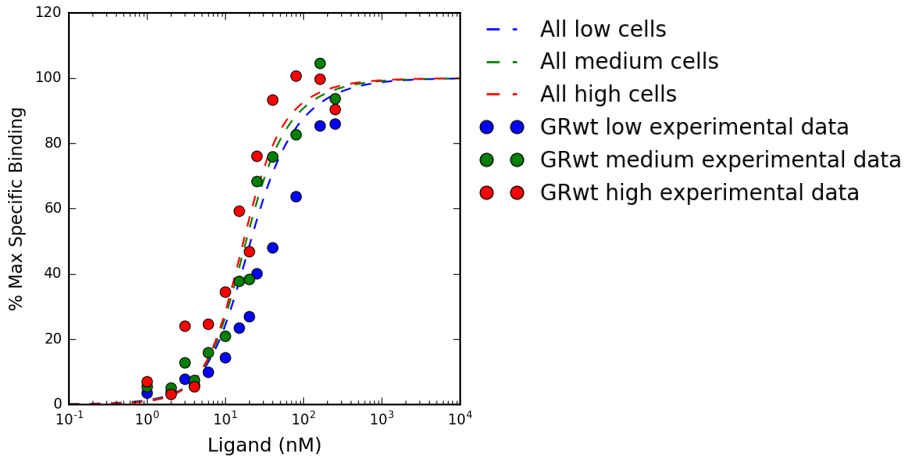

Figure 3.13: The compartmental model reduces to non-compartmental model when only a single compartment is used. Saturation binding data was simulated with 100% of the transfected cells as either low, medium or high GR cells. Experimental data reproduced from Robertson *et al.*[1].

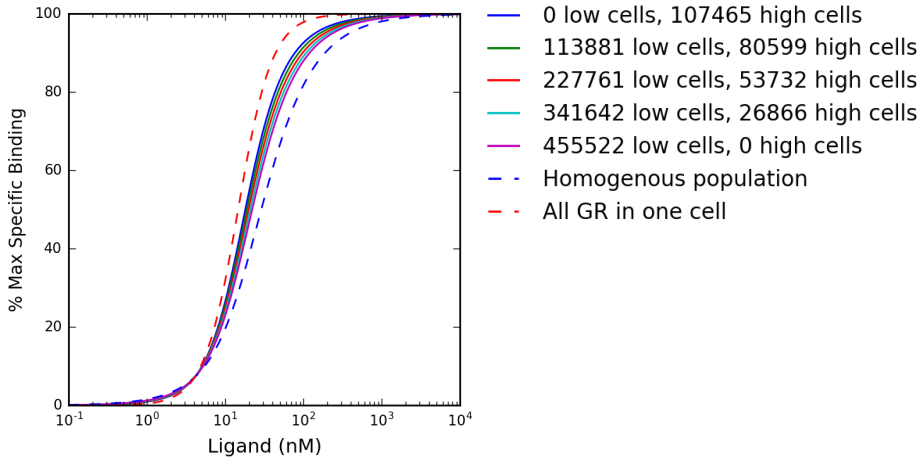

Figure 3.14: Comparison of saturation binding simulations using the compartmental model over a range of GR ratios. Saturation binding experiments were simulated using the compartmental model with different ratios of low and high GR cells. Total GR, calculated as if 20% of cell population were medium transfected cells, was kept constant and distributed into low and high GR cells, represented by solid lines. The blue dashed line represents a simulation with total GR distributed equally amongst all cells in the population. The red dashed line represents a simulation with total GR inside a single cell.

3.5.1 System analysis using the compartmental GR dimerisation model with populated variables

To analyze how the distribution of GR within a population affects ligand binding, compartmental model simulations were compared to experimental data. Saturation binding data was simulated at low, medium and high amounts of GR and with ratios of 2:1:1, 1:2:1 and 1:1:2 of low, medium and high cells (**Figure 3.15**). The total GR was calculated as if 20% of the population were either low, medium or high GR cells and the other 80% were untransfected. When generated with a low amount of GR (**Figure 3.15 (A)**) r^2 values of 0.830, 0.827 and 0.820 were obtained for the fit to low experimental data, 0.981, 0.981 and 0.979 for the fit to medium experimental data and 0.917, 0.920 and 0.926 for the fit to high GR experimental data of 2:1:1, 1:2:1 and 1:1:2 cell distributions, respectively. The shift in K_d and Hill coefficient produced by the compartmental model was not sufficient to emulate the shift in K_d and Hill coefficient observed in the experimental data in **Figure 3.5**. Moreover, the degree of the shift in saturation binding between the 2:1:1 and 1:1:2 GR distributions was not as significant as between 100% low GR cells and 100% high GR cells in **Figure 3.13**. The same goodness of fit was obtained when the simulations were performed with medium (**Figure 3.15 (B)**) and high (**Figure 3.15 (C)**) total GR. This suggests that the shift in K_d and Hill coefficient demonstrated with the non-compartmental model, shown above in Section 3.2.5, was not a function of GR concentration *per se* and instead may be due to a shift in the ratio of GR distribution.

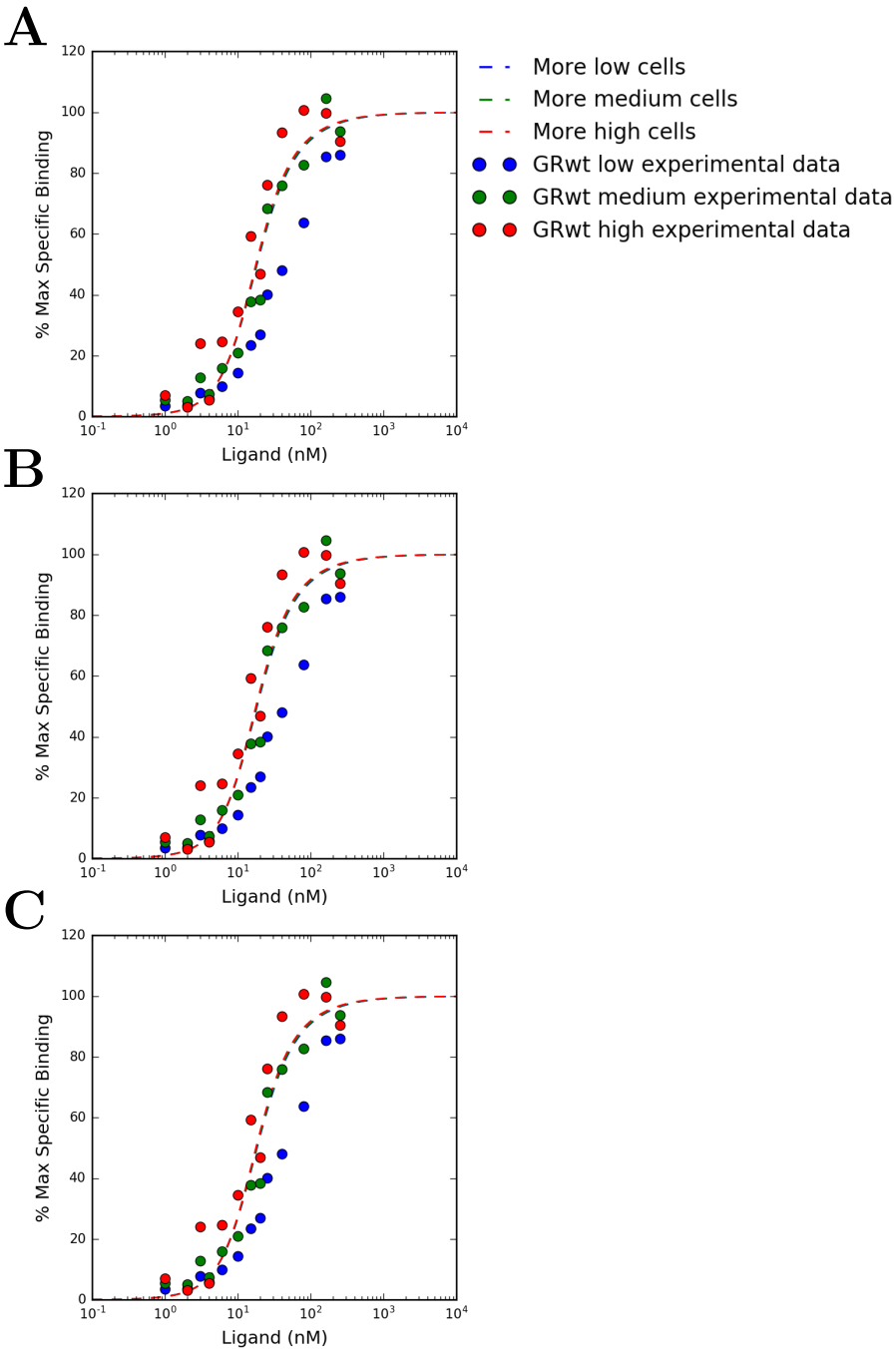

Figure 3.15: Comparison of saturation binding simulations using the compartmental model over a range of GR ratios and concentrations to experimental data. Simulated saturation binding data was generated using the compartmental model at ratios of 2:1:1, 1:2:1 and 1:1:2 of low, medium and high GR cells. Simulations were performed with total GR equivalent to 20% of the cell population possessing **(A)** low, **(B)** medium and **(C)** high GR and the other 80% untransfected. Experimental data reproduced from Robertson *et al.*[1].

Chapter 4

Discussion

4.1 Synopsis

To date, the GR dimerisation cycle (**Figure 2.8**) has not been studied by mathematical modelling and characterization of its constituent reactions with regards to Dex binding is a novel outcome of this study. While topological aspects of nuclear receptor signal transduction have been modeled before[166], the formulation of a mathematical model of the dimerisation cycle and subsequent binding simulation is unique to this project.

The K_d determined for ligand-independent dimerisation is approximately 13-fold higher than the K_d for dimerisation of liganded GR. This indicates that the binding of ligand to the GR causes a conformational change in the protein, which drastically increases the affinity of the GR molecule for homodimerisation. Ligand-independent dimerisation is distinguished from the other reactions in the GR dimerisation cycle in that it reaches equilibrium without addition of ligand. This means that, regardless of the forward and reverse reaction rates, this step of the GR activation pathway is already completed when ligand is added, possibly speeding up the rate of GR activation at higher GR concentrations. Since the kinetics of unliganded GR dimerisation could not be determined, it is difficult to comment on how the relationship between association and dissociation rates might influence the rate of GR activation.

When comparing the K_ds of reactions 1 and 4, 52.3 nM for ligand binding to GR monomer and 211.5 nM^2 for ligand binding to GR dimer, these would appear to indicate that the ligand has a 4-fold higher affinity for the monomer than the dimer. However, reaction 1 measures the affinity of a single ligand while reaction 4 measures the affinity of two ligands binding to GR subunits. Alternatively, the K_d of reaction 4 could be described as the product of two sequential ligand binding reactions, described in Section 3.1, and the 211.5 nM^2 value can be compared to 2735.3 nM^2

i.e. the product of two reactions of ligand binding to GR monomer. Therefore, the GR dimer has approximately 13-fold higher affinity for two ligand molecules than two monomers have. This implies that dimerisation induces a conformational change, which increases the affinity of the GR for ligand, whether this change occurs before ligand binding, after a single ligand binds to the GR dimer or a combination of these two is unclear.

Similar shifts in K_d and Hill coefficient are seen when GR concentration is increased (**Figure 3.6**) as when the ratio of high to low GR cells is increased (**Figure 3.14**). When concurrently increasing the total GR and the ratio of high to low GR cells the expected outcome was that these effects would combine to give a greater shift in K_d and Hill coefficient than either individually. However, **Figure 3.15** shows that when simulations are run using the compartmental model with these two factors adjusted together; no shift in K_d or Hill coefficient is found when total GR is adjusted. Considering that all results are normalized to the total GR in the population, this further implicates cellular GR concentration and not overall population GR concentration as the causative factor of the shifts in K_d and Hill coefficient.

4.1.1 Concentration-dependent shifts in K_d and Hill coefficient are inherent to dimerisation reactions

The alternate pathway of GR activation has been proposed as the mechanism by which the concentration-dependent effects of GR on K_d and Hill coefficient are actuated[1]. However, **Figure 3.3 (B)** shows that even in the absence of ligand-independent dimers, K_d decreases and the Hill coefficient increases with GR concentration. The concentration-dependent effects of GR are present in both pathways of GR activation and therefore are not specific to ligand-independent dimerisation. Moreover, experiments in this study (**Figure 3.10**) as well as in literature[1] using the GRdim mutant, that is to say with dimerisation eliminated, showed that potency and cooperativity did not increase with an increase in total GR. Therefore, ligand binding to GR monomer is not sufficient to produce a GR concentration-dependent shift in K_d and Hill coefficient. Considering that the classical pathway displays this shift (**Figure 3.3 (B)**) and that it is not dependent on ligand binding to GR monomer, the shift is most likely a factor of the GR dimerisation. Unfortunately, this cannot be confirmed experimentally as no experimental system is available in which the classical and alternate pathways are isolated.

Running the model to equilibrium over a range of GR concentrations and without

ligand showed that the relative amount of the total GR as dimers increased and monomers decreased as the GR concentration increased. The numbers of monomeric GR molecules can be calculated by using the formula for K_{d} and the breakdown of the GR population, as shown below:

$$K_{\mathrm{d}} = \frac{[GR_{\mathrm{monomer}}]^2}{[GR_{\mathrm{dimer}}]}$$

$$[GR_{\mathrm{total}}] = [GR_{\mathrm{monomer}}] + 2[GR_{\mathrm{dimer}}]$$

$$[GR_{\mathrm{monomer}}] = \frac{-K_{\mathrm{d}} \pm \sqrt{K_{\mathrm{d}} + 8K_{\mathrm{d}}[GR_{\mathrm{total}}]}}{4}$$

Using this, the proportion of the total GR in the population as monomers and dimers in a GR population were calculated for GR from 10 nM to 100 μM, shown in **Figure 4.1**. The percentage of GR in the population as dimers is under 10% at 10 nM GR and over 95% percentage at 100 μM GR. The K_{d} was constant at all GR concentrations and the proportion of the total GR population as dimers increased with GR concentration. Therefore, the number of pre-formed GR dimers increases disproportionately to the number of GR monomers in the cell as the total number of GRs are increased. The correlation between percentage of the GR population as dimers and total GR concentration has been experimentally shown by Bledsoe *et al.*[116]. However, Bledsoe showed this relationship with Dex-bound GR LBD and obtained a K_{d} of 1.5 μM, indicating that while the LBD is able to form dimers, the rest of the GR protein increases GR-Dex affinity by at least 1000-fold. This non-linear relationship between GR concentration and percentage GR dimers is rooted in the conversion of two GR monomers to a single dimer molecule. Therefore, the shift in proportion of the population that forms ligand-independent dimers is a property of dimerisation reactions in general and not specific to the GR.

Macromolecular reactions are depicted in a way that is a convenient compromise between level of detail and ease of use. These reactions may involve any number of conversions, sometimes atomic or larger, each with their own thermodynamic properties but which are not consequential enough to warrant inclusion in the most common model. Accordingly, many of these minor reactions are omitted from the models used to described these interactions. When reactions are omitted, their thermodynamic properties are absorbed into the apparent dissociation constant of the entire pathway. Therefore, if a constituent reaction has been overlooked or is unknown, the equation used to describe a reaction may be inaccurate. Expressing

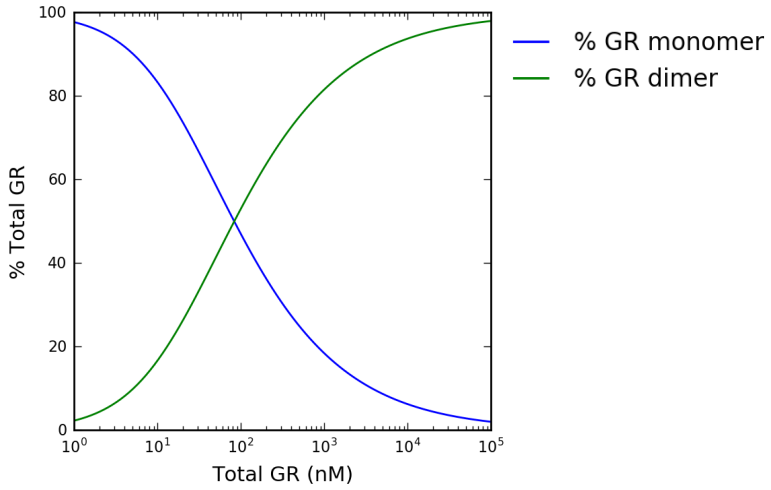

Figure 4.1: Percentage of ligand-independent dimers compared to total GR concentration. The percentage of the total GR population as GR monomers and dimers were calculated from 1 to 100000 nM GR with the K_d for dimerisation kept constant at 83 nM.

the binding of Dex, other ligands, to GR as a single reaction as:

$$2L + 2R \rightleftharpoons (RL)_2$$

does not contain sufficient detail to accurately describe the relationship between fractional occupancy of the GR and GR concentration when GR concentration is varied too far from the experimental data used to populate the model. Instead, expressing this reaction as the entire dimerisation cycle is necessary to capture enough detail for binding in this system to be accurately predicted. The decrease in K_d and increase in Hill coefficient with an increase in GR concentration is likely embedded in the thermodynamics of the overlooked dimerisation reactions of GR-Dex binding.

4.1.2 Concentration-dependent decrease in K_d is a function of a decrease in k_{off}

The GR concentration-dependent shift in K_d of GR-Dex binding found by Robertson *et al.*[1] was replicated in this study, albeit with a different range of K_d values. However, the question remained: is this shift as a result of an increased rate of ligand binding to GR at higher concentrations or as a result of a reduction in the rate of ligand dissociation? The results of this study show that the trend of k_{on} of GR-Dex binding is not influenced by GR concentration and that the k_{off} decreases as GR concentration increases (**Figure 3.10**). Furthermore, the k_{on} trend is preserved, while

the k_{off} is not, when dimerisation is abrogated with the GRdim mutant. Therefore, the GR concentration-dependent decrease in K_d is a function of a decrease in k_{off}.

Having established a correlation between dimerisation and residence time, we can now speculate about the exact mechanism by which k_{off} is decreased by an increase is GR concentration. Dissociation of a ligand requires a physical path out of the ligand binding pocket. This path could be occluded by the other GR molecule in the dimer, or by disruption of co-factors as found in other studies[116], greatly reducing the likelihood of ligand escaping the binding pocket. Therefore, the rate of ligand dissociation from the GR might decrease, which protects the ligand from degradation. However, if dimerisation *per se* caused occlusion of the ligand binding pocket, this would reduce the ability of ligand to bind to ligand-independent GR dimers. In this case, the conformation selection model[141] predicts that the unliganded GR dimers exists as a number of isoforms with a continuum of ligand binding affinity. Alternatively, following the induced fit model of ligand binding[142,143], dimerisation could cause the receptor to undergo an isomerisation reaction where the conformation of the complementarity network in the ligand binding pocket adjusts in such a way that the affinity for the ligand increases. In particular, helices 1, 3 and 5 of the ligand binding pocket, amongst other protein structures, are involved in the dimerisation interface, which alters their conformation around the bound ligand[116]. This would explain why the classical model of GR-ligand binding also shows a shift in K_d and Hill coefficient despite cooperativity being precluded by the lack of multiple ligand binding sites at the moment of ligand binding. The shift in percentage of the population towards GR dimers, shown in **Figure 4.1**, as an increase in GR would lead to a greater number of molecules in the higher affinity state and therefore the population would have a lower rate of dissociation.

4.1.3 Increasing transfection plasmid DNA does not cause increase in protein concentration per transfected cell

The dynamics of transient transfection are likely an overlooked but subtly consequential factor in many studies. The effect of increasing GR plasmid concentration on gene transcription has been studied in the past[181] with regards to titration and squelching effects. However, the analysis was based on the flawed assumption that increased plasmid DNA increases the GR concentration per transfected cell. In our study, expression of a transiently transfected plasmid took 48 h to reach a plateau and lasted up until 96 h (**Figure 3.11**), which is consistent with transient transfection convention. This may be attributed primarily to cells eliminating plasmid

DNA, as well as the influence of mitosis, which dilutes both plasmid concentration per cell as well as the protein level. In this way, the highly transfected cells may become the medium and lowly transfected cells of the next generation.

What is not well understood is how the distribution of protein expression changes with regard to quantity of transfected DNA. When the quantity of plasmid DNA was increased, the absolute number of cells expressing low, medium and high amounts of GR increased, which is to be expected as the greater quantity of plasmid molecules increases the probability of an individual cell being transfected. However, the relative proportion of the transfected cell population expressing low, medium or high amounts of GR remained constant regardless of the amount of plasmid DNA in the transfection. Therefore, the ratio of low, medium and highly transfected cells remained constant in response to increased plasmid DNA, while the overall percentage of the population transfected increased (**Figure 3.11**). Since the saturation binding studies in Robertson *et al.* and the model simulations in this study are normalized to the total receptor concentration, increasing the number of transfected cells in proportion to the total GR in the population should not affect shape of the saturation binding curves. This appears to undermine the assumptions of this and other studies[1] in that the average concentration of GR in transfected COS-1 cells does not appear to increase with an increase in plasmid quantity.

4.2 Critique

As with any research project, a number of the results and methodologies are susceptible to further refinement. The characterization of reactions 2 to 4 of the GR dimerisation cycle has, the best of our knowledge, not been attempted by other researchers and, as a result, the K_d values determined in this study cannot be compared to the literature. The GR dimerisation model is capable of replicating GR concentration-dependent shifts in K_d and Hill coefficient of Dex binding; however, the replicated shifts do not fully match the magnitude of the shift found in the experimental data. This discrepancy could be the result of various factors. This study is particularly vulnerable to inaccuracies in the K_ds of reactions 1 and 3 because fitting of reactions 2 and 4 made use of these values. Another possibility is that there could be a critical aspect of the GR-ligand model which has not been included. Additionally, unliganded GR has been shown to have a number of cellular effects[1,182–186] and it is conceivable that these cellular effects may influence the Dex-GR binding and to a greater extent at higher GR levels. Finally, inaccuracies of the experimental data set cannot be ruled out. Although there is much to be gained by

resolving this discrepancy, it does not diminish the qualitative analysis of the GR dimerisation cycle made using the model.

The binding experiments performed in Robertson *et al.*[1] were reported at 20% transfection efficiency for 40, 400 and 4000 ng GR plasmid DNA transfection. Personal communication with the authors revealed that transfection efficiency was determined by fluorescent microscopy, a less accurate method compared to the FACS method used in this study. In the Robertson study, it was assumed that the same proportion of the population was susceptible to transfection and that these cells were simply transfected with a greater number of plasmid, and therefore contained more GR per transfected cell. Consequently, the authors calculated the GR concentration per transfected cell as 5× the GR concentration in the entire population, which was determined by saturation binding. This assumption does not fit the findings in **Figure 3.11**, which shows that transfection efficiency increased from 16.8% to 58.5% at 48 h as DNA quantity increased from 40 to 4000 ng.

The K_d of ligand binding to monomeric GR was determined using the GRdim mutant, where it was assumed that dimerisation was completely abrogated. However, as mentioned in Section 2.2.4, evidence is emerging that GRdim does form dimers to some extent. The abrogation of trans-activation only implies that conventional, trans-activating dimers are not formed but does not preclude the formation of non-conventional dimers, which likely have impaired DNA binding capability. The formation of non-conventional dimers is substantiated in a protein association study by Presman *et al.*[162], which shows that the GRdim mutant does dimerise to a similar degree as GRwt. In the context of the current study, the ability of GRdim to dimerise confounds determination of the K_d for reaction 1. Following the hypothesis above, namely that the shift in K_d and Hill coefficient is an inherent property of dimerisation, any formation of dimers would lower the K_d determined for reaction 1. Therefore, the K_d determined in this project is likely lower than the actual value for this reaction.

Both the ligand and DNA binding domains of the GRwt have sequences that are involved in dimerisation[116,187,188]. The source of GRdim's dimerisation deficient properties is a point mutation in the D-loop of the DNA binding domain at A458T[160] and it is hypothesized that the residual dimerisation is a result of the dimerisation sequences in the ligand binding domain. In contrast to this, GRmon contains mutations in both the ligand and DNA binding domains and was shown to be completely dimerisation deficient[162]. Being relatively new, GRmon has not been characterized as well as GRdim, particularly with regard to ligand binding properties, which, when considering GRmon's mutation in the ligand binding do-

main, could differ from those of GRdim and GRwt. Currently, the GRmon mutant is only available for the mouse GR; however, considering the similarities between mouse and human GR, they likely possess similar binding properties. Overall, this GRmon mutant is likely a more accurate representation of dimerisation deficiency than GRdim and populating reaction 1 of the GR dimerisation cycle model with the K_d for Dex binding to GRmon could improve simulation accuracy.

The determination of K_d for ligand-independent dimerisation of GR required an analysis of previously published FRET data[1]. The FRET data was generated using single cell microscopy and, as with any single cell measurement, the data may be distorted when population characteristics, such as the average COS-1 cell volume and protein concentration, are applied. In terms of this study, the GR concentration from Robertson *et al.*[1] was used to calculate the K_d of ligand-independent dimerisation. If the transfection efficiencies were higher than the reported value, which is likely considering that transfection efficiency was 58.5% at 48 h for 4000 ng plasmid DNA transfection, then GR concentration would be lower than assumed and, consequently, the K_d of reaction 3 would be lower. Similarly, if the transfection efficiency were lower than the reported value, the K_d would be higher as GR concentration would be higher than assumed. This affects the model both directly, as a change in K_d of reaction 3, as well as indirectly through the fitting of the K_ds of reactions 2 and 4, which depends on the ratio of the K_ds of reactions 1 and 3. Considering the potential for introduction of error when working with single cells and average population characteristics, the similarity of the calculated K_d for the low, medium and high GR concentrations is remarkable with a spread of only 10 nM. This suggests that the large number of well carried out FRET experiments provided a large enough data set to overcome the potential error inherent to FRET experiments.

The fitting of k_{off} of reactions 2 and 4 was particularly susceptible to the accuracy of the experimental data. The K_d reported for GR-Dex binding of the experimental data set used throughout this study[1] was 49.1, 23.9 and 16.8 nM for low, medium and high GR, respectively; however, the average K_d for GR-Dex binding reported in the literature is 6 nM. Following the hypothesis that increasing GR concentration causes an increase in potency, the relatively high K_d values reported for this data may indicate that the GR concentrations used in that study were significantly lower than expected.

The transfection of GR into COS-1 cells in this study produced a heterogeneously distributed GR protein expression within the transfected population. For this reason, cell sorting was attempted; however, despite the efforts to counter the deleterious effects of sorting on cell health and viability, the homogeneous cell pop-

ulations did not survive long enough to perform a whole cell binding experiment. Cell sorting is usually performed in microscopy studies where the cells can be viewed immediately after sorting and cell survival is not a concern. Had the cell sorting been successful, the accuracy of all data determined from population studies would have been improved. This includes the saturation binding experiments from which the K_d for ligand binding to GR monomer (reaction 1) was determined in addition to the K_d values determined for reactions 2 and 4, which were fitted to saturation binding data produced with a heterogeneous population.

In order to improve cell survival, the FACS method could be modified in the following two ways. Firstly, the nozzle size could be increased from 70 to 100 μm as this would reduce the physical strain on the cells as they are sorted[189]. Unfortunately a 100 μm nozzle was not available at the time of this study. Secondly, the sheath fluid could be replaced with supplemented Dulbecco's modified Eagle's medium (DMEM) as the sheath fluid was deemed to be toxic and is added to the sorted suspension mixture as each cell is sorted. However, this could potentially lead to future contamination of the sorting apparatus.

There was a large amount of error in k_{on} and k_{off} values determined from the whole cell binding time course (**Figure 3.10**). It is possible that this method is not optimized for determination of kinetic parameters for highly potent binding reactions, such as steroid-steroid receptor bindings. For example, the binding with the 40 nM incubation saturated after 1 h, which may have caused an inaccurate fit of the k_{on} and k_{off} values. Incubations over longer periods of time, i.e. at lower concentrations of Dex, will produce a longer saturation binding curve, which may improve the accuracy of the binding model. Finally, the popularity of the DEAE-dextran transfection method has fallen since the advent of viral vectors. DEAE*, choloroquin† and DMSO‡ have significant toxicity which can result in aberrant experimental results.

4.3 Context

The findings of this study show that the GR ligand binding system is more sensitive to changes in GR concentration than previously anticipated.

*http://www.sciencelab.com/msds.php?msdsId=9923344
†http://www.sciencelab.com/msds.php?msdsId=9923444
‡http://www.sciencelab.com/msds.php?msdsId=9927347

4.3.1 Medical applications

The sensitivity of the GC signal transduction system to GR concentration has implications in the development of GC resistance, a major concern for chronic GC users[190]. A primary mechanism of GC resistance is the downregulation of the GR[188,191], which following the findings in this study, will reduce the effects of GCs both by reducing the number of receptors and by reducing the efficiency with which ligand binds to the receptor. The inverse is true of conditions that upregulate GR; the effects of GCs will increase disproportionately to the concentration of GR.

GCs are often administered therapeutically and residence time or $t_{1/2}$ is an important consideration for therapeutic regimes. Binding of the GC to the GR and subsequent dimerisation of the GR complex increases residence times and thereby reduces the dissociation rate of GCs and protects them from degradation, inadvertently increasing drug potency. Therefore, systems with a higher GR concentration will not only be activated by GCs at lower concentrations, they will be active for longer periods of time. In this way, in addition to activating palindromic GREs, dimerisation is responsible for increasing the length of time the ligand remains bound to GR and thereby increases the activity of ligands. From this it can be concluded that GR concentration influences ligand activity not only as a substrate but also as a mechanism by which ligand removal is mitigated. In the process of optimizing of drug residence time, a similar susceptibility of the K_{d} to alteration by manipulation of k_{off} has been found by other researchers[137–139]. The findings in this study have significant implications for therapeutic regimes both with regard to drug residence time as well as to tissues and individuals with different levels of GR.

4.3.2 Research implications

This model should be eminently useful for research aimed at exploring the concentration-dependent effects of GR on GC activity. Measuring the concentration of the different GR species in the GR dimerisation cycle is not always feasible as it requires protein interaction methods such as FRET or Numbers and Brightness. However, total GR concentration can be quantified with relative ease with ^{3}H-Dex competitive binding assays or quantitative Western blot to mention a few methods.

Although the concentration-dependent effects of GR have primarily been shown with Dex, it is likely this this effect is present with other, less potent glucocorticoids as well as in other steroid receptor systems. The K_{d} for ligand-independent dimerisation of GR is particularly useful in that, unlike the other dissociation constants, it is not specific for Dex and could be used in a GR dimerisation model for any agonist.

Considering the similarities in activation mechanisms between steroid receptors, it is likely that a similar analysis to the one in the current project could yield novel findings in other steroid receptor research fields.

4.3.3 Future studies

Currently, the model simulates GR-Dex binding at equilibrium and, while analysis at equilibrium has yielded significant insights, the utility of the model would be greatly improved by upgrading it to be time dependent. In order to achieve this, the k_{on} and k_{off} values of each reaction of the GR dimerisation cycle would have to be determined. This could be accomplished in a similar manner as the parameters of the equilibrium model were determined. The k_{on} and k_{off} values of at least two reactions would have to be determined experimentally and the remaining values could be fitted to the whole cell binding data in **Figure 3.9**.

Ideally, the model would be expanded to include the ancillary pathways of GR activation and GC signal transduction. These would include modelling intracellular dynamic distributions of GR with regard to ligand concentration, GR up- and down-regulation as well as ligand removal. Modelling DNA binding of GR is crucial not only for predicting transcriptional activation but also for simulating stability of the GR-ligand complex. GR tetramers have been detected by Presman *et al.*[179], which challenges the paradigm of GR dimers being the end product of ligand binding and, with a few additions, it is not difficult to conceive of modelling the GR oligomerization cycle. Additionally, the GR dimerisation cycle is not specific to Dex and could be extended to include other GCs. Furthermore, to truly model GC transcriptional activity *in vivo*, the heterogeneity of GR distribution within tissues would have to be defined. It is unclear whether this heterogeneity is found in the distribution of proteins between the cells of a tissue *in vivo* and, as concentration can affect binding in a non-linear way, should be investigated. Finally, from a molecular biologist's point of view, the ultimate goal of this project would be to model GR transcriptional outcomes from total GR and ligand concentrations.

4.4 Conclusion

The current project comprised a novel approach of simulating GR-GC binding, which is considered a requisite step of GR activation. A major outcome was the formulation of a mathematical model of the GR dimerisation and Dex binding cycle. Significantly, this model captured the GR concentration-dependent shifts in K_d and Hill coefficient when simulating GR-Dex saturation binding experiments, albeit not

to the same extent as experimental data from literature[1]. Therefore, the decrease in K_d and increase in Hill coefficient with an increase in GR concentration found by Robertson et al.[1] was confirmed in our model. Moreover, this effect was determined to be the result of the dimerisation reaction in the GR activation pathway. Furthermore, this model is capable of simultaneously predicting GR-GC binding in cells of different GR concentrations. Using a method developed in this study, the specific binding of a population of cells can be scaled to relative distribution of GR within that cell population.

The kinetic basis for the decrease in K_d for Dex-GR binding was determined as a concentration-dependent decrease in k_{off}, as k_{on} remained nearly constant with a change in GR concentration. This decrease in k_{off} is eliminated when dimerisation is abrogated and therefore the concentration-dependent shift in K_d is attributed to the dimerisation reactions present in both the classical and alternate pathways of GR activation.

The findings demonstrate that GC-GR binding is more sensitive to GR concentration than has been previously anticipated. Considering the similarities in activation mechanisms between steroids and steroid receptors, it is likely that a similar analysis to the one in this project could yield novel findings in other steroid receptor research fields. This has implications for GC signal transduction research, steroid research in general as well as for therapeutic regimes and GR resistance development.

Chapter 5

Methods and materials

5.1 Experimental methods and materials

Plastic-ware was obtained from reputable suppliers of laboratory equipment such of WhiteSci, Lasec, The Scientific Group and Biocom.

5.1.1 Cell culture

COS-1 cells were obtained from American Type Culture Collection and were cultured in DMEM containing 44 mM sodium bicarbonate and 1 mM sodium pyruvate purchased from Sigma-Aldrich (St. Louis, Missouri, United States). In addition, supplemented DMEM contained 10% Fetal Bovine Serum (FBS), 100 IU/ml of penicillin, 100 μg/ml of streptomycin purchased from Merck (Darmstadt, Germany). Cultures used ranged from passage 6 to 35.

5.1.2 Plasmids

The human GRwt plasmid, pEGFP-C2-hGRwt, was provided by S. Okret (Karolinska Institute, Sweden). Human GRdim plasmid, pEGFP-C2-hGRdim, was produced by Steven Robertson (Stellenbosch University, South Africa) by replacing the wild type GR in pEGFP-C2-hGRwt with dimerisation deficient GRdim. The empty vector, PGL2-Basic, was obtained from Promega. Plasmids were harvested using the NucleoBond®Xtra Maxi plasmid extraction kit as per manufacturers instructions. Plasmid identity was confirmed by restriction enzyme digest with *Sal*1 for pEGFP-C2-hGRwt and pEGFP-C2-hGRdim from Thermo Fischer and *Bam*H1 for PGL2-Basic from Fermentas.

5.1.3 ^{3}H-Dexamethasone whole cell binding

COS-1 cells, transfected 24 h prior, as described below, with 40, 400 or 4000 ng of either pEGFP-C2-hGRwt or pEGFP-C2-hGRdim, were plated into 24 well plates at a density of 0.5×10^5 cells/well 24 h prior to steroid incubation. On the day of incubation, plasmid expression and distribution was tested by means of FACS, as described below. After expression confirmation, cells were washed three times with Phosphate Buffered Saline (PBS) and subsequently incubated with 250 μl DMEM containing either 20 or 40 nM tritiated Dexamethasone (^{3}H-Dex) (PerkinElmer SA (Pty) Ltd), stock specific activity ranging from 71 to 78 Ci/mmol, for up to 4 h. Non-specific binding was determined by concomitant incubation of 10 μM Dex with either of the aforementioned concentrations of ^{3}H-Dex at each time point. The incubation was concluded by aspiration and cells were subsequently washed with 0.2% Bovine Serum Albumin (BSA) in PBS at 4°C three times for 15 min. Thereafter, the cells were lysed with 100 μl passive lysis buffer (0.2% (v/v) Triton, 10% (v/v) glycerol, 2.8% (v/v) TRIS-phosphate-EDTA and 1.44 mM EDTA) and stored at -20°C until scintillation counting. Scintillation counting was performed as described below and counts were normalised to protein concentration determined using the Bradford method[192].

Transfection

The DEAE-dextran transfection method[193] was used in this study. COS-1 cells were plated in 10 cm plates at 10^6 cells/plate 24 h before transfection. Cells were incubated in a transfection mixture containing DMEM with 1% diethylaminoethyl (DEAE) (Sigma-Aldrich), 0.1% chloroquinone and 4000 ng total plasmid DNA for 4 h. Different levels of GR expression were induced by adding either 40, 400 or 4000 ng of pEGFP-C2-hGRwt or pEGFP-C2-hGRdim. Total plasmid DNA was kept constant at 4000 ng by adding the non-expressing plasmid, PGL2-Basic, to compensate for the different quantities of expression plasmid DNA. Following the 4 h incubation, the transfection mixture was replaced and the cells were incubated in 5 ml 10% dimethyl sulfoxide (DMSO) (Sigma-Aldrich) PBS for 5 min. Thereafter, the DMSO was replaced with supplemented DMEM.

Transfection efficiency

Transfection efficiency was tested using the BD FACSAria system by making use of the prosthetic eGFP of the GRwt and GRdim proteins. 24 h after transfection, 2×10^5 cells/well were plated into a 6 well plate and 24 h later were harvested for

flow cytometry. Fluorescein isothiocyanate (FITC) BD-Calibrite 3 beads (BD Biosciences, San Jose) were used as an internal standard. Transfected cells were determined as those with a FITC-A value of over $10^{2.5}$ using a 488 nm laser. Transfected cells were further categorized as low transfected, with a FITC-A range $10^{2.5}$ to $10^{3.3}$, moderately transfected, with a FITC-A range $10^{3.3}$ to $10^{4.2}$, or highly transfected, with a FITC-A range $10^{4.2}$ or higher. An example of this is given in **Appendix E**.

Scintillation counting

Liquid scintillation counting was used to measure the amount of ^{3}H-Dex bound to GR in the cell lysate. Scintillation was measured using a Tri-Carb 2810TR (PerkinElmer) in Pony vials (PerkinElmer). The scintillation mixture contained 80 μl of cell lysate and 1 ml of FLO Scint II scintillation fluid (PerkinElmer). Ligand depletion was calculated using a control counted with 5 μl of 20 or 40 nM ^{3}H-Dex and was always <5%.

Protein determination

Protein concentration of each sample was determined by the Bradford method of protein determination[192] using a Powerwave 340 Biotek to measure absorbance at 595 nM. The sample solution contained 5 μl cell lysate and 200 μl Bradford reagent and was incubated for 30 min before absorbance was determined. Protein concentration was calculated by comparing samples to a BSA standard curve, BSA concentration ranging from 0 to 2 mg/ml, after normalisation to a blank sample.

Determination of kinetic parameters

The forward and reverse reactions occur simultaneously and consequently cannot be determined from a single binding time course. Whole cell binding time courses were conducted at two concentrations of ^{3}H-Dex so that the reaction rate constants could be solved simultaneously using the model below[194]:

$$K_{\mathrm{d}} = \frac{k_{\mathrm{off}}}{k_{\mathrm{on}}}$$

$$k_{\mathrm{ob}} = k_{\mathrm{on}}L + k_{\mathrm{off}}$$

$$occupancy = \frac{L}{K_{\mathrm{d}} + L}$$

$$Y_{\mathrm{max}} = occupancy \times B_{\mathrm{max}}$$

$$Y = Y_{\mathrm{max}}(1 - e^{-k_{\mathrm{ob}}X})$$

where Y is non-specific binding, X is time in minutes, L is the ligand concentration, $B_{\max}$ is the maximum binding at equilibrium, k_{ob} is the observed reaction rate constant and k_{on} and k_{off} are the forward and reverse reaction rate constants, respectively.

Cell sorting

In an attempt to produce a homogeneously GR expressing population, FACS was incorporated into the whole cell binding experimental design. COS-1 cells were transfected as described above, 48 h later the cells were harvested by trypsinisation, washing cells off of a containment vessel following 5 min incubation in trypsin-Ethylenediaminetetraacetic acid (Merck), centrifuged at 2000 rpm for 5 min, the supernatant was aspirated, the cells were resuspended in PBS and sorted using the BD FACSAria according to the eGFP-GR expression categories described in Section 5.1.3. The sorted cells were centrifuged at 2000 rpm for 5 min, the supernatant was aspirated, the cells were resuspended in supplemented DMEM and plated into 24 well plates at a density of 0.5×10^5 cells/well 24 h prior to whole cell time course binding as described above. Sorting cells for the purposes of performing a whole cell binding experiment 24 h later is a novel approach and a number of challenges were encountered.

The cell yield obtained from sorting a transfected 10 cm plate was relatively low when compared to the number of cells required to perform a whole cell binding experiment. The number of transfected 10 cm plates required to generate enough sorted cells would be burdensome to produce and the time required to sort such a large number of cells was not suitable for the experimental design. This issue was resolved by changing the experimental design from plating out only sorted cells for the whole cell binding experiment to plating out a mixture containing 10% sorted transfected cells and 90% unsorted untransfected cells. Unsorted cells were harvested by trypsinisation immediately after sorting of the tranfected cells. The untransfected cells would not influence the whole cell binding as they did not contain GR and therefore could not contribute to specific binding. This reduced the number of cells required for harvesting by 10-fold without influencing the results.

The sorted COS-1 cells did not survive and/or adhere to cell culture plates for 24 h after harvesting and sorting. A number of avenues were explored to try improve the survival and adherence of the cells. First, the pre-sort suspension which contained the cells prior to sorting was changed from PBS to 1% FCS PBS with the justification that this would reduce the harm to the cells in the period between harvesting and sorting. Second, the post-sort medium was changed from 10% FCS

DMEM to 20% FCS DMEM with the justification that this medium is diluted by a factor of 2 during sorting as cells are sorted with a small volume of sheath fluid. Third, the sort speed was reduced from 1000 cells per second to 200 with the justification that the high rate of sorting was causing strain on the cells when they expanded after leaving the nozzle.

5.1.4 Transfection efficiency trial

COS-1 cells were plated into 5×6 well plates at a density of 2×10^5 cells/well 24 h prior to transfection. Wells of each plate were transfected as described above such that each plate contained a low, medium and high transfected and an untransfected well. At times of 24, 48, 72, 96 and 120 h a plate was harvested by trypsinisation and resuspended in PBS before transfection efficiency and distribution was tested using the BD FACSAria system as described above.

5.2 Computational and modelling methods

Modelling and computational analyses were performed within an IPython[195] notebook using the Python[196] programming language with extensive use of the PySCeS[178], NumPy[197], SciPy[198] and Matplotlib[199] packages.

5.2.1 Model construction

The model for GR dimerisation and ligand binding was constructed from the classical and alternate pathways: Ligand binding to GR and subsequent GR-ligand complex homodimerisation and GR homodimerisation followed by binding of two ligands respectively. Classical rate and stoichiometric reactions were used to construct an internally consistent model in compliance with the PySCeS ".psc" file format, shown in **Appendix A**. Additionally, models were constructed containing only the classical and alternate activation pathways, shown in **Appendix B** and **C**, respectively.

Simulating whole cell GR ^{3}H-Dex saturation binding curves

In terms of radiolabelled binding assays, specific binding represents the binding of the radiolabelled ligand to the specific protein of interest and is calculated:

$$B_\mathrm{s} = B_\mathrm{t} - B_\mathrm{ns}$$

where B_t, B_s and B_{ns} are total, specific and non-specific binding, respectively. Total binding was measured after incubation with the ^{3}H-Dex. Non-specific binding was measured after incubation with a competitor to the ^{3}H-Dex, in this case, a molar excess of non-tritiated Dex.

The model was used to simulate GR ^{3}H-Dex whole cell saturation binding curves. The model was initiated with a ligand concentration of 20 nM and a GR concentration of 54, 123 or 229 nM representing either low, medium or high GR, respectively as described by Robertson *et al.*[1] and run to equilibrium. The equilibrium concentration values for RL, ligand bound GR, and RLRL were recorded and specific binding was calculated:

$$B_s = RL + 2 \times RLRL$$

where RL is ligand bound receptor monomer and RLRL is liganded receptor dimer. The liganded dimer is multiplied by two as there are two ligands bound per molecule. This is performed at a range of ligand concentrations and specific binding was calculated and recorded each time. The specific binding at each ligand concentration was scaled to the specific binding at the maximum ligand concentration.

$$B_{sc} = \frac{B_s}{B_{ms}} \times 100$$

where B_{ms} represents the maximum specific binding and B_{sc} represents the scaled specific binding. The resulting scaled specific bindings were plotted against ligand concentrations and were analogous to experimentally generated whole cell binding GR ^{3}H-Dex saturation binding curves.

5.2.2 Calculating ligand independent dimerisation

The data used to calculate ligand independent dimerisation was obtained from published FRET experiments[1]. This data shows homodimerisation of GR in the unliganded and liganded states at different concentrations of GR and therefore could be used to calculate the dissociation constant for ligand independent dimerisation of the GR. Total GR concentration was determined by whole cell ^{3}H-Dex saturation binding. The transfection efficiency reported for this data was 20%, therefore the concentration per transfected cell was 5× higher than that of the average cell. This was compensated for in the calculation by scaling up the GR concentration by a factor of 5 which had the effect of increasing the K_d 5-fold. Total CFP-GR and YFP-GR concentrations were calculated as half the total GR concentration and the maximum possible CFP-GR-YFP-GR heterodimer concentration was calculated as a third of this, using the population breakdown determined by Robertson *et al.*[1].

The FRET signal after 30 min of Dex induction was taken as the maximum FRET signal, i.e. the signal at 100% GR dimerisation, while the FRET signal at t=0 was taken to represent the basal level of unliganded GR dimerisation. The ratio of non-Dex induced FRET signal to maximally induced signal was multiplied by the maximum CFP- and YFP- GR heterodimer concentration which was taken to represent the concentration of heterodimer in the unliganded state. Monomeric CFP- and YFP- GR were calculated using the CFP-YFP GR heterodimer concentration and total the CFP-GR and YFP-GR concentrations as well as the model for determining the concentrations of monomeric CFP- and YFP- GR from FRET time course data, shown below, developed by Robertson *et al.*[1].

$$C = ((3 \times C^2) + 2 \times C \times CY - (CY)^2)/(C + CY)$$

where C represents monomeric CFP- or YFP- GR concentration and CY represents heterodimer concentration.

The % GR monomers, shown in **Table 3.2** was calculated by taking the ratio of CFP-GR or YFP-GR without Dex stimulation, found in **Table 3.1** to the total CFP-GR or YFP-GR. The % GR dimers was calculated from % GR monomers as:

$$\%GR_{\text{dimers}} = 100 - \%GR_{\text{monomers}}$$

The K_{d} of reaction 3, ligand independent GR dimerisation, was calculated from concentrations of unliganded monomer and dimer using the mass action form of the dissociation constant calculation:

$$K_{\text{d}} = \frac{[GR_{\text{monomers}}]^2}{[GR_{\text{dimers}}]}$$

5.2.3 Fitting the dissociation constants

The dissociation constants for dimerisation of liganded GR monomers and ligand binding to unliganded GR dimers were obtained by fitting the GR dimerisation cycle model consisting of the reaction shown above to experimental data using the minimize method of the LmFit Python package[200]. This experimental data was obtained from ^{3}H-Dex saturation binding experiments performed in COS-1 cells transiently transfected with differing amounts of GRwt and GRdim containing plasmids and published previously[1].

The fitting procedure was as follows: a value for the dissociation constant for dimerisation of liganded GR monomers was estimated, using this, and the thermodynamic relationship within the dimerisation cycle, a dissociation constant for ligand

binding to unliganded GR dimers was calculated. The value for GR concentration in the model was set to match one of the data sets from the experimental data. Using the PySCeS package, a parameter scan on ligand concentration was performed and liganded monomer and dimer concentrations were returned. These values were used to calculate specific binding over a range of ligand concentrations, effectively generating a saturation binding curve. The residuals were calculated by subtracting the model generated saturation binding curve, at each concentration of GR, from the experimental data. The residuals were then returned and the process repeated until the dissociation constant for dimerisation of liganded GR which results in the smallest residuals is estimated.

5.2.4 Compartmental model formulation

A compartmental model was generated which contained three replicates of the GR dimerisation cycle, shown in **Appendix D**.

Calculating cell number from fixed glucocorticoid receptor amount

The average amount of GR per cell for low, medium and high cells was determined by Robertson[1]. Using this, the ratio of GR in a low GR cell to that in low, medium and high GR cells is calculated. The distribution between low, medium and high cells is determined by flow cytometry. From these, the fraction of the total GR in each population group is determined. Using this fraction, the total GR is divided into total GR molecules in each cell type. Once again using the GR concentration in low, medium and high cells together with the average COS-1 cell protein concentration and Avogadro's number, the number of low, medium and high cells are calculated. Finally, the specific binding was calculated similarly to the single compartment model, described in Section 5.2.1, and scaled to the relative cell numbers of the different compartments and compared to experimental data. An example of this distribution is given below:

Global variables:

$$N_{\text{Avogadro}} = 6.02 \times 10^{23} \text{ molecules per mol}$$
$$Protein_{\text{COS}-1} = 6.49 \times 10^{-7} \text{mg/cell}$$
$$N_{\text{Transfected cells}} = 2 \times 10^{5} \text{ cells}$$

Method variables as example:

$$
\begin{aligned}
Fraction_{\text{Low}} &= 0.5 \\
Fraction_{\text{Medium}} &= 0.25 \\
Fraction_{\text{High}} &= 0.25
\end{aligned}
$$

$$
\begin{aligned}
GR\ protein_{\text{Low}} &= 335 \times 10^{-15} fmol \text{ GR/mg protein} \\
GR\ protein_{\text{Medium}} &= 763 \times 10^{-15} fmol \text{ GR/mg protein} \\
GR\ protein_{\text{High}} &= 1420 \times 10^{-15} fmol \text{ GR/mg protein}
\end{aligned}
$$

$$
\begin{aligned}
GR\ molecules_{\text{Total}} &= N_{\text{Transfected cells}} \times Protein_{\text{COS}-1} \times N_{\text{Avogadro}} \times GR\ protein_{\text{Medium}} \\
&= 2 \times 10^{5} \times 6.49 \times 10^{-7} \times 6.02 \times 10^{23} \times 763 \times 10^{-15} \\
&= 59.6 \times 10^{9} \text{ molecules}
\end{aligned}
$$

The ratio of GR in low, medium and high cells to low cells:

$$
\begin{aligned}
GR\ ratio_{\text{Low}} &= GR\ protein_{\text{Low}} / GR\ protein_{\text{Low}} \\
&= (335 \times 10^{-15}) / (335 \times 10^{-15}) \\
&= 1 \\
GR\ ratio_{\text{Medium}} &= GR\ protein_{\text{Medium}} / GR\ protein_{\text{Low}} \\
&= (763 \times 10^{-15}) / (335 \times 10^{-15}) \\
&= 2.27 \\
GR\ ratio_{\text{High}} &= GR\ protein_{\text{High}} / GR\ protein_{\text{Low}} \\
&= (1420 \times 10^{-15}) / (335 \times 10^{-15}) \\
&= 4.24
\end{aligned}
$$

Finding the fraction of the total GR in each population group:

$$\begin{aligned}
Relative_{\text{Low}} &= GR\ ratio_{\text{Low}} \times\ Fraction_{\text{Low}} \\
&= 1 \times 0.5 \\
&= 0.5 \\
Relative_{\text{Medium}} &= GR\ ratio_{\text{Medium}} \times\ Fraction_{\text{Medium}} \\
&= 2.27 \times 0.25 \\
&= 0.57 \\
Relative_{\text{High}} &= GR\ ratio_{\text{High}} \times\ Fraction_{\text{High}} \\
&= 4.24 \times 0.25 \\
&= 1.06 \\
Relative_{\text{Denominator}} &= Relative_{\text{Low}} + Relative_{\text{Medium}} + Relative_{\text{High}} \\
&= 0.5 + 0.57 + 1.06 \\
&= 2.13
\end{aligned}$$

Calculating the amount of GR in each population based on fractions above:

$$\begin{aligned}
N_{\text{GR in low cells}} &= GR\ molecules_{\text{Total}} \times\ Relative_{\text{Low}}/Relative_{\text{Denominator}} \\
&= 59.6 \times 10^9 \times 0.5/2.13 \\
&= 14 \times 10^9 \text{ GR molecules} \\
N_{\text{GR in medium cells}} &= GR\ molecules_{\text{Total}} \times\ Relative_{\text{Medium}}/Relative_{\text{Denominator}} \\
&= 59.6 \times 10^9 \times 0.57/2.13 \\
&= 16 \times 10^9 \text{ GR molecules} \\
N_{\text{GR in high cells}} &= GR\ molecules_{\text{Total}} \times\ Relative_{\text{High}}/Relative_{\text{Denominator}} \\
&= 59.6 \times 10^9 \times 1.06/2.13 \\
&= 30 \times 10^9 \text{ GR molecules}
\end{aligned}$$

Calculating the number of low, medium and high cells:

$$\begin{aligned}
N_{\text{Low GR cells}} &= N_{\text{GR in low cells}}/(GR\ protein_{\text{Low}} \times Protein_{\text{COS}-1} \times N_{\text{Avogadro}}) \\
&= 14 \times 10^{9}/(335 \times 10^{-15} \times 6.49 \times 10^{-7} \times 6.02 \times 10^{23}) \\
&= 1.06965 \times 10^{5} \text{ cells} \\
N_{\text{Medium GR cells}} &= N_{\text{GR in medium cells}}/(GR\ protein_{\text{Medium}} \times Protein_{\text{COS}-1} \times N_{\text{Avogadro}}) \\
&= 16 \times 10^{9}/(763 \times 10^{-15} \times 6.49 \times 10^{-7} \times 6.02 \times 10^{23}) \\
&= 0.53673 \times 10^{5} \text{ cells} \\
N_{\text{High GR cells}} &= N_{\text{GR in high cells}}/(GR\ protein_{\text{High}} \times Protein_{\text{COS}-1} \times N_{\text{Avogadro}}) \\
&= 30 \times 10^{9}/(1420 \times 10^{-15} \times 6.49 \times 10^{-7} \times 6.02 \times 10^{23}) \\
&= 0.54074 \times 10^{5} \text{ cells}
\end{aligned}$$

Bibliography

1. Robertson, S., Rohwer, J. M., Hapgood, J. P. & Louw, A. Impact of glucocorticoid receptor density on ligand-independent dimerization, cooperative ligand-binding and basal priming of transactivation: A cell culture model. *PLOS One* **8,** 1–17 (May 2013).
2. Hench, P. & Kendall, E. The effect of a hormone of the adrenal cortex (17-hydroxy-11-dehydrocorticosterone; compound E) and of pituitary adrenocorticotropic hormone on rheumatoid arthritis. *Proceedings of the staff meetings. Mayo Clinic* **24,** 181–197 (1949).
3. *The Nobel Prize in physiology or medicine 1950* Nobel Media AB. (2014).
4. Nestler, E. J., Hyman, S. E. & Malenka, R. C. *Molecular Neuropharmacology: A Foundation for Clinical Neuroscience* 3rd ed. (McGraw Hill Professional, 2008).
5. Alberts, B. *et al. Molecular Biology of the Cell* 4th ed. (ed Alberts, B.) (Garland Science, 2002).
6. Marques-Deak, A., Cizza, G. & Sternberg, E. Erratum: Brain-immune interactions and disease susceptibility. *Molecular Psychiatry* **10,** 972 (2005).
7. Otmishi, P. *et al.* Neuroimmune Interaction in Inflammatory Diseases. *Clinical Medicine Insights: Circulatory, Respiratory and Pulmonary Medicine* **2,** 35–44 (Apr. 2008).
8. Bellavance, M.-A. & Rivest, S. The HPA - immune axis and the immunomodulatory actions of glucocorticoids in the brain. *Frontiers in Immunology* **5** (Mar. 2014).
9. Vale, W., Spiess, J., Rivier, C. & Rivier, J. Characterization of a 41-residue ovine hypothalamic peptide that stimulates secretion of corticotropin and β-endorphin. *Science* **213,** 1394–1397 (1981).

10. Rivier, C. & Vale, W. Modulation of stress-induced ACTH release by corticotropin-releasing factor, catecholamines and vasopressin. *Nature* **305,** 325–327 (1983).

11. Mountjoy, K., Bobbins, L., Mortrud, M. & Cone, R. The cloning of a family of genes that encode the melanocortin receptors. *Science* **257,** 1248–1251 (1992).

12. Cone, R. *et al.* The melanocortin receptors: Agonists, antagonists, and the hormonal control of pigmentation. *Recent Progress in Hormone Research* **51,** 287–317 (1996).

13. Keller-Wood, M. & Dallman, M. Corticosteroid inhibition of ACTH secretion. *Endocrine Reviews* **5,** 1–24 (1984).

14. Breuner, C. & Orchinik, M. Plasma binding proteins as mediators of corticosteroid action in vertebrates. *Journal of Endocrinology* **175,** 99–112 (2002).

15. Berlinger, F. Principles and practice of endocrinology and metabolism. *Journal of the American Medical Association* **264,** 2810 (1990).

16. Yang, S. & Zhang, L. Glucocorticoids and vascular reactivity. *Current Vascular Pharmacology* **2,** 1–12 (2004).

17. Hayashi, R., Wada, H., Ito, K. & Adcock, I. Effects of glucocorticoids on gene transcription. *European Journal of Pharmacology* **500,** 51–62 (2004).

18. Buckingham, J. Glucocorticoids: Exemplars of multi-tasking. *British Journal of Pharmacology* **147,** S258–S268 (2006).

19. Dean, D. & Sanders, M. Ten years after: Reclassification of steroid-responsive genes. *Molecular Endocrinology* **10,** 1489–1495 (1996).

20. Dostert, A. & Heinzel, T. Negative glucocorticoid receptor response elements and their role in glucocorticoid action. *Current Pharmaceutical Design* **10,** 2807–2816 (2004).

21. Stromstedt, P.-E., Poellinger, L., Gustafsson, J.-A. & Carlstedt-Duke, J. The glucocorticoid receptor binds to a sequence overlapping the TATA box of the human osteocalcin promoter: A potential mechanism for negative regulation. *Molecular and Cellular Biology* **11,** 3379–3383 (1991).

22. Meyer, T., Carlstedt-Duke, J. & Starr, D. A weak TATA box is a prerequisite for glucocorticoid-dependent repression of the osteocalcin gene. *Journal of Biological Chemistry* **272,** 30709–30714 (1997).

23. Surjit, M. *et al.* Widespread negative response elements mediate direct repression by agonist-liganded glucocorticoid receptor. *Cell* **145,** 224–241 (2011).

24. Teurich, S. & Angel, P. The glucocorticoid receptor synergizes with jun homodimers to activate AP-1-regulated promoters lacking GR binding sites. *Chemical Senses* **20,** 251–255 (1995).

25. Wang, Y., Zhang, J., Dai, W., Lei, K. & Pike, J. Dexamethasone potently enhances phorbol ester-induced IL-1β gene expression and nuclear factor NF-κB activation. *Journal of Immunology* **159,** 534–537 (1997).

26. Schiller, B., Chodankar, R., Watson, L., Stallcup, M. & Yamamoto, K. Glucocorticoid receptor binds half sites as a monomer and regulates specific target genes. *Genome Biology* **15** (2014).

27. Lim, H.-W. *et al.* Genomic redistribution of GR monomers and dimers mediates transcriptional response to exogenous glucocorticoid in vivo. *Genome Research* **25,** 836–844 (2015).

28. Effect of cortisol on glucose metabolism. *Nutrition Reviews* **20,** 278–280 (1962).

29. Munck, A. The effect of cortisol on glucose uptake by rat epididymal fat pads. *Endocrinology* **68,** 178–180 (1961).

30. Eisenstein, A. Inhibition of gluconeogenic action of cortisol in pyridoxine-deficient rats. *Biochimica et Biophysica Acta* **36,** 580–581 (1959).

31. Leboeuf, B., Renold, A. & Cahill Jr., G. Studies on rat adipose tissue in vitro. IX. Further effects cortisol on glucose metabolism. *The Journal of Biological Chemistry* **237,** 988–991 (1962).

32. Rizza, R., Mandarino, L. & Gerich, J. Cortisol-induced insulin resistance in man: Impaired suppression of glucose production and stimulation of glucose utilization due to a postreceptor defect of insulin action. *Journal of Clinical Endocrinology and Metabolism* **54,** 131–138 (1982).

33. Exton, J. Regulation of gluconeogenesis by glucocorticoids. *Monographs on Endocrinology* **12,** 535–546 (1979).

34. Macfarlane, D., Forbes, S. & Walker, B. Glucocorticoids and fatty acid metabolism in humans: Fuelling fat redistribution in the metabolic syndrome. *Journal of Endocrinology* **197,** 189–204 (2008).

35. Mangos, G. *et al.* Cortisol inhibits cholinergic vasodilatation in the human forearm. *American Journal of Hypertension* **13,** 1155–1160 (2000).

36. Andrews, R. & Walker, B. Glucocorticoids and insulin resistance: Old hormones, new targets. *Clinical Science* **96,** 513–523 (1999).

37. Baxter, J. & Forsham, P. Tissue effects of glucocorticoids. *The American Journal of Medicine* **53,** 573–589 (1972).

38. Metabolic effects of glucocorticoids in man. *Nutrition Reviews* **32,** 301–303 (1974).

39. Xu, C. *et al.* Direct effect of glucocorticoids on lipolysis in adipocytes. *Molecular Endocrinology* **23,** 1161–1170 (2009).

40. Ottosson, M., Lönnroth, P., Björntorp, P. & Edèn, S. Effects of cortisol and growth hormone on lipolysis in human adipose tissue. *Journal of Clinical Endocrinology and Metabolism* **85,** 799–803 (2000).

41. Pazirandeh, A., Xue, Y., Prestegaard, T., Jondal, M. & Okret, S. Effects of altered glucocorticoid sensitivity in the T cell lineage on thymocyte and T cell homeostasis. *The FASEB Journal* **16,** 727–729 (2002).

42. Högger, P., Dreier, J., Droste, A., Buck, F. & Sorg, C. Identification of the integral membrane protein RM3/1 on human monocytes as a glucocorticoid-inducible member of the scavenger receptor cysteine-rich family (CD163). *Journal of Immunology* **161,** 1883–1890 (1998).

43. Piemonti, L. *et al.* Glucocorticoids increase the endocytic activity of human dendritic cells. *International Immunology* **11,** 1519–1526 (1999).

44. Batuman, O., Ferrero, A., Cupp, C., Jimenez, S. & Khalili, K. Differential regulation of transforming growth factor β-1 gene expression by glucocorticoids in human T and glial cells. *Journal of Immunology* **155,** 4397–4405 (1995).

45. Elenkov, I., Papanicolaou, D., Wilder, R. & Chrousos, G. Modulatory effects of glucocorticoids and catecholamines on human interleukin-12 and interleukin-10 production: clinical implications. *Proceedings of the Association of American Physicians* **108,** 374–381 (1996).

46. Franchimont, D. *et al.* Tumor necrosis factor α decreases, and interleukin-10 increases, the sensitivity of human monocytes to dexamethasone: Potential regulation of the glucocorticoid receptor. *Journal of Clinical Endocrinology and Metabolism* **84,** 2834–2839 (1999).

47. Galon, J. *et al.* Gene profiling reveals unknown enhancing and suppressive actions of glucocorticoids on immune cells. *The FASEB Journal* **16,** 61–71 (2002).

48. Wang, Z., Malone, M., He, H., McColl, K. & Distelhorst, C. Microarray analysis uncovers the induction of the proapoptotic BH3-only protein Bim in multiple models of glucocorticoid-induced apoptosis. *Journal of Biological Chemistry* **278,** 23861–23867 (2003).

49. Han, J.-W. *et al.* Expression of bbc3, a pro-apoptotic BH3-only gene, is regulated by diverse cell death and survival signals. *Proceedings of the National Academy of Sciences of the United States of America* **98,** 11318–11323 (2001).

50. Lu, N., Collins, J., Grissom, S. & Cidlowski, J. Selective regulation of bone cell apoptosis by translational isoforms of the glucocorticoid receptor. *Molecular and Cellular Biology* **27,** 7143–7160 (2007).

51. Rogatsky, I. *et al.* Target-specific utilization of transcriptional regulatory surfaces by the glucocorticoid receptor. *Proceedings of the National Academy of Sciences of the United States of America* **100,** 13845–13850 (2003).

52. Casale, F. *et al.* Determination of the in vivo effects of prednisone on Bcl-2 family protein expression in childhood acute lymphoblastic leukemia. *International Journal of Oncology* **22,** 123–128 (2003).

53. Beck, I. *et al.* Crosstalk in inflammation: The interplay of glucocorticoid receptor-based mechanisms and kinases and phosphatases. *Endocrine Reviews* **30,** 830–882 (2009).

54. Hafezi-Moghadam, A. *et al.* Acute cardiovascular protective effects of corticosteroids are mediated by non-transcriptional activation of endothelial nitric oxide synthase. *Nature Medicine* **8,** 473–479 (2002).

55. Sionov, R. V., Spokoini, R., Kfir-Erenfeld, S., Cohen, O. & Yefenof, E. in *Advances in Cancer Research* (eds Vande Woude, G. F. & Klein, G.) 1st ed., 127 –248 (Academic Press, 2008).

56. Sionov, R., Cohen, O., Kfir, S., Zilberman, Y. & Yefenof, E. Role of mitochondrial glucocorticoid receptor in glucocorticoid-induced apoptosis. *Journal of Experimental Medicine* **203,** 189–201 (2006).

57. Whelan, T., Schteingart, D., Starkman, M. & Smith, A. Neuropsychological deficits in cushing's syndrome. *Journal of Nervous and Mental Disease* **168,** 753–757 (1980).

58. Starkman, M. & Schteingart, D. Neuropsychiatric Manifestations of Patients with Cushing's Syndrome: Relationship to Cortisol and Adrenocorticotropic Hormone Levels. *Archives of Internal Medicine* **141,** 215–219 (1981).

59. Starkman, M., Schteingart, D. & Schork, M. Cushing's syndrome after treatment: Changes in cortisol and ACTH levels, and amelioration of the depressive syndrome. *Psychiatry Research* **19,** 177–188 (1986).

60. Varney, N., Alexander, B. & MacIndoe, J. Reversible steroid dementia in patients without steroid psychosis. *American Journal of Psychiatry* **141,** 369–372 (1984).

61. Lupien, S., Maheu, F., Tu, M., Fiocco, A. & Schramek, T. The effects of stress and stress hormones on human cognition: Implications for the field of brain and cognition. *Brain and Cognition* **65,** 209–237 (2007).

62. De Quervain, D.-F., Roozendaal, B. & McGaugh, J. Stress and glucocorticoids impair retrieval of long-term spatial memory. *Nature* **394,** 787–790 (1998).

63. Sternberg, E. & Judd, L. Conference summary and conclusions: A comprehensive approach to predicting and managing mood effects of glucocorticoids. *Annals of the New York Academy of Sciences* **1179,** 229–233 (2009).

64. Fardet, L., Petersen, I. & Nazareth, I. Prevalence of long-term oral glucocorticoid prescriptions in the UK over the past 20 years. *Rheumatology (Oxford, England)* **50,** 1982–1990 (2011).

65. Singer, M. *et al.* The third international consensus definitions for sepsis and septic shock (sepsis-3). *Journal of the American Medical Association* **315,** 801–810 (2016).

66. Bergmann, M., Staples, K., Smith, S., Barnes, P. & Newton, R. Glucocorticoid inhibition of granulocyte macrophage-colony-stimulating factor from T cells is independent of control by nuclear factor-κB and conserved lymphokine element 0. *American Journal of Respiratory Cell and Molecular Biology* **30,** 555–563 (2004).

67. Smoak, K. & Cidlowski, J. Glucocorticoids regulate tristetraprolin synthesis and posttranscriptionally regulate tumor necrosis factor alpha inflammatory signaling. *Molecular and Cellular Biology* **26,** 9126–9135 (2006).

68. Barnes, P. Corticosteroid effects on cell signalling. *European Respiratory Journal* **27,** 413–426 (2006).

69. Clark, A. MAP kinase phosphatase 1: A novel mediator of biological effects of glucocorticoids? *Journal of Endocrinology* **178,** 5–12 (2003).

70. Ito, K., Barnes, P. & Adcock, I. Glucocorticoid receptor recruitment of histone deacetylase 2 inhibits interleukin-1β-induced histone H4 acetylation on lysines 8 and 12. *Molecular and Cellular Biology* **20,** 6891–6903 (2000).

71. Bunim, J., Black, R., Lutwak, L., Peterson, R. & Whedon, G. Studies on dexamethasone, a new synthetic steroid, in rheumatoid arthritis—a preliminary report. *Arthritis & Rheumatism* **1,** 313–331 (1958).

72. *Drug discovery and medicinal chemistry for psychiatric disorders* (eds Rankovic, Z., Hargreaves, R. & Bingham, M.) (Cambridge: Royal Society of Chemistry, 2012).

73. *19th WHO Model List of Essential Medicines* World Health Organisation (Apr. 2015).

74. Tobias, J. & Chambers, T. Glucocorticoids impair bone resorptive activity and viability of osteoclasts disaggregated from neonatal rat long bones. *Endocrinology* **125,** 1290–1295 (1989).

75. Beck, L. *et al.* One systemic administration of transforming growth factor-β1 reverses age- or glucocorticoid-impaired wound healing. *Journal of Clinical Investigation* **92,** 2841–2849 (1993).

76. Perkoff, G., Silber, R., Tyler, F., Cartwright, G. & Wintrobe, M. Studies in disorders of muscle. XII. Myopathy due to the administration of therapeutic amounts of 17-hydroxycorticosteroids. *The American Journal of Medicine* **26,** 891–898 (1959).

77. Afifi, A., Bergman, R. & Harvey, J. Steroid myopathy. Clinical, histologic and cytologic observations. *The Johns Hopkins medical journal* **123,** 158–173 (1968).

78. Muller, R. & Kugelberg, E. Myopathy in Cushing's syndrome. *Journal of Neurology, Neurosurgery, and Psychiatry* **22,** 314–319 (1959).

79. Ng, T., Robson, G. & Denning, D. Hydrocortisone-enhanced growth of Aspergillus spp.: Implications for pathogenesis. *Microbiology* **140,** 2475–2479 (1994).

80. Hwang, J. & Weiss, R. Steroid-induced diabetes: A clinical and molecular approach to understanding and treatment. *Diabetes/Metabolism Research and Reviews* **30,** 96–102 (2014).

81. Wolkowitz, O., Lupien, S. & Bigler, E. The "steroid dementia syndrome": A possible model of human glucocorticoid neurotoxicity. *Neurocase* **13,** 189–200 (2007).

82. Norra, C., Arndt, M. & Kunert, H. Steroid dementia: An overlooked diagnosis? *Neurology* **66,** 155 (2006).

83. Newton, R. & Holden, N. Separating transrepression and transactivation: A distressing divorce for the glucocorticoid receptor? *Molecular Pharmacology* **72,** 799–809 (2007).

84. De Bosscher, K. *et al.* A fully dissociated compound of plant origin for inflammatory gene repression. *Proceedings of the National Academy of Sciences of the United States of America* **102,** 15827–15832 (2005).

85. Stedman, T. L. *Stedman's medical eponyms* 2nd ed. (eds Bartolucci, S. L. & Forbis, P.) (Lippincott Williams & Wilkins, 2005).

86. Carmichael, J., Paterson, I., Crompton, G., Grant, I. & Kay, A. Corticosteroid resistance in chronic asthma. *British Medical Journal (Clinical research ed.)* **282,** 1419–1422 (1981).

87. Irusen, E. *et al.* p38 mitogen-activated protein kinase-induced glucocorticoid receptor phosphorylation reduces its activity: Role in steroid-insensitive asthma. *Journal of Allergy and Clinical Immunology* **109,** 649–657 (2002).

88. Weigel, N. & Moore, N. Steroid receptor phosphorylation: A key modulator of multiple receptor functions. *Molecular Endocrinology* **21,** 2311–2319 (2007).

89. Matthews, J., Ito, K., Barnes, P. & Adcock, I. Defective glucocorticoid receptor nuclear translocation and altered histone acetylation patterns in glucocorticoid-resistant patients. *Journal of Allergy and Clinical Immunology* **113,** 1100–1108 (2004).

90. Hamid, Q. *et al.* Increased glucocorticoid receptor β in airway cells of glucocorticoid- insensitive asthma. *American Journal of Respiratory and Critical Care Medicine* **159,** 1600–1604 (1999).

91. Sousa, A., Lane, S., Cidlowski, J., Staynov, D. & Lee, T. Glucocorticoid resistance in asthma is associated with elevated in vivo expression of the glucocorticoid receptor β-isoform. *Journal of Allergy and Clinical Immunology* **105,** 943–950 (2000).

92. Orii, F. *et al.* Quantitative analysis for human glucocorticoid receptor α/β mRNA in IBD. *Biochemical and Biophysical Research Communications* **296,** 1286–1294 (2002).

93. Farrell, R. *et al.* High multidrug resistance (P-glycoprotein 170) expression in inflammatory bowel disease patients who fail medical therapy. *Gastroenterology* **118,** 279–288 (2000).

94. Farrell, R. & Kelleher, D. Glucocorticoid resistance in inflammatory bowel disease. *Journal of Endocrinology* **178,** 339–346 (2003).

95. Loke, T.-K. *et al.* Systemic glucocorticoid reduces bronchial mucosal activation of activator protein 1 components in glucocorticoid-sensitive but not glucocorticoid-resistant asthmatic patients. *Journal of Allergy and Clinical Immunology* **118,** 368–375 (2006).

96. Adcock, I., Lane, S., Brown, C., Lee, T. & Barnes, P. Abnormal glucocorticoid receptor-activator protein 1 interaction in steroid-resistant asthma. *Journal of Experimental Medicine* **182,** 1951–1958 (1995).

97. Ishiguro, Y. *et al.* Macrophage migration inhibitory factor has a proinflammatory activity via the p38 pathway in glucocorticoid-resistant ulcerative colitis. *Clinical Immunology* **120,** 335–341 (2006).

98. Nobili, S., Landini, B., Giglioni, B. & Mini, E. Pharmacological strategies for overcoming multidrug resistance. *Current Drug Targets* **7,** 861–879 (2006).

99. Hoi, A., Iskander, M. & Morand, E. Macrophage migration inhibitory factor: A therapeutic target across inflammatory diseases. *Inflammation and Allergy - Drug Targets* **6,** 183–190 (2007).

100. Gross, K. & Cidlowski, J. Tissue-specific glucocorticoid action: a family affair. *Trends in Endocrinology and Metabolism* **19,** 331–339 (2008).

101. Simons Jr., S. What goes on behind closed doors: Physiological versus pharmacological steroid hormone actions. *BioEssays* **30,** 744–756 (2008).

102. Cosío, B., Torrego, A. & Adcock, I. Molecular mechanisms of glucocorticoids [Mecanismos moleculares de los glucocorticoides]. *Archivos de Bronconeumologia* **41,** 34–41 (2005).

103. De Bosscher, K., Van Craenenbroeck, K., Meijer, O. & Haegeman, G. Selective transrepression versus transactivation mechanisms by glucocorticoid receptor modulators in stress and immune systems. *European Journal of Pharmacology* **583,** 290–302 (2008).

104. Lu, N. *et al.* International union of pharmacology. LXV. The pharmacology and classification of the nuclear receptor superfamily: Glucocorticoid, mineralocorticoid, progesterone, and androgen receptors. *Pharmacological Reviews* **58,** 782–797 (2006).

105. Bookout, A. L. *et al.* Anatomical Profiling of Nuclear Receptor Expression Reveals a Hierarchical Transcriptional Network. *Cell* **126,** 789–799 (Aug. 2006).

106. Ebrecht, M. *et al.* Tissue specificity of glucocorticoid sensitivity in healthy adults. *The Journal of Clinical Endocrinology and Metabolism* **85,** 3733–3739 (Oct. 2000).

107. Paoletti, P. *et al.* Characteristics and biological role of steroid hormone receptors in neuroepithelial tumors. *Journal of Neurosurgery* **73,** 736–742 (Nov. 1990).

108. Ho, A. D., Stojakowits, S., Pralle, H., Dörner, M. & Hunstein, W. Glucocorticoid receptor level, terminal deoxynucleotidyl transferase activity and initial responsiveness to prednisone and vincristine in leukemia. *Klinische Wochenschrift* **61,** 455–459 (May 1983).

109. Sun, X., Fischer, D. R., Pritts, T. A., Wray, C. J. & Hasselgren, P.-O. Expression and binding activity of the glucocorticoid receptor are upregulated in septic muscle. *American Journal of Physiology - Regulatory, Integrative and Comparative Physiology* **282,** R509–R518 (2002).

110. Carlstedt-Duke, J. *et al.* Domain structure of the glucocorticoid receptor protein. *Proceedings of the National Academy of Sciences of the United States of America* **84,** 4437–4440 (1987).

111. Beato, M., Herrlich, P. & Schütz, G. Steroid hormone receptors: Many actors in search of a plot. *Cell* **83,** 851–857 (1995).

112. Kumar, R. & Thompson, E. The structure of the nuclear hormone receptors. *Steroids* **64,** 310–319 (1999).

113. Avenant, C., Ronacher, K., Stubsrud, E., Louw, A. & Hapgood, J. Role of ligand-dependent GR phosphorylation and half-life in determination of ligand-specific transcriptional activity. *Molecular and Cellular Endocrinology* **327,** 72–88 (2010).

114. Chen, W. *et al.* Glucocorticoid receptor phosphorylation differentially affects target gene expression. *Molecular Endocrinology* **22,** 1754–1766 (2008).

115. Galliher-Beckley, A. & Cidlowski, J. Emerging roles of glucocorticoid receptor phosphorylation in modulating glucocorticoid hormone action in health and disease. *IUBMB Life* **61,** 979–986 (2009).

116. Bledsoe, R. *et al.* Crystal structure of the glucocorticoid receptor ligand binding domain reveals a novel mode of receptor dimerization and coactivator recognition. *Cell* **110,** 93–105 (2002).

117. Schoch, G. *et al.* Molecular Switch in the Glucocorticoid Receptor: Active and Passive Antagonist Conformations. *Journal of Molecular Biology* **395,** 568–577 (2010).

118. McMaster, A. & Ray, D. Drug Insight: Selective agonists and antagonists of the glucocorticoid receptor. *Nature Clinical Practice Endocrinology and Metabolism* **4,** 91–101 (2008).

119. Voutsas, I. F. *et al.* A novel quantitative flow cytometric method for measuring glucocorticoid receptor (GR) in cell lines: correlation with the biochemical determination of GR. *Journal of Immunological Methods* **324,** 110–119 (July 2007).

120. Lu, Y.-S. *et al.* Effects of glucocorticoids on the growth and chemosensitivity of carcinoma cells are heterogeneous and require high concentration of functional glucocorticoid receptors. *World Journal of Gastroenterology* **11,** 6373–6380 (2005).

121. Pratt, W., Galigniana, M., Harrell, J. & DeFranco, D. Role of hsp90 and the hsp90-binding immunophilins in signalling protein movement. *Cellular Signalling* **16,** 857–872 (2004).

122. Freedman, N. & Yamamoto, K. Importin 7 and Importin α/Importin β Are Nuclear Import Receptors for the Glucocorticoid Receptor. *Molecular Biology of the Cell* **15,** 2276–2286 (2004).

123. Htun, H., Barsony, J., Renyi, I., Gould, D. & Hager, G. Visualization of glucocorticoid receptor translocation and intranuclear organization in living cells with a green fluorescent protein chimera. *Proceedings of the National Academy of Sciences of the United States of America* **93,** 4845–4850 (1996).

124. Savory, J. *et al.* Discrimination between NL1- and NL2-mediated nuclear localization of the glucocorticoid receptor. *Molecular and Cellular Biology* **19,** 1025–1037 (1999).

125. Caamaño, C., Morano, M., Dalman, F., Pratt, W. & Akil, H. A conserved proline in the hsp90 binding region of the glucocorticoid receptor is required for hsp90 heterocomplex stabilization and receptor signaling. *Journal of Biological Chemistry* **273,** 20473–20480 (1998).

126. Davies, T., Ning, Y.-M. & Sánchez, E. A new first step in activation of steroid receptors. Hormone-induced switching of FKBP51 and FKBP52 immunophilins. *Journal of Biological Chemistry* **277,** 4597–4600 (2002).

127. Ronacher, K. *et al.* Ligand-selective transactivation and transrepression via the glucocorticoid receptor: Role of cofactor interaction. *Molecular and Cellular Endocrinology* **299,** 219–231 (2009).

128. Defranco, D. *et al.* Nucleocytoplasmic shuttling of steroid receptors. *Vitamins and Hormones* **51,** 315–338 (1995).

129. Reik, A., Schütz, G. & Francis Stewart, A. Glucocorticoids are required for establishment and maintenance of an alteration in chromatin structure: Induction leads to a reversible disruption of nucleosomes over an enhancer. *EMBO Journal* **10,** 2569–2576 (1991).

130. Yang, J., Liu, J. & DeFranco, D. Subnuclear trafficking of glucocorticoid receptors in vitro: Chromatin recycling and nuclear export. *Journal of Cell Biology* **137,** 523–538 (1997).

131. Black, B., Holaska, J., Rastinejad, F. & Paschal, B. DNA binding domains in diverse nuclear receptors function as nuclear export signals. *Current Biology* **11,** 1749–1758 (2001).

132. Schaaf, M. & Cidlowski, J. Molecular determinants of glucocorticoid receptor mobility in living cells: The importance of ligand affinity. *Molecular and Cellular Biology* **23,** 1922–1934 (2003).

133. Tago, K., Tsukahara, F., Naruse, M., Yoshioka, T. & Takano, K. Regulation of nuclear retention of glucocorticoid receptor by nuclear Hsp90. *Molecular and Cellular Endocrinology* **213,** 131–138 (2004).

134. Copeland, R. Evaluation of enzyme inhibitors in drug discovery. A guide for medicinal chemists and pharmacologists. *Methods of Biochemical Analysis.* **46,** 1–265 (2005).

135. Copeland, R. *Enzymes: a practical introduction to structure, mechanism, and data analysis* (VCH Publishers, 1996).

136. Fischer, E. Einfluss der configuration auf die wirkung der enzyme. *Berichte der Deutschen Chemischen Gesellschaft* **27,** 2985–2993 (1894).

137. Copeland, R., Pompliano, D. & Meek, T. Drug-target residence time and its implications for lead optimization. *Nature Reviews Drug Discovery* **5,** 730–739 (2006).

138. Tummino, P. & Copeland, R. Residence time of receptor-ligand complexes and its effect on biological function. *Biochemistry* **47,** 5481–5492 (2008).

139. Copeland, R. The dynamics of drug-target interactions: Drug-target residence time and its impact on efficacy and safety. *Expert Opinion on Drug Discovery* **5,** 305–310 (2010).

140. Swinney, D. Biochemical mechanisms of drug action: What does it take for success? *Nature Reviews Drug Discovery* **3,** 801–808 (2004).

141. Koshland, D. Application of a theory of enzyme specificity to protein synthesis. *Proceedings of the National Academy of Sciences* **44,** 98–104 (1958).

142. Ma, B., Kumar, S., Tsai, C.-J. & Nussinov, R. Folding funnels and binding mechanisms. *Protein Engineering* **12,** 713–720 (1999).

143. Tsai, C.-J., Kumar, S., Ma, B. & Nussinov, R. Folding funnels, binding funnels, and protein function. *Protein Science* **8,** 1181–1190 (1999).

144. Bhabha, G. *et al.* A dynamic knockout reveals that conformational fluctuations influence the chemical step of enzyme catalysis. *Science* **332,** 234–238 (2011).

145. Hammes, G., Chang, Y.-C. & Oas, T. Conformational selection or induced fit: A flux description of reaction mechanism. *Proceedings of the National Academy of Sciences of the United States of America* **106,** 13737–13741 (2009).

146. Garvey, E. Structural mechanisms of slow-onset, two-step enzyme inhibition. *Current Chemical Biology* **4,** 64–73 (2010).

147. Swinney, D. Can binding kinetics translate to a clinically differentiated drug? From theory to practice. *Letters in Drug Design and Discovery* **3,** 569–574 (2006).

148. Lu, H. & Tonge, P. Drug-target residence time: Critical information for lead optimization. *Current Opinion in Chemical Biology* **14,** 467–474 (2010).

149. Encío, I. & Detera-Wadleigh, S. The genomic structure of the human glucocorticoid receptor. *Journal of Biological Chemistry* **266,** 7182–7188 (1991).

150. Oakley, R., Sar, M. & Cidlowski, J. The human glucocorticoid receptor β isoform: Expression, biochemical properties, and putative function. *Journal of Biological Chemistry* **271,** 9550–9559 (1996).

151. De Castro, M. *et al.* The non-ligand binding β-isoform of the human glucocorticoid receptor (hGRβ): Tissue levels, mechanism of action, and potential physiologic role. *Molecular Medicine* **2,** 597–607 (1996).

152. Yudt, M., Jewell, C., Bienstock, R. & Cidlowski, J. Molecular origins for the dominant negative function of human glucocorticoid receptor beta. *Molecular and Cellular Biology* **23,** 4319–4330 (2003).

153. Hollenberg, S. *et al.* Primary structure and expression of a functional human glucocorticoid receptor cDNA. *Nature* **318,** 635–641 (1985).

154. Giguère, V., Hollenberg, S., Rosenfeld, M. & Evans, R. Functional domains of the human glucocorticoid receptor. *Cell* **46,** 645–652 (1986).

155. Bamberger, C., Bamberger, A.-M., De Castro, M. & Chrousos, G. Glucocorticoid receptor β, a potential endogenous inhibitor of glucocorticoid action in humans. *Journal of Clinical Investigation* **95,** 2435–2441 (1995).

156. Oakleyt, R., Jewell, C., Yudt, M., Bofetiado, D. & Cidlowski, J. The dominant negative activity of the human glucocorticoid receptor β isoform. Specificity and mechanisms of action. *Journal of Biological Chemistry* **274,** 27857–27866 (1999).

157. Kino, T. *et al.* Glucocorticoid receptor (GR) β has intrinsic, GRα-independent transcriptional activity. *Biochemical and Biophysical Research Communications* **381,** 671–675 (2009).

158. Heck, S. *et al.* A distinct modulating domain in glucocorticoid receptor monomers in the repression of activity of the transcription factor AP-1. *EMBO Journal* **13,** 4087–4095 (1994).

159. Jewell, C., Scoltock, A., Hamel, B., Yudt, M. & Cidlowski, J. Complex human glucocorticoid receptor dim mutations define glucocorticoid induced apoptotic resistance in bone cells. *Molecular Endocrinology* **26,** 244–256 (2012).

160. Reichardt, H. *et al.* DNA binding of the glucocorticoid receptor is not essential for survival. *Cell* **93,** 531–541 (1998).

161. Ponce de León, V., Mérillat, A.-M., Tesson, L., Anegón, I. & Hummler, E. Generation of TALEN-mediated GRdim knock-in rats by homologous recombination. *PLOS One* **9,** 1–6 (Feb. 2014).

162. Presman, D. M. *et al.* Live cell imaging unveils multiple domain requirements for In vivo dimerization of the glucocorticoid receptor. *PLOS Biology* **12,** 1–14 (Mar. 2014).

163. Segard-Maurel, I. *et al.* Glucocorticosteroid receptor dimerization investigated by analysis of receptor binding to glucocorticosteroid responsive elements using a monomer-dimer equilibrium model. *Biochemistry* **35,** 1634–1642 (1996).

164. Oren, I., Fleishman, S., Kessel, A. & Ben-Tal, N. Free diffusion of steroid hormones across biomembranes: A simplex search with implicit solvent model calculations. *Biophysical Journal* **87,** 768–779 (2004).

165. Gronemeyer, H., Gustafsson, J.-Å. & Laudet, V. Principles for modulation of the nuclear receptor superfamily. *Nature Reviews Drug Discovery* **3,** 950–964 (2004).

166. Kolodkin, A. *et al.* Design principles of nuclear receptor signaling: How complex networking improves signal transduction. *Molecular Systems Biology* **6** (2010).

167. Hill, A. V. The possible effects of the aggregation of the molecules of hæmoglobin on its dissociation curves. *The Journal of Physiology* **40,** iv–vii (1910).

168. Fanestil, D. & Edelman, I. Characteristics of the renal nuclear receptors for aldosterone. *Proceedings of the National Academy of Sciences of the United States of America* **56,** 872–879 (1966).

169. Gardner, R. Nuclear thyroid hormone receptors: Evidence for association with nucleolar chromatin. *Biochemical and Biophysical Research Communications* **67,** 625–633 (1975).

170. Reddy, T. *et al.* Genomic determination of the glucocorticoid response reveals unexpected mechanisms of gene regulation. *Genome Research* **19,** 2163–2171 (2009).

171. De Kloet, E., Meijer, O., Vreugdenhil, E. & Joëls, M. The yin and yang of nuclear receptors: Symposium on nuclear receptors in brain. *Trends in Endocrinology and Metabolism* **11,** 245–248 (2000).

172. Nordeen, S., Kuhnel, B., Lawler-Heavner, J., Barber, D. & Edwards, D. A quantitative comparison of dual control of a hormone response element by progestins and glucocorticoids in the same cell line. *Molecular Endocrinology* **3,** 1270–1278 (1989).

173. Van Steensel, B. *et al.* Localization of the glucocorticoid receptor in discrete clusters in the cell nucleus. *Journal of Cell Science* **108,** 3003–3011 (1995).

174. Polman, J. *et al.* A genome-wide signature of glucocorticoid receptor binding in neuronal PC12 cells. *BMC Neuroscience* **13** (2012).

175. Liu, J. & DeFranco, D. Protracted nuclear export of glucocorticoid receptor limits its turnover and does not require the exportin 1/CRM1-directed nuclear export pathway. *Molecular Endocrinology* **14,** 40–51 (2000).

176. Franco, R. *et al.* The two-state dimer receptor model: A general model for receptor dimers. *Molecular Pharmacology* **69,** 1905–1912 (Mar. 2006).

177. Gibbs, W. A method of geometrical representation of the thermodynamic properties of substances by means of surfaces. *Transactions of the Connecticut Academy* **1,** 382–404 (1873).

178. Olivier, B. G., Rohwer, J. M. & Hofmeyr, J.-H. S. Modelling cellular systems with PySCeS. *Bioinformatics* **21,** 560–561 (Sept. 2004).

179. Presman, D. *et al.* DNA binding triggers tetramerization of the glucocorticoid receptor in live cells. *Proceedings of the National Academy of Sciences of the United States of America* **113,** 8236–8241 (2016).

180. Girard, C., Barbier, O., Veilleux, G., El-Alfy, M. & Bélanger, A. Human uridine diphosphate-glucuronosyltransferase UGT2B7 conjugates mineralocorticoid and glucocorticoid metabolites. *Endocrinology* **144,** 2659–2668 (2003).

181. Szapary, D., Xu, M. & Simons Jr., S. Induction properties of a transiently transfected glucocorticoid-responsive gene vary with glucocorticoid receptor concentration. *Journal of Biological Chemistry* **271,** 30576–30582 (1996).

182. Matthews, L. *et al.* Cell cycle phase regulates glucocorticoid receptor function. *PLOS One* **6** (2011).

183. Ritter, H., Antonova, L. & Mueller, C. The unliganded glucocorticoid receptor positively regulates the tumor suppressor gene BRCA1 through GABP beta. *Molecular Cancer Research* **10,** 558–569 (2012).

184. Ritter, H. & Mueller, C. Expression microarray identifies the unliganded glucocorticoid receptor as a regulator of gene expression in mammary epithelial cells. *BMC Cancer* **14** (2014).

185. Kotitschke, A., Sadie-Van Gijsen, H., Avenant, C., Fernandes, S. & Hapgood, J. Genomic and nongenomic cross talk between the gonadotropin-releasing hormone receptor and glucocorticoid receptor signaling pathways. *Molecular Endocrinology* **23,** 1726–1745 (2009).

186. Verhoog, N., Du Toit, A., Avenant, C. & Hapgood, J. Glucocorticoid-independent repression of tumor necrosis factor (TNF) α-stimulated Interleukin (IL)-6 expression by the glucocorticoid receptor: A potential mechanism for protection against an excessive inflammatory response. *Journal of Biological Chemistry* **286,** 19297–19310 (2011).

187. Dahlman-Wright, K., Wright, A., Gustafsson, J. & Carlstedt-Duke, J. Interaction of the glucocorticoid receptor DNA-binding domain with DNA as a dimer is mediated by a short segment of five amino acids. *Journal of Biological Chemistry* **266,** 3107–3112 (1991).

188. Luisi, B. *et al.* Crystallographic analysis of the interaction of the glucocorticoid receptor with DNA. *Nature* **352,** 497–505 (1991).

189. Davies, D. in *Flow Cytometry: Principles and Applications* (ed Macey, M. G.) (Humana Press Inc., Totowa, 2007).

190. Rodriguez, J., Monsalves-Alvarez, M., Henriquez, S., Llanos, M. & Troncoso, R. Glucocorticoid resistance in chronic diseases. *Steroids* **115,** 182–192 (2016).

191. Cohen, S. *et al.* Chronic stress, glucocorticoid receptor resistance, inflammation, and disease risk. *Proceedings of the National Academy of Sciences of the United States of America* **109,** 5995–5999 (2012).

192. Bradford, M. A rapid and sensitive method for the quantitation of microgram quantities of protein utilizing the principle of protein-dye binding. *Analytical Biochemistry* **72,** 248–254 (1976).

193. Maes, R., Sedwick, W. & Vaheri, A. Interaction between DEAE-dextran and nucleic acids. *Biochimica et Biophysica Acta - Nucleic Acids And Protein Synthesis* **134,** 269–276 (1967).

194. GraphPad Prism. *Equation: Association kinetics (two ligand concentration)* Version 5.00 for Windows. GraphPad Software (La Jolla, California, USA, 2007).

195. Pérez, F. & Granger, B. E. IPython: A System for Interactive Scientific Computing. *Computing in Science & Engineering* **9,** 21–29 (2007).

196. *Python Language Reference, version 2.7* Python Software Foundation. <http://www.python.org>.

197. Walt, S. v. d., Colbert, S. C. & Varoquaux, G. The NumPy Array: A Structure for Efficient Numerical Computation. *Computing in Science & Engineering* **13,** 22–30 (2011).

198. Jones, E., Oliphant, T., Peterson, P., *et al. SciPy: Open source scientific tools for Python* (2001).

199. Hunter, J. D. Matplotlib: A 2D Graphics Environment. *Computing in Science & Engineering* **9,** 90–95 (2007).

200. Newville, M., Stensitzki, T., Allen, D. B. & Ingargiola, A. *LMFIT: Non-Linear Least-Square Minimization and Curve-Fitting for Python* <doi:10.5281/zenodo.11813> (2014).

Appendices

Appendix A

Glucocorticoid receptor dimerisation cycle model

The Glucocorticoid receptor dimerisation cycle model ".psc" file. R1, represents reaction 1, ligand binding to monomeric GR; R2, represents reaction 2, homodimerisation of liganded GR; R3, represents reaction 3, homodimerisation of unliganded GR; and R4, represents reaction 4, binding of two ligands to unliganded GR homodimer. L represents the ligand Dex and is fixed as Dex is present in excess in the experiments therefore ligand depletion did not occur. R represents the monomeric unliganded GR, RL represents liganded monomeric GR, RLRL represents liganded GR homodimer and RR represents unliganded GR homodimer. k1 to k4 and k_1 to k_4 represent the forward and reverse reaction rate constants of reactions 1 to 4, respectively.

```
## Glucocorticoid receptor dimerisation cycle model .psc file
# Concentrations in nM
# Time units in minutes
FIX: L

R1:
    R + L = RL
    R * L * k1 - RL * k_1
R2:
    {2}RL = RLRL
    RL**2 * k2 - RLRL * k_2
R3:
    {2}R = RR
    R**2 * k3 - RR * k_3
R4:
    RR + {2}L = RLRL
    RR * L**2 * k4 - RLRL * k_4

#InitEx
L = 20

#InitPar
k1 = 1
k_1 = 52.3
k2 = 1
k_2 = 6.4
k3 = 1
k_3 = 83.0
k4 = 1
k_4 = 211.5

#InitVar
R = 54
RL = 0
RR = 0
RLRL = 0
```

Appendix B

Glucocorticoid receptor classical activation pathway model

The Glucocorticoid receptor dimerisation cycle model ".psc" file. R1, represents reaction 1, ligand binding to monomeric GR and R2, represents reaction 2, homodimerisation of liganded GR. L represents the ligand Dex and is fixed as Dex is present in excess in the experiments therefore ligand depletion did not occur. R represents the monomeric unliganded GR, RL represents liganded monomeric GR and RLRL represents liganded GR homodimer. k1 and k2 and k_1 and k_2 represent the forward and reverse reaction rate constants of reaction 1 and 2, respectively.

```
## Glucocorticoid receptor classical activation pathway model .psc file
# Concentrations in nM
# Time units in minutes
FIX: L

R1:
    R + L = RL
    R * L * k1 - RL * k_1
R2:
    {2}RL = RLRL
    RL**2 * k2 - RLRL * k_2

#InitEx
L = 20

#InitPar
k1 = 1
k_1 = 52.3
k2 = 1
k_2 = 6.4

#InitVar
R = 54
RL = 0
RLRL = 0
```

Appendix C

Glucocorticoid receptor alternate activation pathway model

The Glucocorticoid receptor dimerisation cycle model ".psc" file. R1, represents reaction 1, homodimerisation of unliganded GR and R2, represents reaction 2, binding of two ligands to unliganded GR homodimer. L represents the ligand Dex and is fixed as Dex is present in excess in the experiments therefore ligand depletion did not occur. R represents the monomeric unliganded GR, RLRL represents liganded GR homodimer and RR represents unliganded GR homodimer. k1 and k2 and k_1 and k_2 represent the forward and reverse reaction rate constants of reaction 1 and 2, respectively.

```
## Glucocorticoid receptor alternative activation pathway model .psc file
# Concentrations in nM
# Time units in minutes
FIX: L

R1:
    {2}R = RR
    R**2 * k1 - RR * k_1
R2:
    RR + {2}L = RLRL
    RR * L**2 * k2 - RLRL * k_2

#InitEx
L = 20

#InitPar
k1 = 1
k_1 = 83.0 # got from the % dimerisation data in paper (corrected x5)
k2 = 1
k_2 = 211.5 # fitted from GRwt Low

#InitVar
R = 54
RR = 0
RLRL = 0
```

Appendix D

Glucocorticoid receptor dimerisation cycle compartmental model

The glucocorticoid receptor dimerisation cycle compartmental model ".psc" file. R1, represents reaction 1, ligand binding to monomeric GR in the low GR compartment; R2, represents reaction 2, homodimerisation of liganded GR in the low GR compartment; R3, represents reaction 3, homodimerisation of unliganded GR in the low GR compartment; and R4, represents reaction 4, binding of two ligands to unliganded GR homodimer in the low GR compartment. Reactions 5 to 8 correspond to reactions 1 to 4 respectively with the exception that they relate to the medium GR compartment. Reactions 9 to 12 correspond to reactions 1 to 4 respectively with the exception that they relate to the high GR compartment. L represents the ligand Dex and is fixed as Dex is present in excess in the experiments therefore ligand depletion did not occur. Rlow, Rmed and Rhigh represents the monomeric unliganded GR in the low, medium and high GR compartments, respectively; RLlow, RLmed and RLhigh represents liganded monomeric GR in the low, medium and high GR compartments, respectively; RLlowRLlow, RLmedRLmed and RLhighRLhigh represents liganded GR homodimer in the low, medium and high GR compartments, respectively; and RlowRlow, RmedRmed and RhighRhigh represents unliganded GR homodimer in the low, medium and high GR compartments, respectively. k1 to k4 and k_1 to k_4 represent the respective forward and reverse reaction rate constants of reactions 1 to 4, 5 to 8 and 9 to 12.

```
## Glucocorticoid receptor dimerisation cycle compartmental model .psc file
# Concentrations in nM
# Time units in minutes
FIX: L

# Low GR population
R1:
    Rlow + L = Rlow_L
    Rlow * L * k1 - Rlow_L * k_1
R2:
    {2}Rlow_L = Rlow_LRlow_L
    Rlow_L**2 * k2 - Rlow_LRlow_L * k_2
R3:
    {2}Rlow = RlowRlow
    Rlow**2 * k3 - RlowRlow * k_3
R4:
    RlowRlow + {2}L = Rlow_LRlow_L
    RlowRlow * L**2 * k4 - Rlow_LRlow_L * k_4
# Medium GR population
R5:
    Rmed + L = Rmed_L
    Rmed * L * k1 - Rmed_L * k_1
R6:
    {2}Rmed_L = Rmed_LRmed_L
    Rmed_L**2 * k2 - Rmed_LRmed_L * k_2
R7:
    {2}Rmed = RmedRmed
    Rmed**2 * k3 - RmedRmed * k_3
R8:
    RmedRmed + {2}L = Rmed_LRmed_L
    RmedRmed * L**2 * k4 - Rmed_LRmed_L * k_4
# High GR population
R9:
    Rhigh + L = Rhigh_L
    Rhigh * L * k1 - Rhigh_L * k_1
R10:
    {2}Rhigh_L = Rhigh_LRhigh_L
    Rhigh_L**2 * k2 - Rhigh_LRhigh_L * k_2
R11:
    {2}Rhigh = RhighRhigh
```

```
    Rhigh**2 * k3 - RhighRhigh * k_3
R12:
    RhighRhigh + {2}L = Rhigh_LRhigh_L
    RhighRhigh * L**2 * k4 - Rhigh_LRhigh_L * k_4

#InitEx
L = 20

#InitPar
k1 = 1
k_1 = 52.3
k2 = 1
k_2 = 6.4
k3 = 1
k_3 = 83.0
k4 = 1
k_4 = 211.5

#InitVar
Rlow = 54
Rlow_L = 0
RlowRlow = 0
Rlow_LRlow_L = 0

Rmed = 123
Rmed_L = 0
RmedRmed = 0
Rmed_LRmed_L = 0

Rhigh = 229
Rhigh_L = 0
RhighRhigh = 0
Rhigh_LRhigh_L = 0
```

Appendix E

An example of FACS determination of transfection efficiency and distribution, as described in Section 5.1.3.

FACSDiva Version 6.1.3

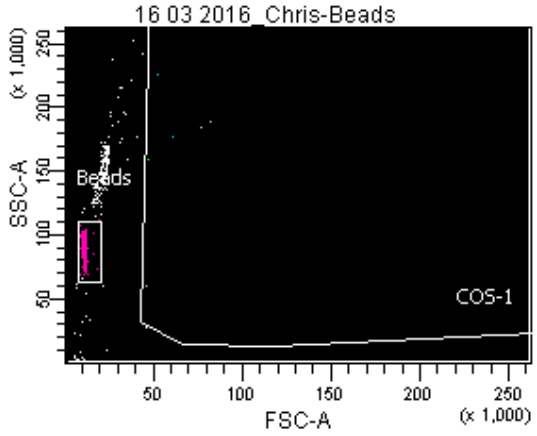

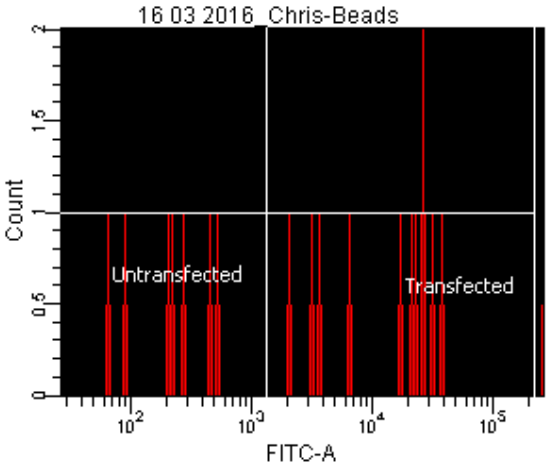

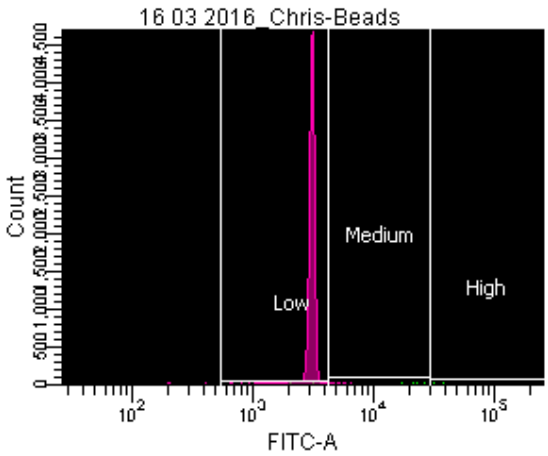

Tube: Beads

Population	#Events	%Parent	%Total
All Events	16,067	####	100.0
COS-1	19	0.1	0.1
Untransfected	7	36.8	0.0
Transfected	11	57.9	0.1
Low	3	27.3	0.0
Medium	6	54.5	0.0
High	2	18.2	0.0
Beads	15,147	94.3	94.3
P1	15,147	100.0	94.3

Experiment Name: GFP 2016 Chris data
Specimen Name: 16 03 2016_Chris
Tube Name: Beads

Population	#Events	%Parent	FITC-A Geo Mean	FITC-A Median
Untransfected	7	36.8	204	216
Transfected	11	57.9	12,429	21,134
Low	3	27.3	2,846	3,087
Medium	6	54.5	18,433	22,117
High	2	18.2	34,771	34,958
Beads	15,147	94.3	3,033	3,072
P1	15,147	100.0	3,033	3,072

FACSDiva Version 6.1.3

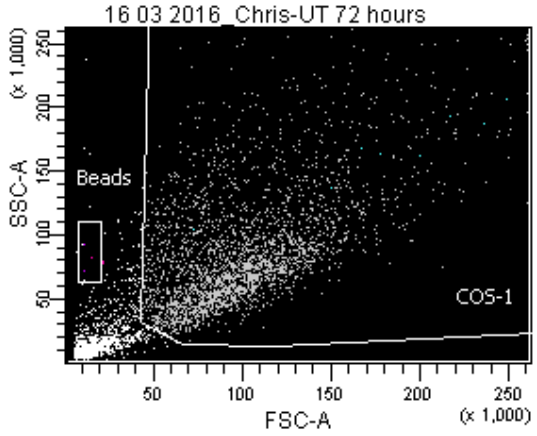

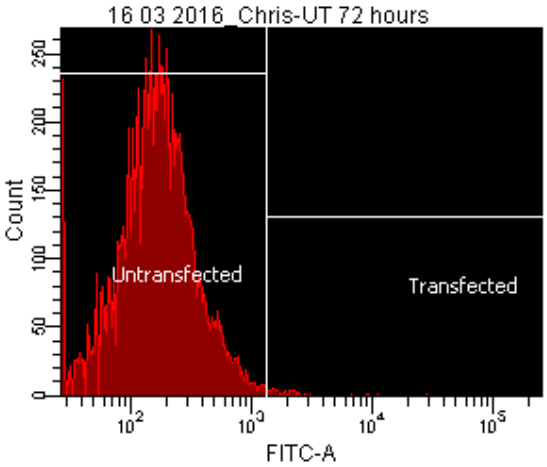

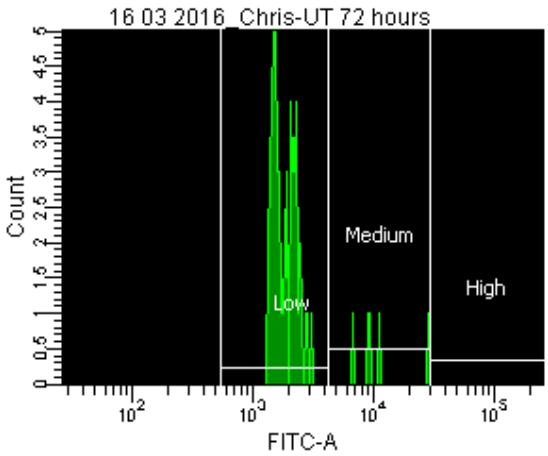

Tube: UT 72 hours

Population	#Events	%Parent	%Total
All Events	14,108	####	100.0
COS-1	10,000	70.9	70.9
Untransfected	9,942	99.4	70.5
Transfected	58	0.6	0.4
Low	53	91.4	0.4
Medium	5	8.6	0.0
High	0	0.0	0.0
Beads	24	0.2	0.2
P1	15	62.5	0.1

Experiment Name: GFP 2016 Chris data
Specimen Name: 16 03 2016_Chris
Tube Name: UT 72 hours

Population	#Events	%Parent	FITC-A Geo Mean	FITC-A Median
Untransfected	9,942	99.4	####	162
Transfected	58	0.6	2,116	1,855
Low	53	91.4	1,808	1,738
Medium	5	8.6	11,174	9,260
High	0	0.0	####	####
Beads	24	0.2	####	87
P1	15	62.5	147	148

FACSDiva Version 6.1.3

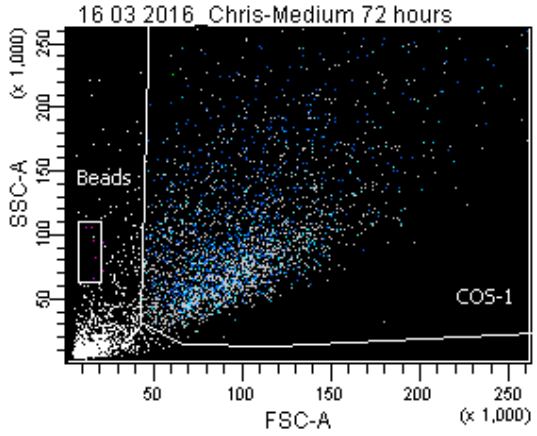

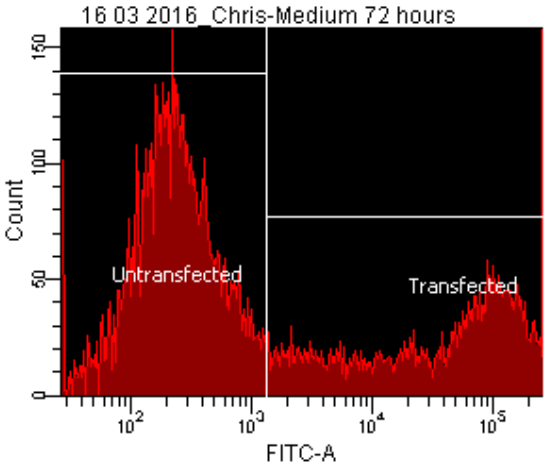

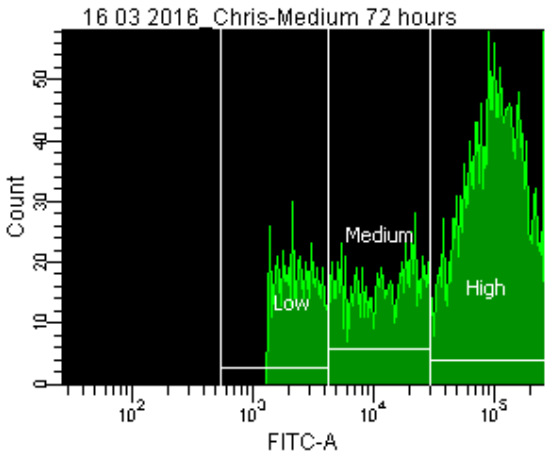

Tube: Medium 72 hours

Population	#Events	%Parent	%Total
All Events	15,099	####	100.0
COS-1	10,000	66.2	66.2
Untransfected	6,302	63.0	41.7
Transfected	3,698	37.0	24.5
Low	553	15.0	3.7
Medium	861	23.3	5.7
High	2,284	61.8	15.1
Beads	36	0.2	0.2
P1	18	50.0	0.1

Experiment Name: GFP 2016 Chris data
Specimen Name: 16 03 2016_Chris
Tube Name: Medium 72 hours

Population	#Events	%Parent	FITC-A Geo Mean	FITC-A Median
Untransfected	6,302	63.0	####	220
Transfected	3,698	37.0	36,459	61,018
Low	553	15.0	2,301	2,307
Medium	861	23.3	11,436	11,780
High	2,284	61.8	110,194	111,771
Beads	36	0.2	####	44
P1	18	50.0	243	175